Genesis of Mylonite and Structure of Francis Peak, Wasatch Mountains, Utah

A THESIS
SUBMITTED TO THE FACULTY OF THE GRADUATE SCHOOL
OF THE UNIVERSITY OF MINNESOTA
BY

William James Dunlap

IN PARTIAL FULFULLMENT OF THE REQUIREMENTS
FOR THE DEGREE OF
MASTER OF SCIENCE

November, 1990

Abstract

This thesis focuses on progressive deformation and mylonite formation from three common protolith rock types, layered gneiss, amphibolite and granitic rock. Protolith rock types and deformed equivalents were sampled in the Farmington Canyon Complex on Francis Peak in the northern Wasatch Mountains of Utah. Genesis of mylonitic foliation and lineation was promoted by grain-scale processes such as recrystallization, strain, solution transfer, metamorphic reaction and fluid influx. Despite the extreme textural transition that takes place during mylonitization, protolith rock type can often be identified even after complete recrystallization.

Geometric and kinematic field data were used to constrain the tectonic history of the rocks and to construct a model for the development of structures associated with the mylonites. Mylonitization probably took place during an obscure Proterozoic deformation or the Cretaceaous Sevier Orogeny, although kinematic data suggest that the former is more likely.

Acknowledgements

Those mentioned below either directly or indirectly influenced my writing. Nonetheless, I willingly take full responsibility for the singularity in the thesis-time continuum which these writings have spawned, and understand that I may be prosecuted for my failure to comply with Intergalactic Thesis Duration Law #92685-101290.

For keeping my spirit healthy I thank Lynette Maki, Heidi Johnson, Heidi Larson, Heidi Hugdahl, Stacy Angeles, Anne Stanfield, Ashley Albritton, Natalie Ziehwein, Mary McQuillan, Lisa Redman, Rowina Kilpatrick, Farah Rahman, Carrie Ann Modean, and Lynn Lanz.

I received assistance in the field from John Green, Mike Ellis and Jim Grant and I gratefully acknowledge this contribution. John Green rode up Farmington Canyon in my truck and sat on the passenger side, near the cliff. I will never forget that hair-raising ride and I'm sure he won't either.

Much of the structural interpretation was developed through interaction with Mike Ellis. He helped me interpret the microstructure and its evolution during deformation. Many thanks to Mike for his eager assistance. I sincerely thank Tim Holst for his diligence in correcting the many revisions of this thesis. Tim gave invaluable advice on the regional geology of northern Utah and also made sure that my interpretation of the structure of Francis Peak was written as objectively as possible. Thank you Tim. I must also thank Mike Spicuzza, fellow disciple of the Jagman, for being a good friend and for acting as backboard for the veritable plethora of ideas that I bounced off him.

Finally I would like to express my deep gratitude to Jim Grant for being an excellent advisor, a careful scientist, and a good friend. I met Jim at Carleton College in June of 1985 when he was there visiting his daughter. I had just finished my B.S. at Carleton, but I was not going to graduate school. I went to talk with Jim about the possibility of doing a Masters at Duluth. After we had chatted for a few minutes about life he asked me, "Do you really want to do geology?", and it was then that I decided I would be a geologist. I thank Jim for careful editing of this thesis, for being assessable and eager to help with problems, and for moulding me into a professional scientist. Thank you Jim, I owe you more than I can say.

TABLE OF CONTENTS:

CHAPTER FOUR:

CHAPTER FIVE:

CHAPTER ONE

INTRODUCTION

The principal objective of this thesis is to document the formation of mylonite as a function of progressive deformation. Mylonite is a compact, banded, chert-like rock that is well-foliated and always associated with zones of anomalously high strain (Lapworth, 1885). In general, mylonites are found on or near fault surfaces and in shear zones. The undeformed precursors of mylonites can be almost any rock type. To understand the genesis of mylonites it is desirable to analyze mylonites produced from a variety of protoliths. Mylonites that form from different protoliths, but form under the same metamorphic conditions, should show subtle variations in microstructure, reflecting a variable response to the same deformation. Mylonites and an array of unmylonitized probable equivalents are found in northern Utah, in a slice of Archean rocks called the Farmington Canyon Complex (Fig. 1).

The study area is situated 24 kilometers north of Salt Lake City, Utah, and just east of Interstate 15 in the Wasatch Mountains. Spanning from Farmington Canyon north to Francis Peak, the study area occupies ten sections of the Bountiful Peak and Peterson quadrangles and covers about eleven square kilometers. Francis Peak, elevation 2910 meters, stands 1600 meters above Great Salt Lake, with the study area occupying the uppermost 900 meters of the peak (Fig. 1). Francis Peak can be accessed from the town of

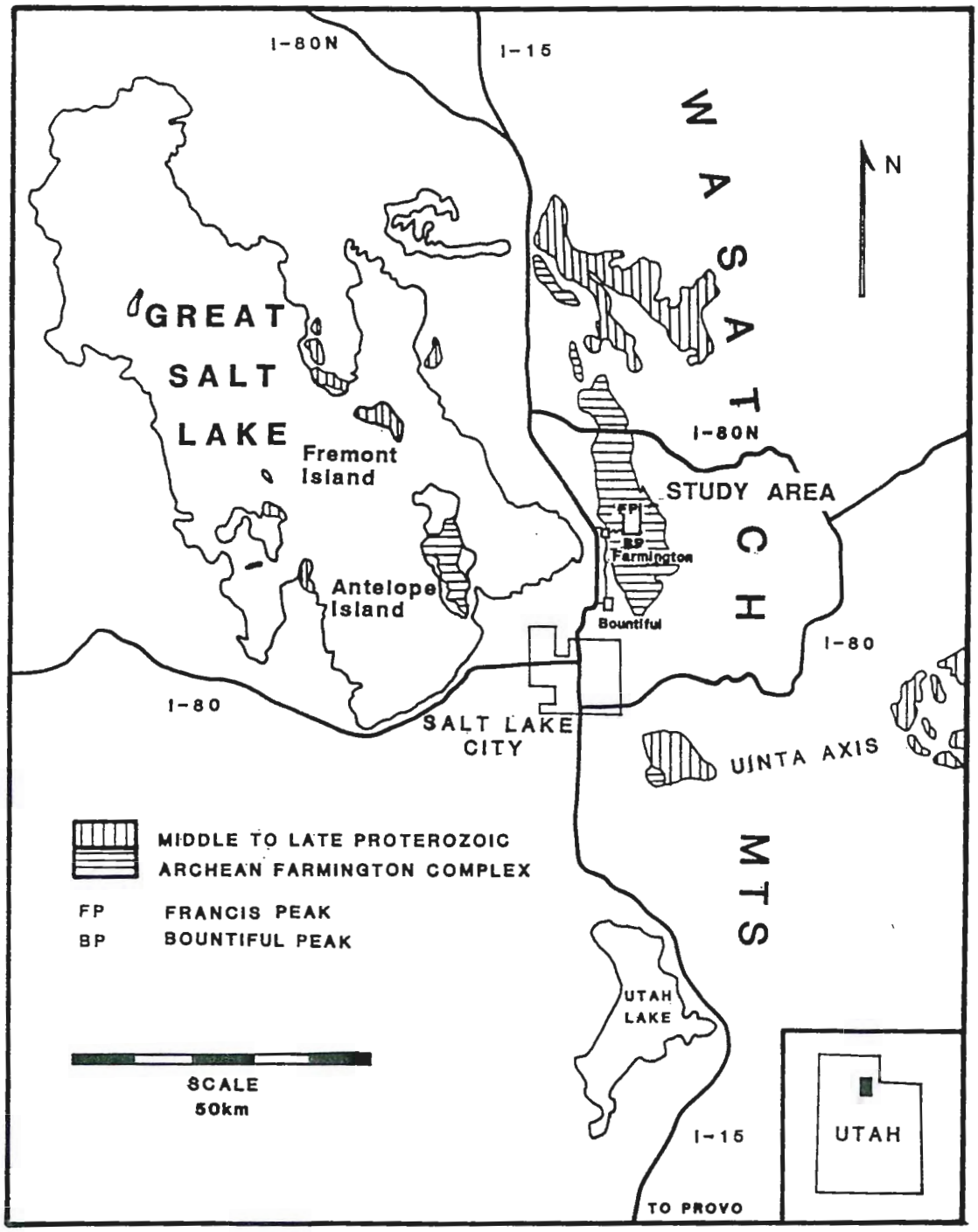

Fig. 1 Location map showing Archean Farmington Complex, middle to late Proterozoic sediments and the study area (after Hintze, 1975).

Farmington by driving up Farmington Canyon 15 kilometers to Bountiful campground, and by proceeding 6.5 kilometers further north along the ridge.

The rocks of the study area comprise the 2.6 billion year old schists and gneisses of the Farmington Canyon Complex. These rocks were isoclinally folded and metamorphosed at 2.6 Ga and were subsequently openly folded and metamorphosed to amphibolite grade at 1.8 Ga, locally overprinting the earlier fabric (Hedge, 1983). Mylonitization of Farmington Canyon Complex schists and gneisses, with local retrogression to greenschist facies, occured prior to Tertiary normal faulting (Bryant, 1978) during either a Proterozoic deformation or Cretaceous thrusting. Tertiary Basin-and-Range normal faulting has elevated the complex as a block bounded on the east and west by west-dipping normal faults. The northern Wasatch Mountains were glaciated during the Pleistocene (Hintze, 1973) leaving impressive east-facing cirques.

The author spent five weeks in the field area in the summer of 1986. Major faults and rock types were mapped on a 1:10,000 scale and nearly 800 structural measurements were taken. Sampling of the mylonites and their less deformed precursors at 57 locations has provided excellent coverage of the area laterally as well as 900 meters vertically. Many of the rocks on the peak have been heaved by frost action, yet undisturbed oriented samples were taken at almost every location.

The purpose of this thesis is to elucidate the genesis of mylonite in the context of the structural setting and accompanying

metamorphism, both of which controlled mylonite formation in the Farmington Canyon Complex. First, the structural position of the Farmington Canyon Complex within the Sevier thrust belt is presented. Second, the geology of the study area including the map, description of lithologies, metamorphism, structural geometry of thrust faults, and penetrative fabrics will be discussed. Third, analyses of textures and microstructures from oriented samples will be presented. Finally, an interpretation of the progressive deformation of the protoliths will be made, based largely on the microstructures and deformation mechanisms determined from thin-sections.

CHAPTER 2

REGIONAL GEOLOGY

In this chapter, the regional tectonic setting and tectonic history of Utah will be reviewed in order to understand the tectonic framework within which the mylonites of the Farmington Canyon Complex formed. The areal extent of the rocks of the region will be described in order to set a framework for a more detailed description of the structure. Next, the geochronology of Farmington Canyon Complex rocks is discussed, including a short review of Proterozoic and Paleozoic history and Tertiary Basin-and-Range faulting. Finally, a thorough description of the structural development of the Sevier orogenic belt is given.

The regional geology of northeastern Utah and southwestern Wyoming is covered by the following maps: the U.G.M.S. Geologic Map of Utah, scale 1:500,000 (Hintze, 1980), and the Geological Survey of Wyoming's Wyoming Geologic Highway Map, scale 1:1,000,000 (Love and Christiansen, 1986). The U.S.G.S. (Bryant, 1984, map I-1447) has also published a reconnaissance map of the Farmington Canyon Complex on a 1:50,000 scale.

The most striking feature of the topography of northeastern Utah is the north-south line of the Wasatch Mountains (Fig. 1). This range separates the Basin-and-Range province from a region of

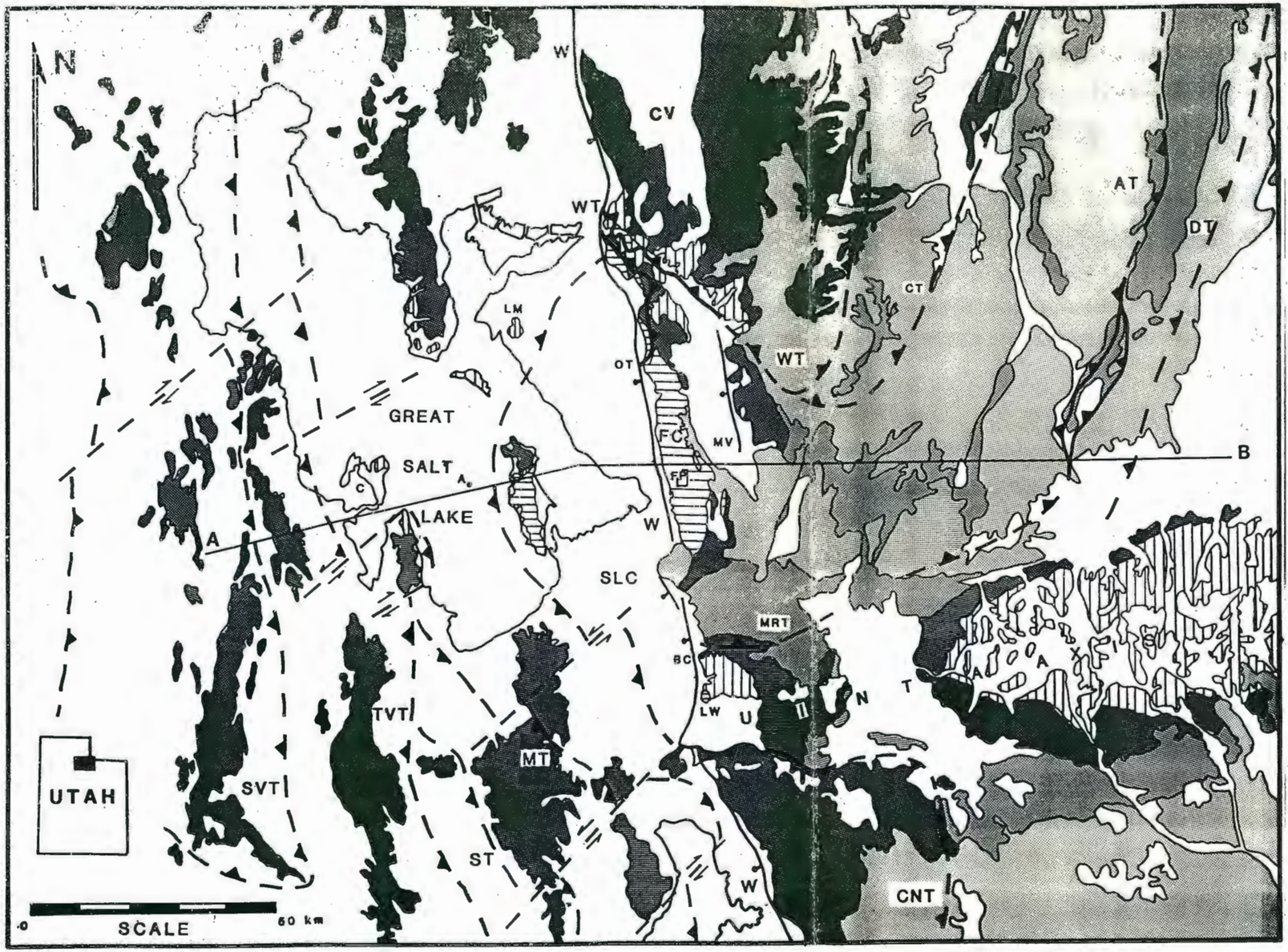

LEGEND

- Post-Eocene (unaffected by thrusting)
- Paleocene-Eocene (Deposited synthrusting)
- Mesozoic
- Paleozoic
- middle and upper Proterozoic
- Archean Farmington Complex

MAJOR THRUSTS

DT Darby
AT Absaroka
WT Willard
CNT Charleston-Nebo
MT Midas
ST Stockton
TVT Tintic Valley
SVT Skull Valley

MINOR THRUSTS

OT Ogden
MRT Mount Raymond
CT Crawford

NORMAL FAULTS

W Wasatch
MV Morgan Valley

LOCATIONS

FP Francis Peak
FC Farmington Complex
SLC Salt Lake City
BC Big Cottonwood Formation
LW Little Willow Formation
A Antelope Island
C Carrington Island
F Fremont Island
LM Little Mountain
CV Cache Valley

Fig. 2 Geologic map of north-central Utah and southwest Wyoming (after, Crittenden, 1972; Royse et al., 1975; Blackstone, 1977; Hintze, 1980; Tooker, 1983; Zoback, 1983; and Love and Christiansen, 1986). Cross-section line A-B corresponds to figure 4.

higher elevation to the east. Figure 2 shows the regional geology about the present study area.

The Farmington Canyon Complex is the principal exposure of Archean basement in the Cordilleran fold and thrust belt (Blackstone, 1977). Common rock types are gneiss, schist, migmatite, granite, pegmatite, phyllonite and mylonite. On figure 2 exposures of Archean basement are found in three areas: the present study area, Antelope Island, and southeast of Salt Lake City in Little Cottonwood Canyon. More than half of Antelope Island is Farmington Canyon Complex gneiss with 90 meters of upper Proterozoic sediments overlying the gneiss (Crittenden, 1972). A thick pile of Cambrian Tintic Quartzite is unconformable on the Proterozoic sediments. Eight kilometers to the west of Antelope Island, Amoco Production Company cored blastomylonitic, garnet-biotite-muscovite gneiss at a depth of 3167 meters (Hedge et al., 1983). This gneiss is probably correlative with the Farmington Canyon Complex gneisses on Antelope Island. To the north, Proterozoic sediments are exposed on Fremont Island, but no underlying Archean gneiss is present. To the south, along the Wasatch fault, the Archean Little Willow Formation crops out in Little Cottonwood Canyon. This formation consists primarily of quartzofeldspathic gneiss and lesser amounts of amphibolite and pelitic schist (Kohlman, 1980). These rocks are unconformably overlain to the north and east by middle to upper Proterozoic quartzites and argillites of the Big Cottonwood Formation. The Little Willow Formation is further bounded by a Tertiary quartz monzonite stock to the south and by the Wasatch fault to the west.

Proterozoic tillites and continental margin sediments were deposited unconformably on Archean gneisses and schists, but are not found in depositional contact with Farmington Canyon Complex rocks (Fig. 2). Proterozoic rocks, locally in thrust contact with Archean rocks, have been brought to the surface as large thrust sheets. In general, Proterozoic and younger rocks have been stripped off Archean basement as a result of prolonged deformation during the Cretaceous (Armstrong, 1968). The most important exposures of Proterozoic rocks lie to the northeast of the Farmington Canyon Complex in the Willard thrust sheet and to the southeast along the Uinta axis. Laramide arching along the Uinta axis has exposed Proterozoic rocks on an east-west line (Hintze, 1973).

Paleozoic and Mesozoic rocks were deposited unconformably on either Proterozoic sediments or Archean basement in the Great Basin of Utah and Nevada (Fig. 2). Their present distribution is largely due to thrusting and later Tertiary and Quaternary normal faulting (Crittenden, 1972). Cambrian Tintic Quartzite is in depositional contact with the Farmington Canyon Complex, effectively rimming the complex to the east. Paleozoic sediments also rim the arched Uinta axis. To the north, at the southern edge of the Idaho-Wyoming thrust belt, ramp anticlines and thrusts are marked by the appearance of Mesozoic rocks with dominantly west dips. West of the Wasatch Mountains, Paleozoic and Tertiary rocks cap north-south striking range blocks.

Geochronology of the Farmington Canyon Complex and related rocks

The relative chronology of geologic events that affected the Farmington Canyon Complex has been deduced from field evidence. The earliest deformation involved isoclinal folding. Interlayered gneiss, amphibolite and pegmatite were isoclinally folded, with concomitant formation of an axial planar schistosity defined by biotite. These folds were openly refolded during a second event that involved metamorphism of the rocks to amphibolite grade. The intrusive rocks were cool by the time a third, low-grade deformational event was initiated, as evidenced by brittle deformation of the feldspars. This event involved thrusting, mylonitization and greenschist facies metamorphism. Normal faults cut across all preexisting structures and have brecciated rocks in the study area.

Hedge et al. (1983) found that Rb-Sr whole-rock data from the Farmington Canyon Complex yield a scatter of ages from 2600-3600 Ma, suggesting that the complex is made of material older than 2600 Ma. They support this suggestion with meager Sm-Nd whole-rock data that give scattered ages from 2740-3430 Ma. Hedge et al. (1983) believe that these Archean dates may arise due to partial metamorphic reequilibration of sediments from a terrane older than 2600 Ma.

High-grade metamorphism may have affected the Farmington Complex at 2600 Ma (Hedge et al., 1983). Bryant and Graff (1980) infer an Archean granulite facies metamorphism on the existence of

a few relict hypersthenes. These rocks can apparently be found above the Ogden thrust, 16 km to the north of the present study area. Their evidence is rather unconvincing. Rismeyer (1981) concluded that isoclinal folding of the complex occurred prior to intrusion of the granitic rocks. He found minerals characteristic of amphibolite facies assemblages, such as sillimanite, to have grown in an axial planar orientation. Since Rb-Sr and Sm-Nd whole-rock clocks in the gneiss were not reset by intrusion of the granites (Hedge et al., 1983), it seems reasonable that the complex was affected by amphibolite facies metamorphism at around 2600 Ma.

Unlayered granitic gneisses from Antelope Island and core from an Amoco drill hole 8 kilometers west of the island have been dated by Hedge et al. (1983). These rocks yield ages of 1993 +/- 22 Ma and 2023 +/- 4 Ma, respectively, by the U/Pb method on zircons. Presumably, the age data records crystallization of the granitic precursors of the gneisses (Bryant and Graff, 1980).

Hedge et al. (1983) have dated granitic bodies and associated layered gneisses from the Farmington Canyon Complex. The granites and gneisses exhibit an Rb-Sr whole-rock isochron age of 1808 +/- 34 Ma. A very high initial $^{87}Sr/^{86}Sr$ ratio of .769 suggests that the granites were derived largely from crustal sources and may be partial melts of leucocratic layers in the gneiss. Zircons from both the granites and adjacent layered gneisses were analyzed using the U/Pb method. A concordia plot of both sets of data yields an upper intercept age of 1780 +/- 20 Ma and a lower intercept age of 70 Ma. Some scatter in the data is attributed to lead loss, which may have

occured during Cretaceous shearing and retrogression. Hedge et al. (1983) conclude that the Farmington Canyon Complex was strongly metamorphosed at 1790 Ma. Open folding and amphibolite facies regional metamorphism appears to have been concomitant with intrusion of granitic rocks (Rismeyer, 1981). Isotopic age dates younger than 1790 Ma have not been obtained from Farmington Canyon Complex rocks.

To summarize, the Farmington Complex was metamorphosed at approximately 2600 Ma. The complex was isoclinally folded prior to intrusion of the granitic rocks. At about 2020 Ma, intrusion of granitic rocks occurred in the gneisses buried below Great Salt Lake. The complex was intruded by granitic rocks, openly folded, and metamorphosed to amphibolite grade at about 1790 Ma.

Proterozoic and Paleozoic history

The following review of the tectonosedimentary history of northern Utah and eastern Nevada is critical to the understanding of regional thrust sheet geometry around the study area.

During the middle and upper Proterozoic, Farmington Canyon Complex basement, and other basement rocks of possible Archean age in northern Utah, received thick blankets of sediment. In general, these late Precambrian sediments form a westward thickening wedge (Crittenden, 1972). Isopach maps of late Precambrian strata show that the northern Wasatch Mountains

received a relatively thin blanket of sediment (less than 300 meters), whereas the Uinta axis and Cache Valley regions accumulated more than 3000 meters of sediment (Eardley, 1969). These thick sequences are thought to be related to aulacogens (King, 1977). The present study area contains no Proterozoic sediments, but Antelope Island has 90 meters of upper Proterozoic Mineral Fork tillite (Eardley, 1969; Armstrong, 1968; Bryant and Graff, 1980) between the older metaigneous rocks and the overlying Cambrian quartzite (Crittenden, 1972). Middle and upper Proterozoic sediments are also exposed at the base of horsts in northwestern Utah (King, 1977). Previous workers have defined large thrust sheets which contain middle to upper Proterozoic rocks. These sheets are circumjacent to the present study area, the only occurrence of Archean rocks west of the foreland fold and thrust belt (King, 1977).

The Great Basin of western Utah and eastern Nevada was the depocenter of an enormous, westward thickening wedge of sediment deposited during the Paleozoic and early Mesozoic (Tooker, 1983). The following is based on excellent descriptions of the history of the Great Basin by Armstrong (1968) and Roberts et al. (1965). Basin sedimentation was affected by mild uplift on the Uinta axis from Colorado to central Nevada in the early Ordovician (Fig. 3). The Devonian-Mississippian Antler orogeny, which affected central and eastern Nevada, involved thrusting of basin sediments eastward during another phase of uplift on the Uinta axis. Note that thrust traces in the Antler belt are displaced by uplift on the Uinta axis. Basin sedimentation continued with contributions from land masses

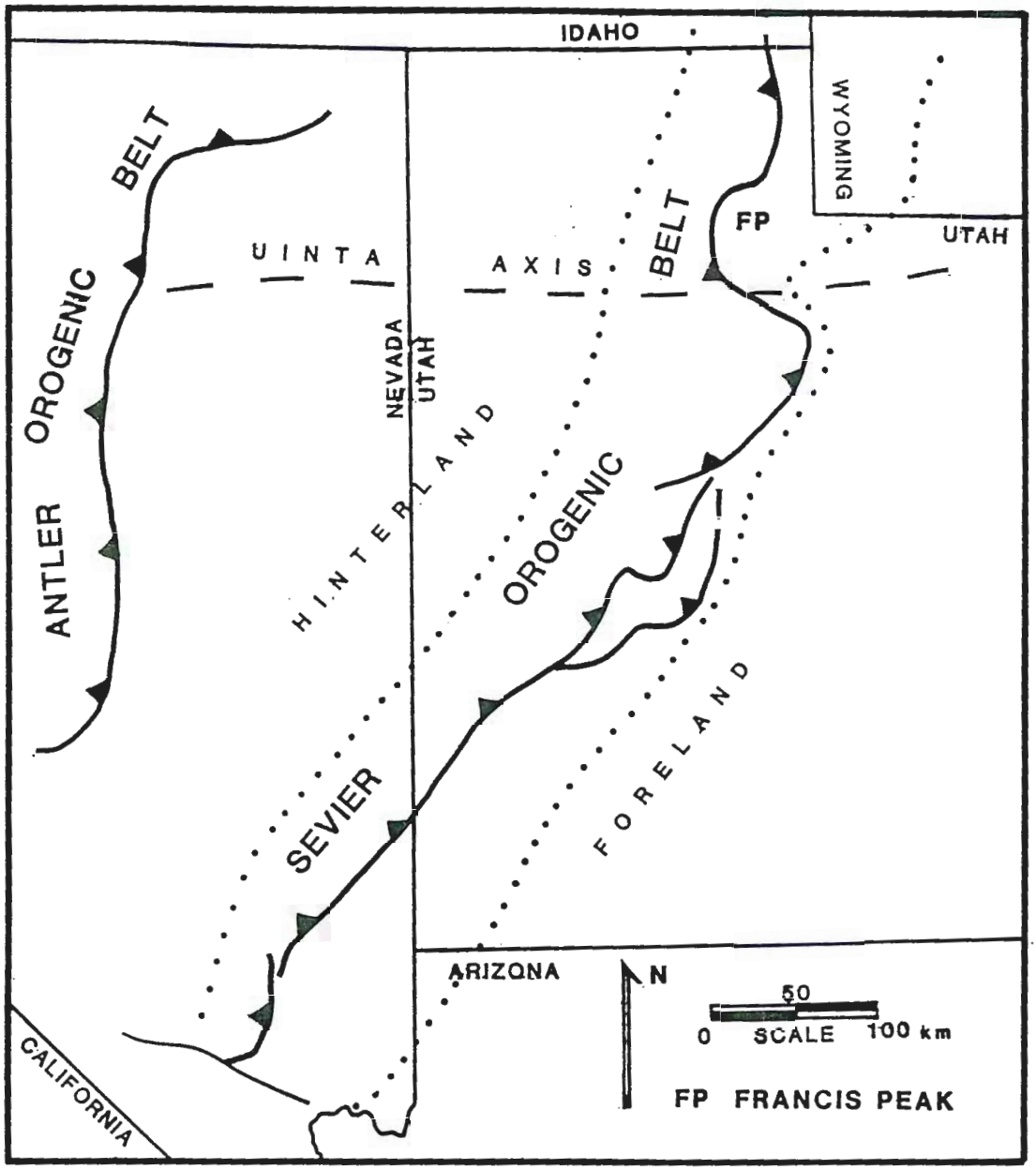

Fig. 3 Tectonic map of eastern Nevada and western Utah.

to the east and west during Pennsylvanian-Permian time. Subsidence of the basin was resisted along the Uinta axis, dividing the late Paleozoic basin in half. Isopachs suggest that uplift in western Utah, related to the initiation of Sevier orogenic activity, started in the Permian (Armstrong, 1968).

Effects of Tertiary and younger faulting

In northern Utah, Mesozoic structures were reactivated during the Tertiary. Flat-lying Mesozoic decollements and thrust faults had displaced Precambrian, Paleozoic and Mesozoic strata tens of kilometers eastward (Armstrong, 1972). Later, Tertiary Basin-and-Range normal faults dissected the Sevier belt thrust sheets as well as utilized the weakness produced by Mesozoic faults (Armstrong, 1972). The normal faults are generally N-S striking and probably listric, with vertical displacements of a few kilometers (Zoback, 1983). Distinction between Mesozoic and Tertiary structures is thus difficult and recognition of continuous large-scale Mesozoic faults is almost impossible, especially in the region around the Farmington Canyon Complex. For a complete description of Tertiary and younger faulting consult the appendix.

The Wasatch fault, the major west-dipping normal fault that bounds the Wasatch Mountains on the west, is generally considered the eastern limit of Basin-and-Range normal faulting. However, Tertiary normal faults are recognized east of the Wasatch fault. The

Morgan Valley fault, which lies ten kilometers to the east of the study area, is a minor N-S striking, 50-60 degree west-dipping, possibly listric normal fault. This fault is expressed topographically by the arcuate trend of the eastern edge of Morgan Valley (Hopkins et al., 1983). Movement on the fault may have rotated Farmington Canyon Complex gneiss, early Tertiary Wasatch Formation and Norwood Tuff in the hanging wall, as evidenced by the Tertiary units that now dip 20-40 degrees east. The present study area, bounded by these two major normal faults, may have been rotated up to 40 degrees to the east on a N-S horizontal axis in response to movement on one or both faults. However, according to the cross-sections of Royse (1975) the stratified rocks of Morgan Valley were deposited synthrusting (Mullens, 1971) on the east-dipping limb of a ramp anticline. The rotation may have been accomplished by both syndepositional thrust rotation and Tertiary normal faulting. Evidence for significant Tertiary faulting further to the east on the more stable Colorado Plateau is non-existent (Zoback, 1983).

Zoback (1983) has used gravity and seismic data to analyze the offsets on normal faults in north-central Utah. According to Zoback, the Wasatch fault (Fig. 2) has a minimum displacement of 3-5 kilometers near Farmington and flattens to a 30 degree dip at a depth of 10-12 kilometers. Minimum vertical displacement on the Wasatch fault near Salt Lake City is 3-4 kilometers, from base of the sediments on the basin block to top of the Wasatch Range. Recent work by Parry and Bruhn (1987) on CO_2-H_2O-NaCl fluid inclusions from an altered and deformed quartz monzonite in the footwall of

the Wasatch fault in the Little Cottonwood area reveals that since equilabration the rocks were brought to the surface from as much as 11 kilometers depth. This implies that the Farmington Canyon Complex may have had up to 11 kilometers of basement and cover rocks overlying the complex before offset on the Wasatch fault occured. If this is true, then Zoback's (1983) estimates are truly minimums, and the actual displacement on the Wasatch Fault is locally large enough to have exposed midcrustal rocks.

Structural Development of the Sevier Thrust Belt

Quiet sedimentation in the Great Basin was interupted in the mid-Triassic with uplift in central Utah and the beginning of Sevier orogenic activity (Armstrong, 1968). Uplift continued along the Uinta axis, bisecting the Great Basin and creating high ground by the late Jurassic. Sediments were shed into the Rocky Mountain foreland basin during Cretaceous time. Synorogenic conglomerates were shed eastward from the uplifted Sevier belt while the thrust sheets advanced eastward from the western topographic high (Mullens, 1971). Considering the age of sediments shed from the advancing mountains, movement on thrusts started in the hinterland in the late Jurassic and migrated eastward until the Eocene (Armstrong, 1968; Armstrong and Oriel, 1965).

Tooker (1983) claims that the Uinta axis and adjacent northern Utah highlands acted as a buttress to advancing Sevier thrust sheets.

The result of this buttressing was the sharp reentrant in thrust traces between Salt Lake City and Ogden. The reentrant separates the Idaho-Wyoming thrust belt from the southern extent of the Sevier belt. Further to the east, in the foreland of the thrust belt, thrust traces have been deflected by the Uinta axis (Fig. 2). As the sheets advanced they encountered relatively shallow basement along the axis, forcing thrusts to come to the surface earlier than thrusts unaffected by the axis (Blackstone, 1977).

By the mid-Cretaceous, Eocambrian (700-570 Ma) quartzite clasts were being deposited in abundance along the thrust front, which implies that thrusts had brought Eocambrian rocks to the surface. In southeastern Nevada thrusts placed Eocambrian and Cambrian rocks over Mesozoic and Paleozoic strata (Fig. 3). Along strike in southwestern Utah, thrusts moved Eocambrian and Cambrian rocks over Jurassic rocks.

Further to the north in the Wasatch Mountains, the Charleston-Nebo thrust system shows the same older-on-younger superposition of Eocambrian and Cambrian quartzites on mid-Jurassic rocks; thick (21,000 m.) basin deposits are thrust over thin (3,000 m.) shelf sediments (Royse et al., 1975). The lateral continuity of these thick basin sediments has been demonstrated (Fig. 2), from where the hangingwall rocks of the Charleston-Nebo thrust are exposed, to the hanging wall of the Willard thrust system 20 miles to the northeast of the present study area (Roberts et al., 1965; Crittenden, 1972; Royse et al., 1975). Thus, it is reasonable that there was a relatively

continuous thrust sheet of Eocambrian and Phanerozoic cover overlying the Farmington Canyon Complex.

According to Tooker (1983), the Charleston-Nebo thrust (CNT) and the Willard thrust (WT), of Crittenden (1972) are structurally linked. If true, this constitutes a connection between the Idaho-Wyoming thrust belt and the Sevier belt. The WT-CNT sheet, which spans the Farmington Canyon Complex from south to north, forms the hanging wall above the complex, and contains no Archean rocks. In the vicinity of the northern Utah reentrant, Proterozoic sediments are almost the exclusive base of this sheet. Rocks of the immediate hanging wall of the WT-CNT sheet are found on Little Mountain, Fremont, Carrington and Stansbury islands. To the north of the study area, Proterozoic hanging wall rocks can be found in a foreland dipping duplex above the WT. To the south, the CNT, which is for the most part obscured by post-Eocene alluvium and volcanic rocks, carries Proterozoic Big Cottonwood Formation in the hanging wall and has cut up section, juxtaposing Cambrian and mid-Jurassic sediments (Armstong, 1968).

East of the Farmington Canyon Complex, in the foreland thrusts of the system (Fig. 2), undetached basement sits 4,500-11,800 meters below the surface (Royse et al., 1975). The Crawford, Absaroka and Darby thrust sheets all have westward dips at the surface. The Crawford, a minor thrust, is recognizable in southwestern Wyoming, but disappears below younger Tertiary sediments, alluvium and volcanic rocks directly to the east of the present study area. Do any of these foreland thrusts connect with

the CNT and the southern extent of the Sevier thrust system, or are they all truncated at the Uinta axis? As mentioned previously, a connection between the WT and CNT is quite likely. Perhaps the Mount Raymond thrust (MRT) also joins the CNT. Blackstone (1977) would prefer to connect the CNT with the MRT instead of the WT because the WT would have to step up section to join the CNT. As supporting evidence Blackstone (1977) submits that the MRT and CNT sole in the same age rock. The Absaroka Thrust is likely continuous with the MRT and may, as first proposed by Royse et al. (1975), form a floor thrust or decollement below Farmington Canyon Complex rocks. The present author prefers that the Absaroka thrust and the Willard thrust form the floor and roof thrust, respectively, of Farmington Canyon Complex rocks (Fig. 4) and that both thrusts merge with the Charleston-Nebo thrust to the south (south of plane of section, Fig. 4).

Royse et al. (1975) believe the spacing between major thrusts in northern Utah to be a function of the spacing of ramps along the regional sole thrust, deeper rocks coming to the surface after ascending the ramp. Royse et al. (1975) make the observation that it was easier to carry a doubled section over a ramp than to triple the section, thus the outcrop pattern. Note the spacing of major thrusts on figure 2, and that, in general, none of the thrust traces intersect each other. Locally, lateral ramps and basement thrusting have disrupted the regular thrust pattern around the Farmington Complex.

Many range blocks in northwestern Utah have flat-lying faults at their bases that could be considered the hinterland extension of a

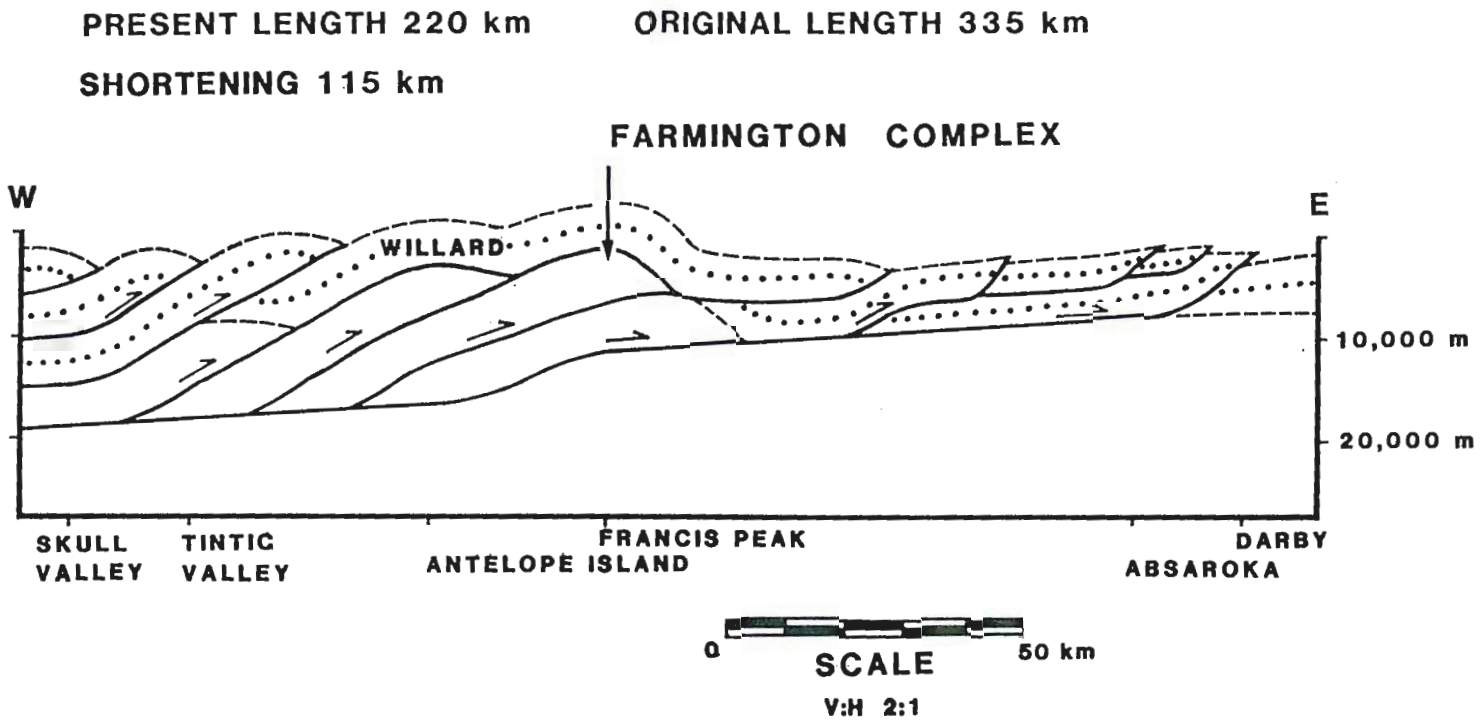

Fig. 4 Schematic balanced cross-section through the Francis Peak study area. Basement rocks unornamented, Phanerozoic cover dotted and contacts dashed. (after Royse, 1975 and Tooker, 1983)

Sevier-age regional detachment (Misch, 1960, in Armstrong, 1968). Roberts et al. (1965) have suggested that the decollement at the base of the Raft River ranges (see Hintze, 1980) is the sole of the Willard thrust. However, not many of the sub-horizontal faults at the base of these ranges can be termed thrust faults. Armstrong (1972) has demonstrated that these decollements may be low-angle denudation (normal) faults: some are not thrusts at all and some have utilized previous thrust planes for renewed movement during Tertiary extension.

When in the Mesozoic did thrusting of Farmington Canyon Complex rocks take place? The Complex sits between the Willard and Absaroka thrusts (Fig. 4). Mullens (1971) has analyzed the synorogenic conglomerates that were shed from uplifted thrust sheets and deposited in low areas between the Wasatch Range and the trace of the Absaroka thrust. These conglomerates were deposited as a result of erosion of WT hanging-wall rocks, Farmington Complex gneisses and schists and Cambrian Tintic quartzite. Mullens found the conglomerates to be separable into the late Cretaceous Echo Canyon Formation, late Cretaceous to Paleocene Evanston Formation and Paleocene to Eocene Wasatch Formation. The Echo Canyon is up to 950 meters thick and contains some material from the late Proterozoic to early Paleozoic rocks of the Willard allochthon. The abundance of Cambrian Tintic quartzite clasts in the Echo Canyon Formation indicate that Farmington Complex rocks were near the surface. The appearance of sediments from the Willard sheet indicates that the rocks were exposed to

erosion in the Cretaceous. The Evanston Formation, which is up to 425 meters thick, contains two divisions, an upper coarse sandstone unit and a thick basal conglomerate derived from exposure of the Willard allochthon. Abundant angular quartz grains in the upper grit and micaceous sandstones of the formation were probably derived from the Farmington Canyon Complex. Mullens and Crittenden (1969) have established that uppermost Cretaceous Evanston sits horizontally on WT sheet rocks, which means that movement on the fault ended before the Paleocene. They also state that earliest movement on this fault post-dates deposition of early Cretaceous sediments in the region, which effectively brackets WT sheet movement to the Cretaceous. Mullens (1971) has observed the Wasatch Formation to lie unconformably on top of Echo Canyon, Evanston and Farmington rocks. He has found the Wasatch Formation to be thickest, 1525 meters, in the Morgan Valley, where conglomerates derived from both the WT allochthon and the Farmington Canyon Complex lie unconformably on Farmington rocks. The gneiss and schist clasts from the complex are angular, less durable and tend to be found near the Wasatch-Farmington Canyon Complex contact. A reasonable inference from this geometry would be that thrusting in the Farmington Canyon Complex continued into the Paleocene and possibly the Eocene and tilted Wasatch rocks.

There are several minor thrusts that dictate the internal geometry of the Farmington Canyon Complex. In the northern portion of the Complex, the Ogden thrust carries Farmington gneiss over itself, forming a foreland dipping duplex (Crittenden, 1972).

Some authors choose to project the Ogden thrust southward so that the whole of Farmington rocks in the Wasatch Mountains have overridden the equivalent Archean rocks of Antelope Island (Bryant, 1984; Hollet, 1979; Bruhn and Beck, 1981; Bruhn and Smith, 1984). This extreme interpretation suggests that a Farmington allochthon was displaced tens of kilometers during movement on the Willard thrust. However, these thrusts are probably minor splays with little displacement (Crittenden, 1972) and may represent footwall failure during WT movement (Dunlap and Ellis, 1986, Ellis and Dunlap, 1987, 1988). Most authors believe the Farmington Canyon Complex to be allochthonous above the Absaroka thrust (Crittenden, 1972; Armstrong, 1968; King, 1977; Royse et al., 1975; Tooker, 1983). The present author prefers the geometry shown in Figure 4. Also, the possibility of a hinterland-dipping thrust between Antelope Island and the Farmington Canyon Complex cannot be ignored.

The attitude and morphology of Farmington Canyon Complex rocks is that of a basement-cored anticline lying on a basal thrust that dips west and extends into both the foreland and hinterland. Royse et al. (1975) have shown that Paleozoic rocks are folded over an anticline of Farmington Canyon Complex rocks. The present author would infer that this anticline is a ramp anticline, the result of Farmington Canyon Complex basement traveling over a footwall ramp (Fig. 4). The eastern extent of the Farmington Thrust sheet at depth, about 9000 meters, is only about 15 km. east of outcrops in the present study area (Royse et al., 1975, Plate I).

To summarize, the study area on Francis Peak is located in the eroded core of a ramp anticline of Farmington Canyon Complex gneisses and schists, above the Absaroka thrust (Fig. 4). These rocks are part of an extensive sheet that is laterally continuous, as shown on Bryant's map (1984). Farmington Canyon Complex rocks lie in the reentrant and in the footwall of the eroded Willard thrust sheet, a regional thrust in the 700 km. long Sevier thrust belt.

CHAPTER THREE

GEOLOGY OF THE FRANCIS PEAK AREA

In the vicinity of Francis Peak, the Farmington Canyon Complex consists of partly retrograded, amphibolite facies schists and gneisses, and their mylonitized equivalents. The most common rock is layered gneiss (Fig. 5), contrary to the map divisions of Bryant (1984) who shows Francis Peak to be largely migmatite and gneiss. The protoliths of the phyllonites and mylonites are quite variable and will be discussed in detail. Later portions of this chapter address retrogression of the rocks during deformation, the structural geometry, and the mesoscopic penetrative fabric of the rocks. In this thesis, "**deformation**" refers only to the mylonitization of the schists and gneisses, unless otherwise specified, and not to the deformation and metamorphism that produced them.

The rocks of Francis Peak can be catagorized under three headings:

1) Layered Quartzofeldspathic Gneisses
    A) Biotite gneiss
    B) Garnet biotite gneiss
    C) Chlorite epidote gneiss
2) Amphibolite Gneiss
3) Granitic rocks
    A) Granite
    B) Quartz syenite
    C) Pegmatite

Deformed equivalents of the above rock types are phyllonite, mylonite and ultra-mylonite. These deformed rocks will be described under each of the above headings.

Layered Quartzofeldspathic Gneiss

Biotite Gneiss

Layered biotite gneiss and its deformed equivalents constitute about 30% of the outcrop mapped along the ridge and a much higher percentage in the relatively undeformed portions of the complex, such as the lower half of Farmington Canyon.

Layered biotite gneiss is gray to black, fine to medium grained, folded and lineated, and weathers to a light brown (Fig. 6). Sample F-57 is the type layered gneiss for purposes of this study (Fig. 7). Dominant mineralogy is quartz, plagioclase, alkali feldspars and biotite (Table 1). The quartz and feldspars form an interlocking, equigranular aggregate of grains 1-3 mm. across. Biotite occurs as flakes which form folia that envelop or transect quartz and feldspar lenses.

Mineral lineations are observable on most foliation surfaces. The mineral lineation is partially formed by the elongation of ellipsoidal quartz and feldspar grains in the plane of foliation. The lineation is further defined by elongate flakes of biotite.

Fig. 5 Radar towers on Francis Peak, looking west. Vertical dimension is 200 meters. Dark rock is layered gneiss, light rock is pegmatite. Note north dipping fault surface on upper right (arrow).

Fig. 6 Layered biotite gneiss, the most abundant protolith in the field area. Fold axes are perpendicular to photo. Note two scales of layering. Rocks located just below Francis Peak to the east.

MODES OF LAYERED QUARTZOFELDSPATHIC GNEISSES

	Biotite gneiss (3)	Garnet biotite gneiss (3)	Chorite epidote gneiss (4)
Qtz	29.5	30	12
Plag	14.5	25	38
K-spar	24.5	27	5
Biot	31.5	5	8
Musc	-	-	-
Chlorite	-	-	22
Epidote	-	-	15
Garnet	-	3	-

MODES OF MYONITIC LAYERED GNEISSES (BG)

	Mylonitic BG (5)	BG Phyllonite (4)	BG Mylonite (6)
Qtz	31	40	49
Plag	16	7	7.5
K-spar	27	18.2	14.3
Biot	-	2.5	0.8
Musc	2	-	0.5
Chl	25	32.3	27

Table 1. Modes of layered quartzofeldapathic gneiss and deformed equivalents. Calculated from a limited number of thin-sections (# in parentheses). Modes are average composition and are only given as rough estimates; due to sampling bias and cut of thin-sections. Note variability of sample composition in following figures.

Fold axes are generally subparallel to the mineral lineation, but may deviate significantly from parallelism if the rocks are deformed. Fold axes of the tightest folds approximate the mineral lineation and lie in the plane of foliation. Axes of more open folds are generally at higher angles to lineation. Folds in the layered gneiss vary from open to isoclinal and have wavelengths from 1 cm. to at least several meters. The folds are disharmonic and may have sheared-out limbs. Biotite in the hinges of folds is axial planar, suggesting that the biotite has been recrystallized and/or rotated during the deformation associated with formation of the gneiss.

Compositional layering appears as alternating light and dark gray bands. Biotite content, relative to quartz and feldspar, dictates the darkness of the layers. Individual layers are millimeters to centimeters wide and may pinch-out laterally. Larger-scale variations are defined by sets of layers of a similar shade of gray, up to one meter wide.

Quartz, feldspar and biotite grains have long dimensions that define a schistosity parallel to layering (Fig. 8). Quartz is mildly deformed, interstitial with respect to feldspars, and shows deformation bands, subgrains, recrystallized grains, and rarely thin recrystallized margins. Plagioclase is partially sericitized along fractures, cleavage and twin planes, and may be myrmekitic. Microcline is unaltered, may be perthitic and may exhibit wide deformation bands. Orthoclase is unaltered like microcline, largely untwinned, and may also be perthitic. Biotite forms thin, elongated,

Fig. 7 Typical folded layered gneiss, sample F-57. Light layers are quartz and feldspar rich, dark layers are biotite rich. Sample surface is nearly orthogonal to fold axes.

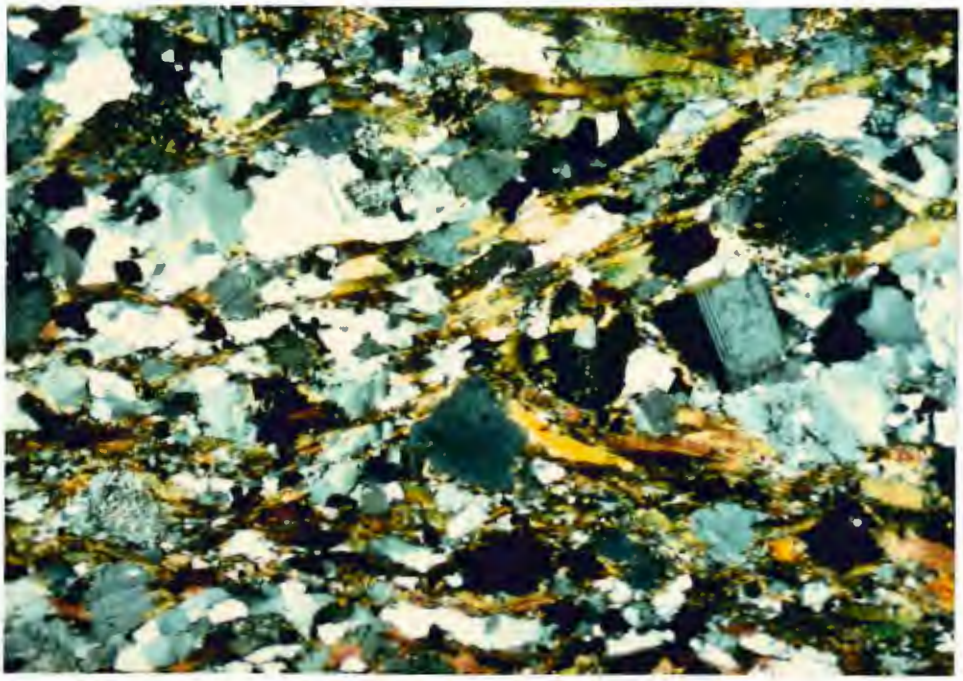

Fig. 8 Photomicrograph of Sample F-57, relatively unmylonitized layered gneiss. Note layers are rich or poor in biotite. Field of view is 5 mm. across, polars crossed.

subhedral books that define the cleavage. Accesory tourmaline, apatite, magnetite, sphene and zircon were observed.

Mylonitization of the layered gneiss produced a spectrum of deformed rocks that vary widely in texture and composition, but not mineralogy. The composition of mylonitized rocks is largely dependent on the amount of micas and epidote that grew during and after deformation. The deformed rocks are mylonitic gneiss, phyllonite, mylonite and ultra-mylonite in loose order of decreasing mica content and increasing deformation (Figs. 9, 10, 11). Of these tectonites, mylonitic gneiss and phyllonite are the most common (Fig. 12), mylonite and ultra-mylonite less common.

As deformation and alteration increase, feldspars, mostly plagioclase, break down to phyllosilicates, plus or minus epidote, and form a phyllonitic foliation. This foliation of sericite/muscovite, chlorite and epidote anastamoses around lenses of quartz, plagioclase and K-feldspar with micas forming tails on plagioclase. The lenses have long axes that lie in the foliation. Increased deformation results in a phyllonite with minor ribbons of quartz and porphyroclasts of K-feldspar.

Alteration products in the deformed rocks include chlorite, muscovite/sericite, and epidote, formed at the expense of biotite, plagioclase and K-feldspar (Fig. 13). Biotite is absent in the deformed layered gneiss except in a few samples where retrogression to chlorite is incomplete. Chlorite has replaced cleavage flakes of biotite crystals. Magnetite is almost always present with chlorite, and may also be an alteration mineral. Plagioclase in the deformed layered

Fig. 9 Mylonitic layered gneisses. Layering in top sample has been disaggregated. Bottom sample is less deformed and has foliation which is oblique to original gneissic layering (note arrow). Samples F-1.

Fig. 10 Layered gneiss phyllonite, samples F-2. Note abundance of dark micas, lineated foliation surfaces (parallel to pencil) and remnant quartz and feldspar porphyroclasts.

Fig. 11 Layered gneiss mylonite samples from location F-53. Note duplex-like, shear band structure in top sample, ribbons of quartz in bottom-center sample, and ribbons of recrystallized feldspar (light) in right sample.

Fig. 12
Typical outcrop of layered gneiss that exhibits range from mylonitic gneiss (top) to folded protolith (below). Note fold under field book. Location F-18, facing north.

gneiss is highly fractured and altered to muscovite/sericite plus or minus epidote. Some plagioclase grains are so highly altered that they appear as a mass of fine sericite. Less altered grains look cloudy. K-feldspar is rarely altered and occurs as porphyroclasts. Epidote occurs as porphyroblasts up to 3 mm. in diameter or porphyroclasts in broken granular trails strung-out along foliation.

Phyllonite contains more mica than the mylonitic gneiss (Fig. 14) and appears greener and browner. Texturally the phyllonites resemble their deformed gneissic counterparts, though the foliation is more intense. Feldspars occur as porphyroclasts in a foliated matrix of fine quartz and micas. The folia are alternately richer or poorer in chlorite and sericite, and show an excellent lineation on a fresh surface. Thin (1 mm. to 1 cm.), quartz-rich ribbons lie in the foliation. Pods of deformed gneiss may be enveloped by phyllonite (Fig. 15).

Layered gneiss mylonite consist of thin (1 mm. to 1 cm.) layers of recrystallized quartz and feldspar with minor films of micas (Fig. 16). Quartz-rich layers may contain a foliation that is oblique to the layering, subtending angles of less than 45 degrees. Layers of recrystallized feldspar are commonly altered to micas. Quartz and feldspar layers are separated by thin films of micas usually less than 1 mm. across. Individual layers are up to a meter or more in length parallel to the mineral lineation. Laterally, these layers are truncated by shear bands every few centimeters. A striking lineation is defined by either blades of recrystallized mica or strained and recrystallized quartz grains. Shear bands and

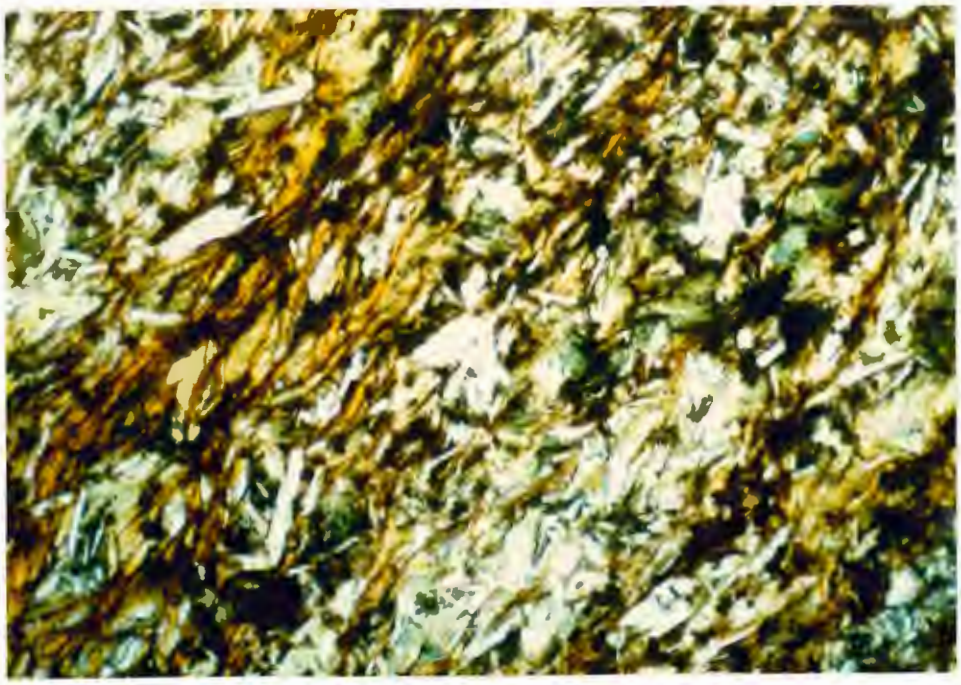

Fig. 13 Typical alteration products in the deformed layered gneisses. Note white muscovite and green chlorite. Granular epidote may also be common in the deformed gneisses. Field of view 5mm, plane light. Sample F-50-8.

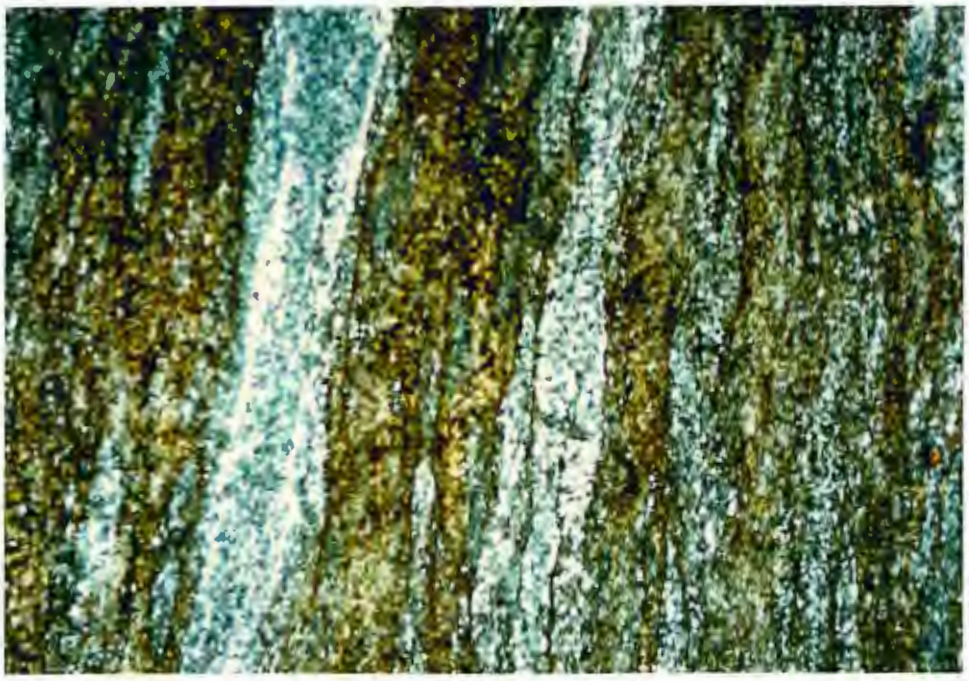

Fig. 14 Photomicrograph of layered gneiss phyllonite. Dark layers are mica-rich and light layers are quartz-rich. Field of view 5 mm. across, polars crossed. Sample F-51-7.

Fig. 15 Mylonitic gneiss that is folded and enveloped by a phyllonitic-chlorite-sericite matrix. Lens cap for scale in upper left portion of photo. Location F-49.

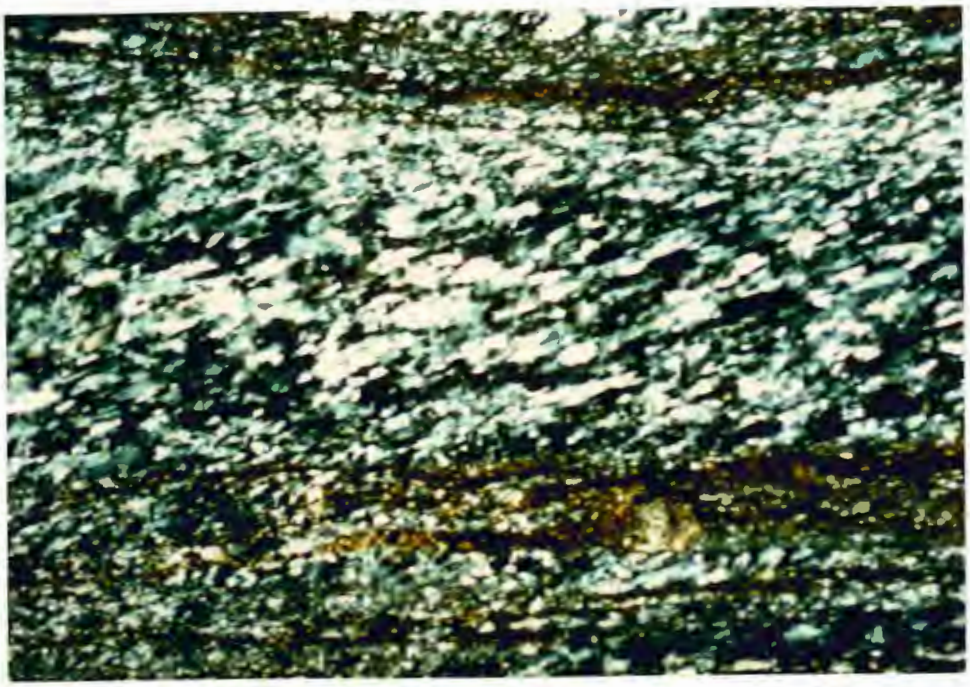

Fig. 16 Photomicrograph of layered gneiss mylonite. Layers are either rich in quartz and feldspar or mica. Note oblique foliation. Field of view 3 mm., polars crossed. Sample F-53-8.

porphyroclasts are locally abundant. The color of the layered gneiss mylonite is usually dark gray, but may be dark green to rusty if chlorite and epidote are abundant. Folds in the mylonite are either open or isoclinal with few in between these two extremes. The mineral lineation is often folded and may intersect fold axes at angles up to 90 degrees.

Garnet Biotite Gneiss

Garnet biotite gneiss looks much the same as the non-garnetiferous layered gneiss, except that it appears rusty when weathered. Garnets range in size from 1 mm. to 3 cm., and are dark red and euhedral (Fig. 17). The garnets tend to grow in the biotite-rich layers of the thinly laminated gneiss.

Garnet, sillimanite and cordierite are common in the pelitic gneisses of the Farmington Complex that remained unaffected by deformation. Garnets are abundant in the present study area, but sillimanite and cordierite have not been found. Sillimanite has been found in the present study area by Bryant (1984) and is common in the layered gneiss on Bountiful Peak (Rismeyer, 1981), where it occurs as macroscopic and microscopic prisms and swirling fibrous masses.

Deformation of the layered garnet biotite gneiss tends to involve retrogression of the garnet. Garnets that have been highly deformed and little altered are flattened, fractured and slightly elongate,

Fig. 17 Samples F-34 of biotite-poor garnet gneiss and biotite-rodded garnet gneiss.

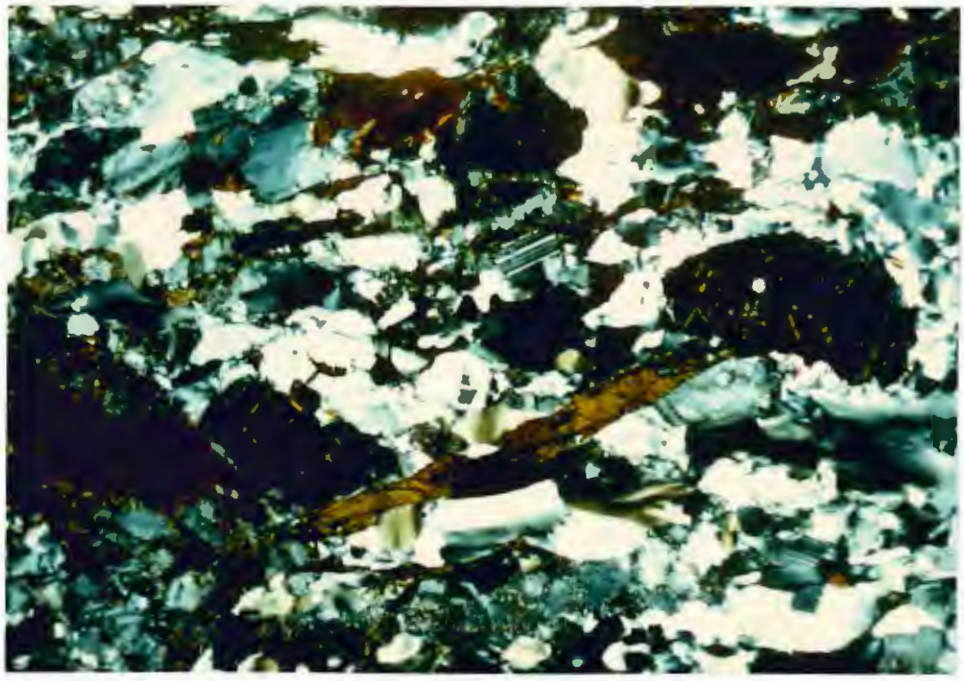

Fig. 18 Photomicrograph of a deformed garnet gneiss. Garnets are black, biotites are dark brown, and quartz and feldspars are gray to white. Field of view 5 mm., polars crossed. Sample F-31-2.

defining a poor lineation (Fig. 18). Mildly deformed, highly altered garnets have chlorite plus or minus epidote along fractures, or may be totally replaced by books of chlorite and stubby prisms of epidote. Possible pseudomorphs of pyrophyllite or muscovite after sillimanite have been found in rocks which contain deformed garnet pseudomorphs. However, x-ray diffraction analyses indicate that there is only possible muscovite pseudomorphs present, and no pyrophyllite, the likely retrograde product of sillimanite.

Chlorite Epidote Gneiss

Chlorite epidote gneiss is a retrograded, dark gray, medium grained rock composed of chlorite-epidote intergrowths (1 mm. across), plagioclase, K-feldspar, quartz and biotite crystals (Fig. 19). The rock is generally a darker gray than the biotite gneiss, and may be the retrograde equivalent of a biotite hornblende gneiss. Layers rich in chlorite, epidote and biotite weather to a rusty brown. Chlorite epidote gneiss was found only on Francis Peak, where deformation is relatively mild, suggesting that its origin is different from that of the biotite gneiss. Unfortunately, the nature of this rock prior to retrogression is unknown.

Biotite books are long and thin and occur in trails that may envelop quartz and feldspar grains (Fig. 20). Chlorite and epidote form ellipsoidal masses. Plagioclase and quartz are round to subhedral forms and may exist as coarse myrmekitic intergrowths.

Fig. 19 Samples of retrograde chlorite-epidote gneiss. Clockwise from top samples are F-54-1, F-52-2, F-44-1 and F-52-1. Samples F-54-1 and F-52-1 are little deformed. Samples F-52-2 and F-44-1 are moderately deformed.

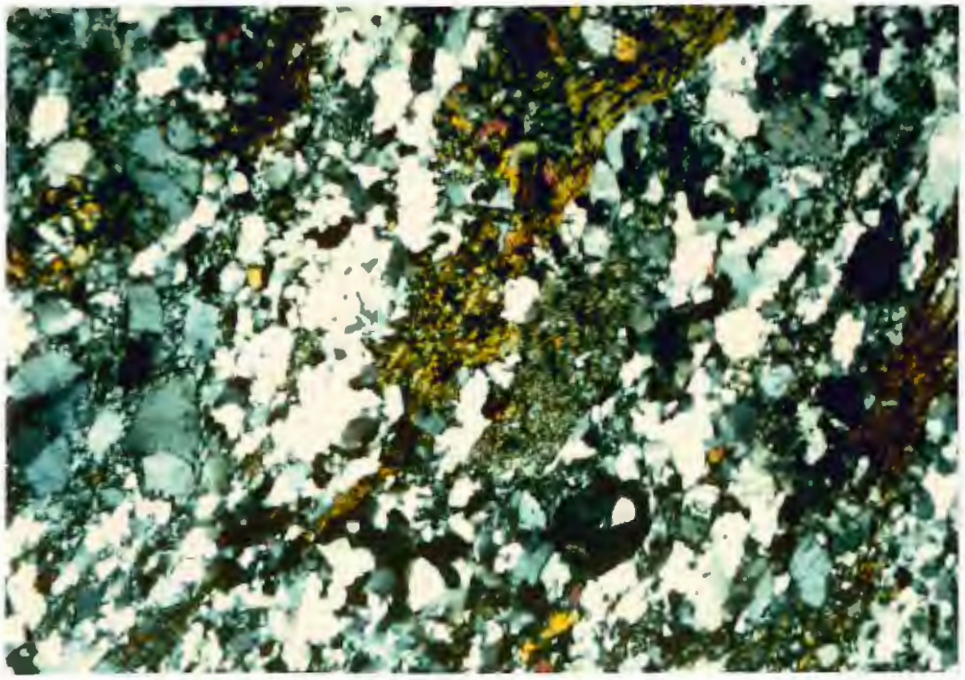

Fig. 20 Photomicrograph of chlorite-epidote gneiss. Biotite is dark brown and chlorite-epidote masses are green and yellow. Field of view is 5 mm. across, polars crossed. Sample F-54-1.

Minor K-feldspar occurs as subhedral grains. Plagioclase, and to a lesser extent, K-feldspar, tends to be altered to sericite on the margins.

The mineral lineation is defined by biotite and chlorite-epidote masses. Stubby, slightly elongate chlorite-epidote masses lie with long axis subparallel to that of biotite flakes and trails, collectively defining the mineral lineation.

Layering in the chlorite-epidote gneiss is weak to well-defined and may be folded. The foliation occurs as discrete layers richer or poorer in chlorite, epidote, and biotite. However, the weakly foliated chlorite-epidote gneiss is characterized by subtle changes in the modal percentage of chlorite, epidote, and biotite. These modal variations take place on a centimeter scale in the well-foliated gneiss and on a centimeter to meter scale in the weakly-foliated gneiss. A weak cleavage is defined by the coplaner nature of the basal plates of biotite grains.

Deformation of the chlorite epidote gneiss results in schists, phyllonites and mylonites that are similar to those produced from the biotite gneiss. However, undeformed chlorite epidote gneiss is richer in chlorite, epidote and biotite than the biotite gneiss. Deformed chlorite epidote gneiss therefore contains a larger percentage of schistose folia. Breakdown of hornblende to chlorite and epidote, and biotite to chlorite may have occurred during deformation and retrograde metamorphism. Recognition of chlorite epidote gneiss in the field was a problem, but was fascillitated by noting the cylindrical shape of chlorite masses that may have

replaced the hornblende. Also, the abundance of epidote in thin-section was helpful in identifying deformed chlorite epidote gneiss.

Amphibolite Gneiss

Amphibolite gneiss is dark gray, black and white speckled, massive to well-foliated, lineated and commonly kinked or openly folded (Fig. 21). Amphibolite gneiss is composed of 1-12 mm. subhedral to euhedral hornblende, 1-3 mm. subhedral plagioclase, and progressively lesser amounts of quartz, biotite and K-feldspar. Amphibolite gneiss has less distinct foliation than the layered gneisses and a much larger grain size.

Mineral lineation in amphibolite gneiss is weak to moderately well-defined, variable in orientation, and less distinct than in the layered gneisses. This lineation is defined by the allignment of hornblende prisms. Ellipsoidal masses of quartz and feldspar also define the lineation and have long axes subparallel with the hornblende lineation.

Foliation in the amphibolite gneiss is moderately well-formed, discontinuous and variable in attitude (Fig. 22). Layers of interlocking quartz and feldspar grains form a planar network, 1 mm. to 3 cm. wide, that is interspersed with hornblende grains. Pegmatite veins containing large hornblendes are commonly boudinaged.

Fig. 21
Outcrop of amphibolite gneiss. These rocks have not been affected by mylonitization. Layering is not as well-formed as that in the layered gneiss. Field book is 20 cm long. Location F-46.

Fig. 22
Samples of amphibolite gneiss F-14, F-31 and F-46. Note variation in composition. Upper left sample has more plagioclase (white). Sample on right, F-46, is kinked.

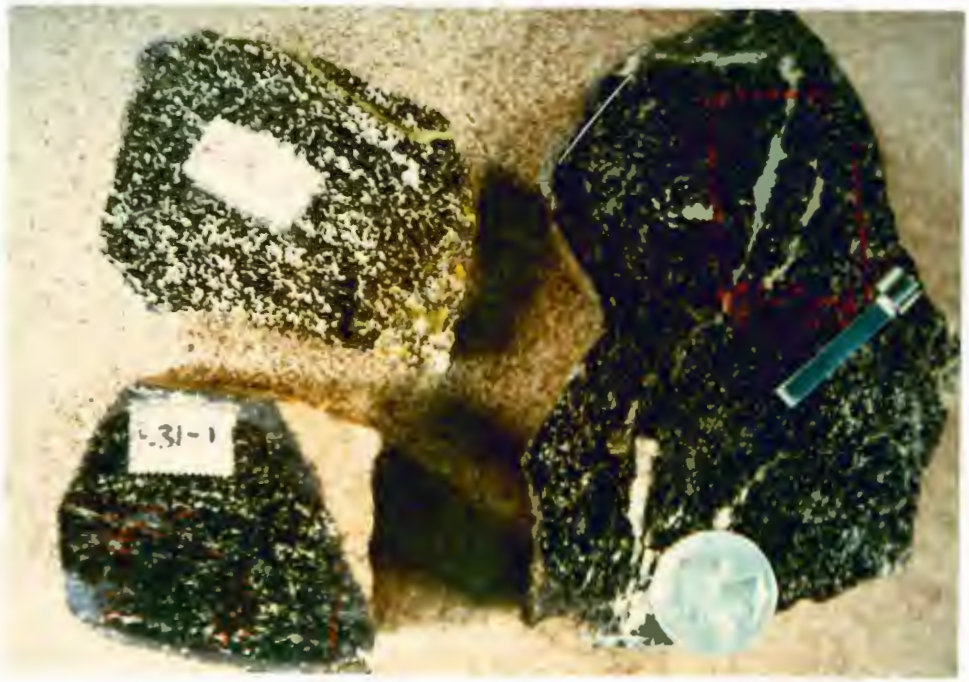

Folding in the amphibolite gneiss is surprisingly rare, yet, at F-46 the gneiss is pervasively kinked. The kinks have a wavelength of several centimeters. Foliation and lineation was affected by the kinking, long hornblende prisms bent at the kink plane (Fig. 23). Kink axes lie in the foliation, subperpendicular to the mineral lineation.

Deformation of the amphibolite gneiss almost always results in a retrograde chlorite-epidote phyllonite (Fig. 24). There are, however, a few examples of mylonite in the study area that are the highly deformed counterparts of the amphibolite gneiss. These mylonites are remarkably rich in quartz. Phyllonite and mylonite may be interlayered, suggesting that they formed during the same deformation. Transitional rocks, between deformed gneiss and phyllonite or mylonite, are curiously absent.

Mildly deformed amphibolite gneiss has flattened hornblende, quartz and feldspar grains and posseses an excellent foliation. Foliation is defined by the planar orientation of chlorite flakes and flattened original grains. Elongate masses of fine-grained chlorite and epidote define a subtle lineation which is best formed on surfaces of preferential slip. Hornblende is retrograded to chlorite and traces of epidote along cleavage, plagioclase is preferentially altered to sericite on rims or in cores, and quartz exhibits a wide range of recrystallization textures. Chlorite and granular masses of epidote, which extend as tails away from the hornblende, define the new foliation and lineation, the original foliation and lineation being mostly destroyed.

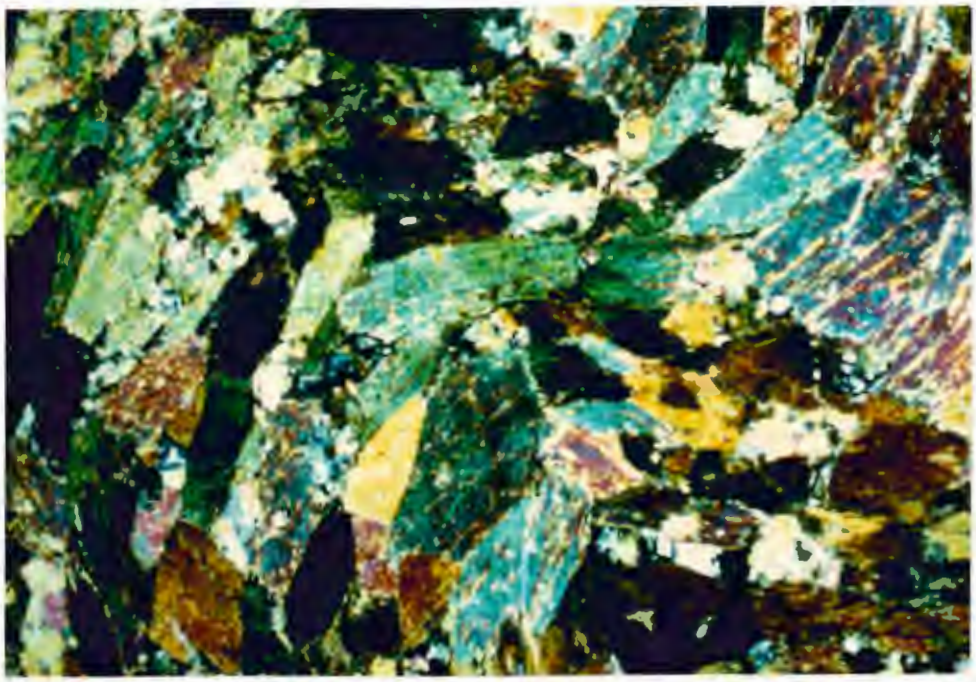

Fig. 23 Photomicrograph of amphibolite gneiss. Note bent blue-green hornblende grain in the kink plane (center). Field of view is 5 mm. across, polars crossed. Sample F-46.

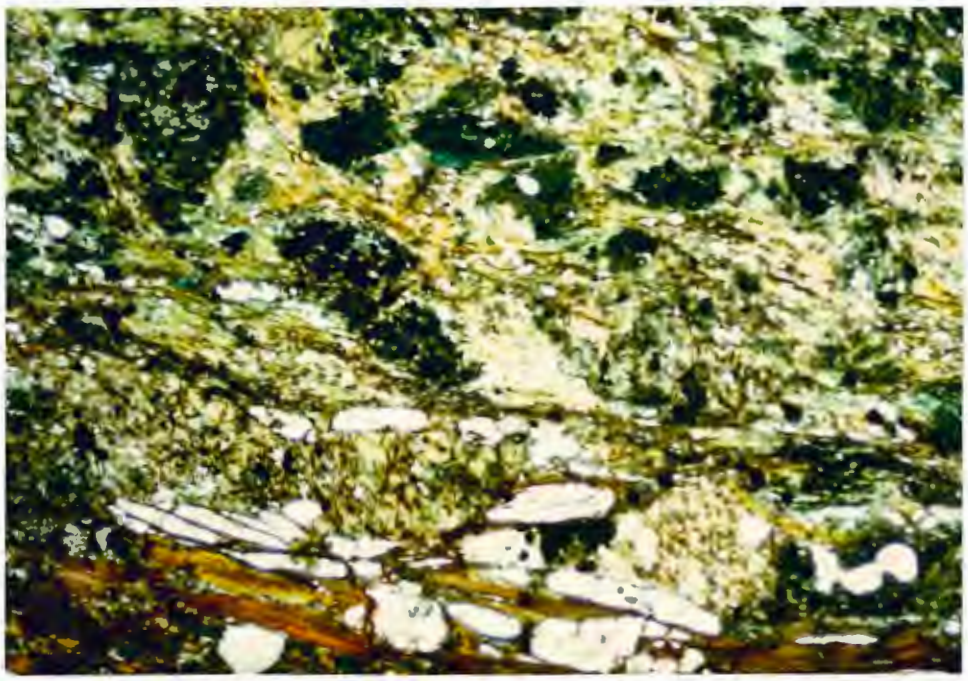

Fig. 24 Photomicrograph of deformed and retrograded amphibolite gneiss phyllonite. Chlorite is green, sericite clear to light green, hornblende dark green, biotite-chlorite brown, and the clear mineral (fish) is of the serpentine group. Field of view is 5 mm., plane light. Sample F-31-2.

Only a few thin (1 cm. to 3 m.) layers of mylonite were found in the amphibolite gneiss. The mylonite can be recognized by the pale green color of the abundant epidote or by the quartz ribbons (Fig. 25). Foliation occurs as alternating, 1-5 mm., chlorite and epidote-rich layers and quartz-rich layers. A schistosity dominates the chlorite-rich layers. Quartz-rich layers contain little else except quartz and minor chlorite and epidote, and tend to pinch-out laterally.

In thin-section the amphibolite mylonite appears much as other mylonites from the study area (Fig. 26) except for two important observations: 1) epidote is as abundant as chlorite in the schistose folia, and 2) the overall grain size of the chlorite and especially the quartz in the schistose foliation is much finer than average. Quartz ribbons in the mylonite are coarser grained, relatively pure, and may exhibit an oblique foliation.

Granitic Rocks

Granite

The granite is white to light pink and massive, usually meduim to coarse grained, but locally porphyritic, pegmatitic or graphic. It consists of quartz, plagioclase and K-feldspar (Figs. 27 and 28), accesory apatite and zircon, and locally garnet or muscovite.

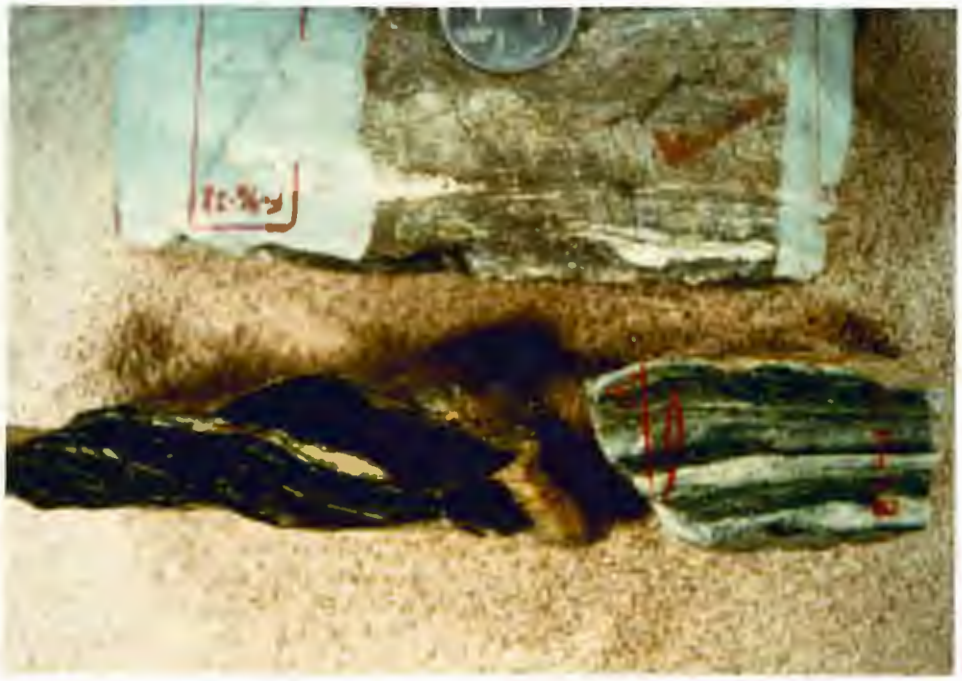

Fig. 25 Samples of amphibolite gneiss mylonite are F-46-3, F-14-3 and F-11-1 clockwise from top. Sample F-46-3 contains thin quartz ribbons near the bottom. F-11-1 is phyllonitic and contains a foliation that is oblique to edges of sample. F-14-1 is a quartz ribbon ultramylonite.

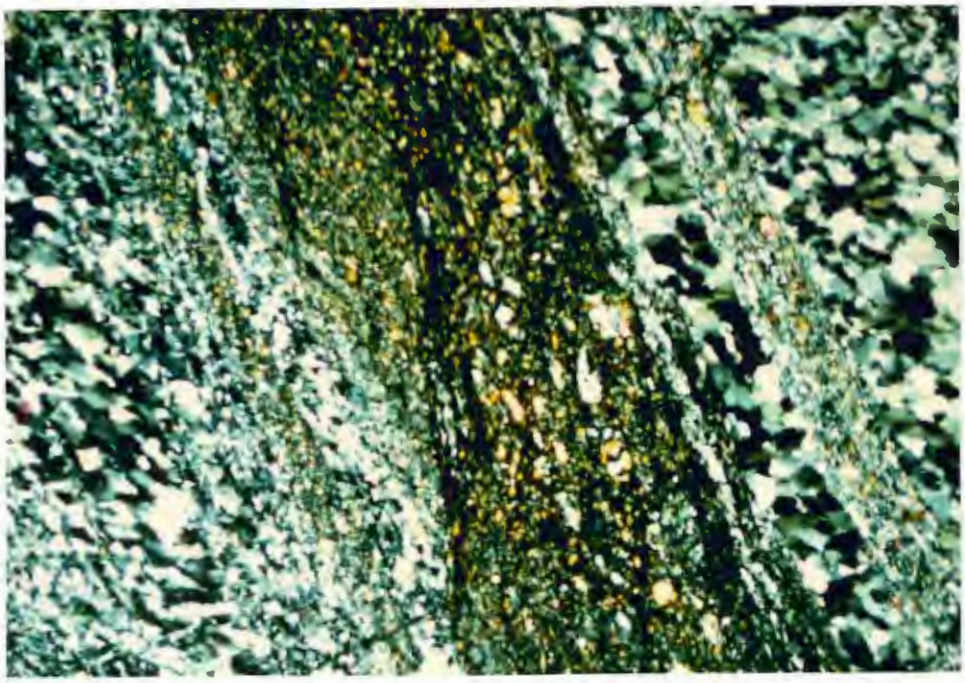

Fig. 26 Photomicrograph of amphibolite gneiss ultramylonite from previous figure. Note dextral shear band in mica layer and oblique foliation in quartz layers. Field of view is 3 mm. across, polars crossed. Sample F-14-3.

Fig. 27 Samples of least deformed granite, F-51-2, F-51-3, F-27-2, clockwise form right. Variation in color depends on composition, K-feldspar-rich rocks being pinker. Pegmatitic granite on right is mildly deformed.

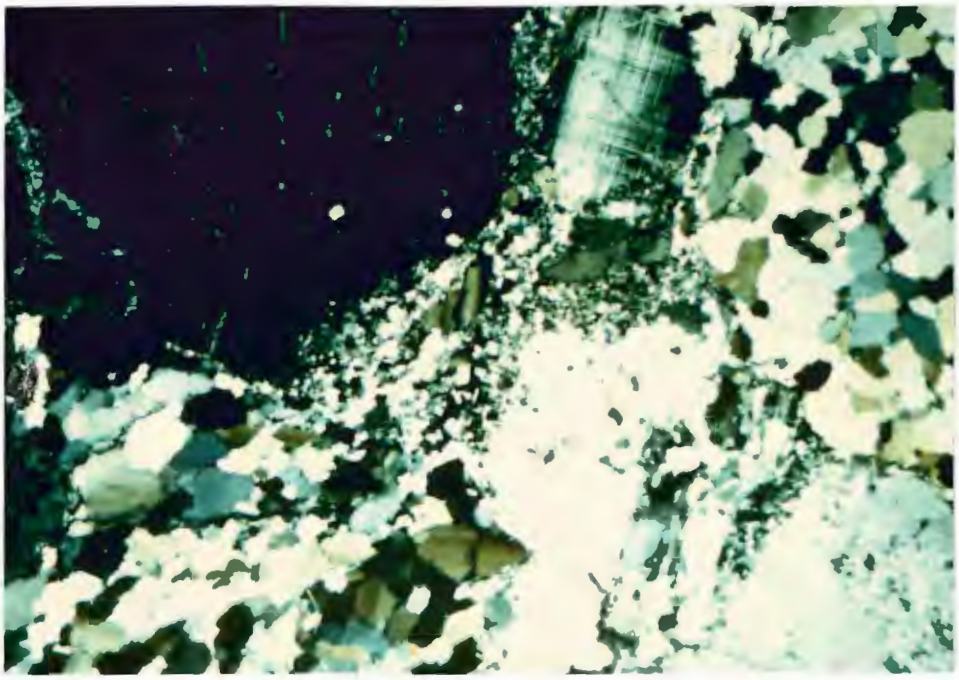

Fig. 28 Photomicrograph of least deformed granite. Large quartz grains are recrystallized to myriad polygonal grains. Broken orthoclase fragment from rim of large grain has inverted to microcline in response to deformation. Field of view is 5 mm. across, polars crossed. Sample F-26-3.

The granites intruded the gneisses during the 1790 Ma metamorphic event (Hedge, et al., 1983). Granite, second in abundance to the gneisses, exhibits highly sheared contacts with the gneisses in all cases. Contacts with the gneisses are sharp and mostly undeformed on Bountiful Peak and only minor, open folding is associated with intrusion (Rismeyer, 1981). The granite bodies have been dismembered in the most deformed parts of the study area. The largest granite bodies lie in the eastern portions of sections 3 and 10 (Fig. 29 and plate 1), east of the Francis Peak Fault Zone. Even in this relatively undeformed block the granites are deformed and have probably been rotated and dismembered as a function of shearing between lithologies.

Garnet granite is white in color, rich in plagioclase, locally pegmatitic, with euhedral garnets up to 12 mm. in diameter. The garnets are not uniform in size and are not homogeneously distributed. The largest garnets are associated with the most coarse-grained granite, and are probably primary phenocrysts. Muscovite granite is also pegmatitic, with the coarsest textured rock containing the largest books of muscovite. Muscovite books 1-2 cm. thick and 1-4 cm. across appear to have crystallized in contact with feldspars up to 20 cm. long.

The texture of the granite is variable and often spectacular (Fig. 30). A description of each texture is merited because each rock type responds differently to deformation. The massive, equigranular granite contains grains of 1 cm. or less in an homogeneous mass of subhedral to euhedral grains. The pegmatitic granite consists of very

Fig. 29 Looking south across the eastern half of the study area. Note westward dip of penetrative fabric and large quartz syenite body on peak. Trees are approximately 10 meters high.

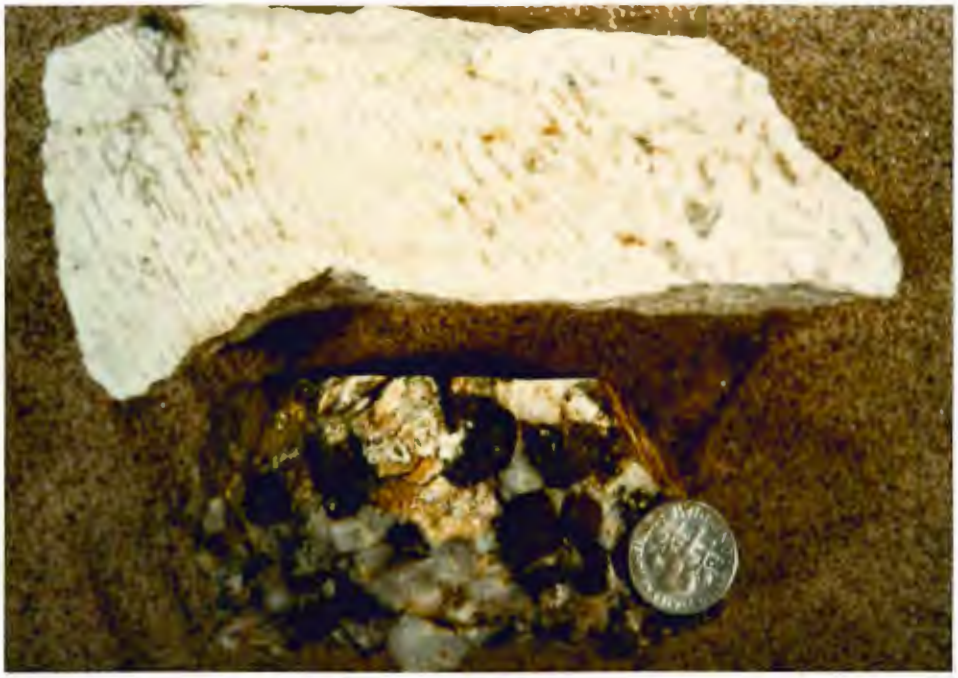

Fig. 30 Samples of granite that exhibit graphic (sample F-39-3) and porphyritic textures (sample F- 39-1). Feldspar is in optical continuity in thin-section.

coarse subhedral to euhedral crystals of K-feldspar, plagioclase and somewhat smaller, interstitial, anhedral quartz. Porphyritic granite closely resembles the pegmatitic granite, but the quartz is only medium grained and less abundant. Graphic granite contains K-feldspar crystals at least 20 cm. long, and possibly 1-2 m. long, that are intergrown with planes of quartz continuous for a few centimeters. In thin-section, graphic granite consists of large single orthoclase crystals punctuated by planar quartz grains, the orientation of which is dictated by the crystal structure of the orthoclase (Fig. 31).

Deformation products of the granite range from mildly deformed rock to mylonite, as with the layered gneiss. However, whereas the deformed layered gneisses are texturally homogeneous, the deformed granites are texturally inhomogeneous (Fig. 32, 33). For example, a mildly deformed granite may consist of crude layers of quartz and feldspar punctuated by layer-parallel micaceous folia. Other deformed granites may be either distinctly mica-poor or entirely micaceous with knots of quartz, yet still recognizable as a deformed granite. More intense deformation of the granite leads to greater consistency in texture.

The mica-rich folia in the deformed granites are either schistose or phyllonitic and are composed of some combination of muscovite, chlorite, epidote and clinozoisite. Epidote is granular and variable in grain size. Where the mica-rich layering is minor, micaceous folia may envelop lenses of quartz and feldspar. These layers are anastamosing to massive and vary in width from 1 mm. to over a

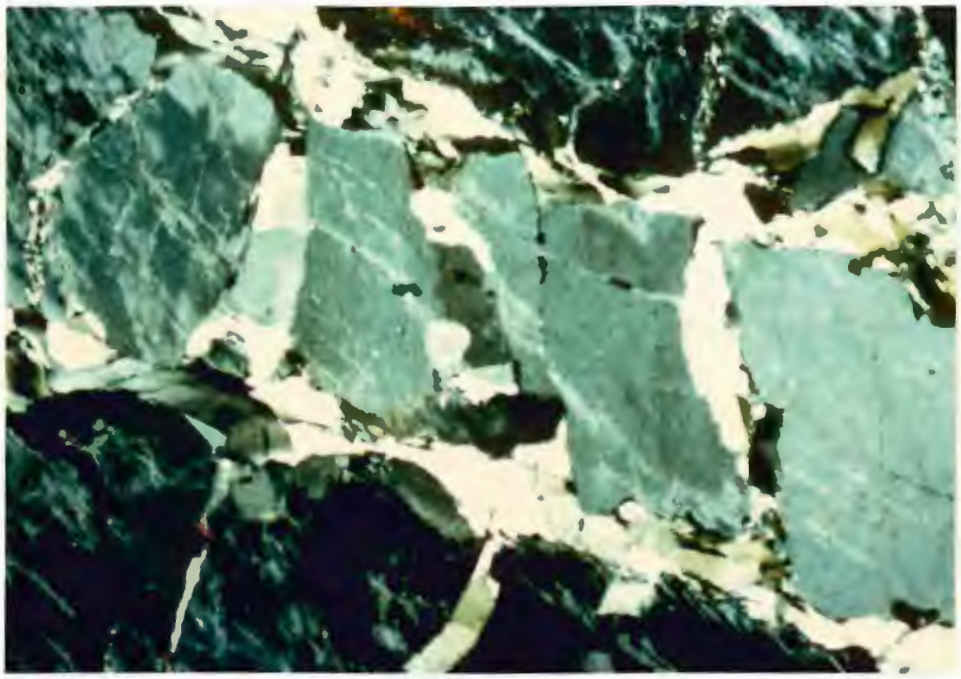

Fig. 31 Photomicrograph of mildly deformed graphic granite from previous figure. Large continuous orthoclase is divided by planes of quartz. Field of view is 5 mm. across, polars crossed. Sample F-39-3.

Fig. 32 Samples of deformed granite, F-47-2, F-39-3, F-47-1 clockwise from top. Feldspars acted rigidly while quartz deformed and recrystallized into ribbons. Veins of retrograde minerals have invaded fractures.

Fig. 33 Deformed and highly sericitized granite. Plagioclase and K-feldspar are completely retrograded to muscovite, and quartz forms white ellipsoidal knots. Sample F-27-5.

Fig. 34 Deformed and brecciated quartz syenite. Deformed lenses of K-feldspar have long dimensions parallel to pencil. Brecciated and deformed rock in alteration conduit has long dimension parallel with phyllonitic foliation (dark, mica-rich rock) and perpendicular to pencil. Location F-12.

meter (Fig. 34). Deformed granite with anastamosing micaceous folia appears much the same in thin-section as the unaltered, deformed granite, except for the mica layers (Fig. 35). The folia wrap around porphyroclasts of quartz or feldspar and lend the rock a crude spaced cleavage. The highly altered deformed granite does not appear anything like the unaltered deformed granite in thin-section (Fig. 36). Feldspars, plagioclase in particular, are completely altered to sericite. Sericitized feldspars do not deform in a brittle manner, but rather flatten into ellipsoidal masses or ribbons of sericite. Quartz grains are highly strained, yet they maintain their continuity as knots the size of original quartz grains.

Unaltered deformed granite exhibits recrystallized quartz and feldspar (Fig. 28). The quartz exists as aggregates of recrystallized ellipsoidal grains with serated grain boundaries and a myriad deformation bands. Feldspars are fractured and deformed. Fractures are more common at the edges of the grains and usually partially follow cleavage planes. Recrystallization is not widespread in feldspar, but an indistinct polygonization is common. Recrystallization in feldspar usually occurs along fractures and at grain margins. Open folds in the feldspars are common and are best observed in twinned plagioclase. Twins in plagioclase and K-feldspar are strongly affected by deformation, and appear to have either grown or shrunk in response to the internal deformation. Polysynthetic twinning in plagioclase will either fade out in patches along grain margins or grow at a high angle to the relict twins.

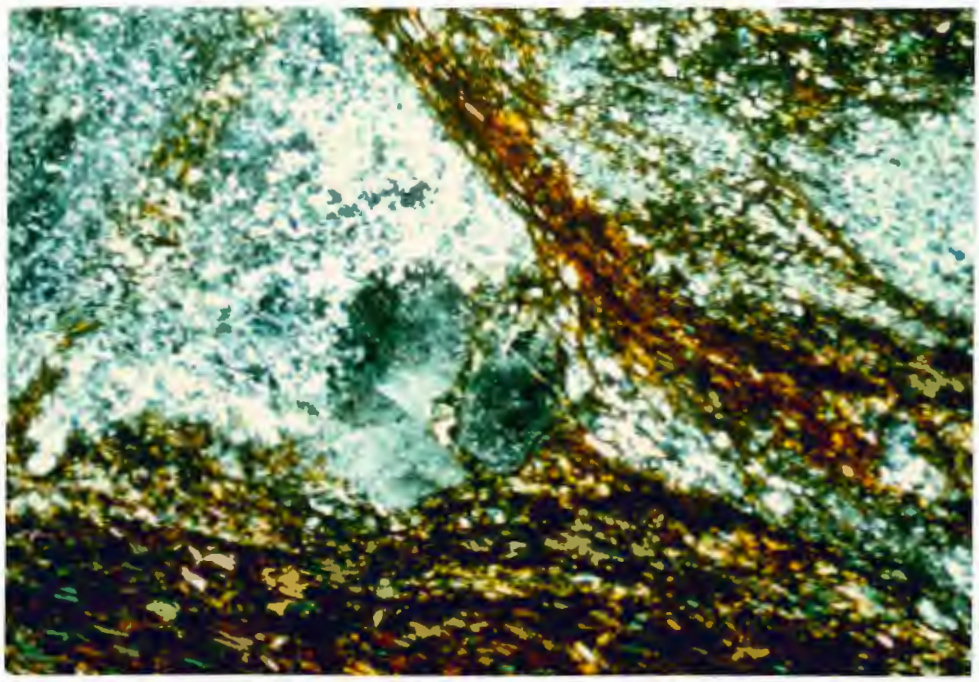

Fig. 35 Deformed granite with foliation formed by biotite, chlorite, muscovite and epidote. Orthoclase is fractured and recrystallized. Field of view is 5 mm. across, polars crossed. Sample F-18-2.

Fig. 36 Photomicrograph of deformed granite from figure 33. Original quartz grains are deformed and recrystallized. Feldspar is completely sericitized and deformed. Field of view is 5 mm. across, polars crossed. Sample F-27-5.

Untwinned K-feldspar may show microcline twinning along fractures or in patches at grain margins.

A continuous gradation between altered deformed granite and phyllonite is observed in the field, over distances of one to several tens of meters. Despite this, there are two important differences between the rock types. First, the schistosity in the phyllonite is better developed, more continuous and wraps around quartz knots (Fig. 37). In the altered deformed granite the schistosity is often truncated by mildly flattened original grains of quartz. Second, the ellipsoidal shape of flattened original grains of quartz and feldspar is not present in the phyllonite.

Foliation is much more continuous in the well lineated and layered granite mylonites. Large porphyroclasts of quartz and feldspar, which constitute 100% of the unaltered deformed granite, are rare in the granitic mylonite. Porphyroclasts in the mylonite are on the order of 0.1 mm across and are usually K-feldspar. The main difference between the granitic phyllonites and mylonites is that they have different modal proportions of feldspars and micas. The phyllonite may consist of up to 50% mica, with little feldspar, whereas the mylonite contains only minor mica, with abundant feldspar porphyroclasts and fine-grained recrystallized feldspar (Figs. 37-40).

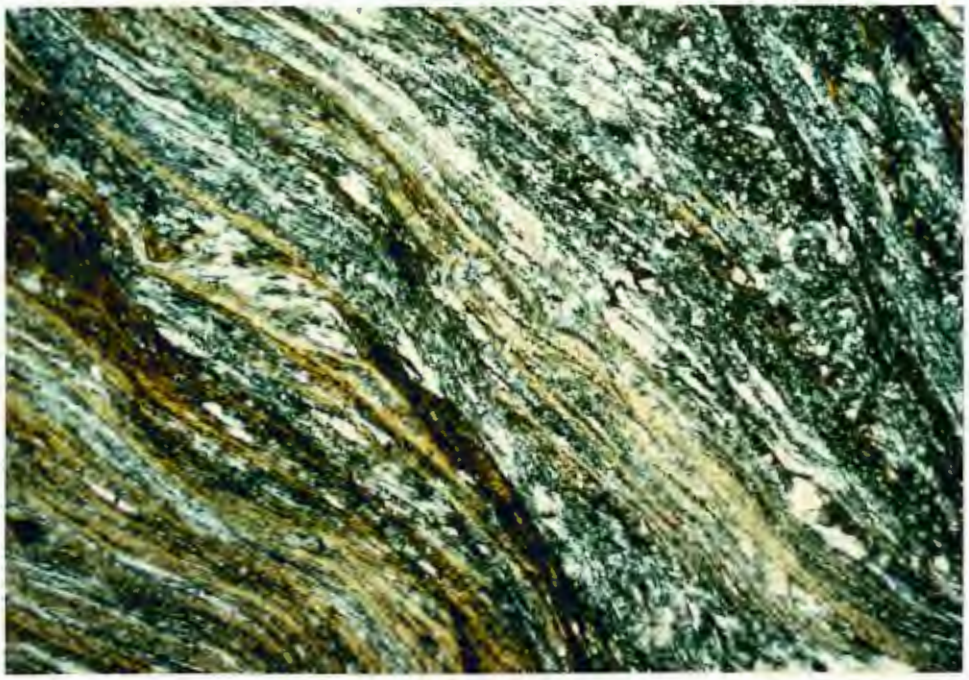

Fig. 37 Photomicrograph of phyllonite from granite. Individual layers are derived from one or more flattened original grains of quartz (light) and deformed and altered feldspars (dark, mica-rich). Field of view is 5 mm. across, polars crossed. Sample F-44-3.

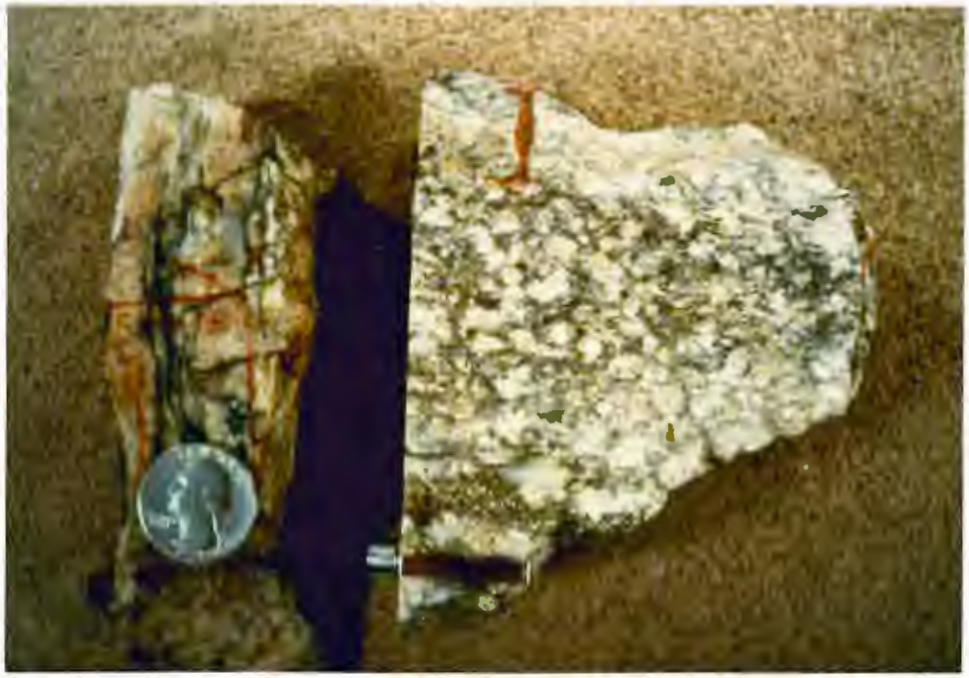

Fig. 38 Samples of granite mylonite. Left sample (F-9-1) contains thin quartz ribbons. Right sample (F-9-2) has abundant feldspar porphyroclasts in a ductilely deformed matrix of quartz.

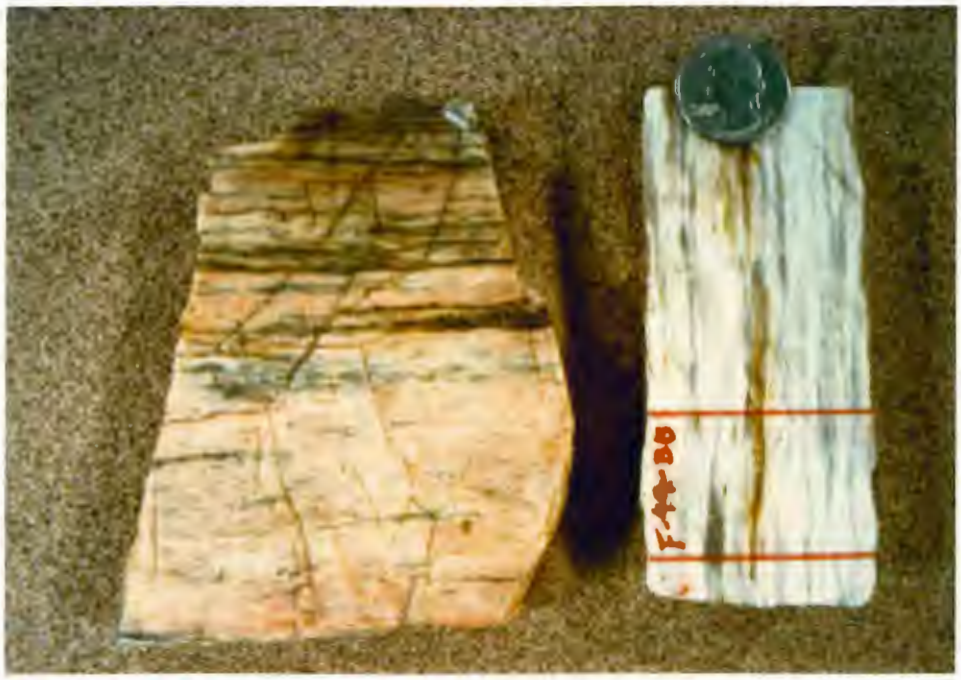

Fig. 39 Samples of granite ultramylonite. Left sample (F-50) is from the quartz syenite and right sample (F-49) is from a pegmatite. Note that quartz as well as feldspars are completely recrystallized due to ductile deformation.

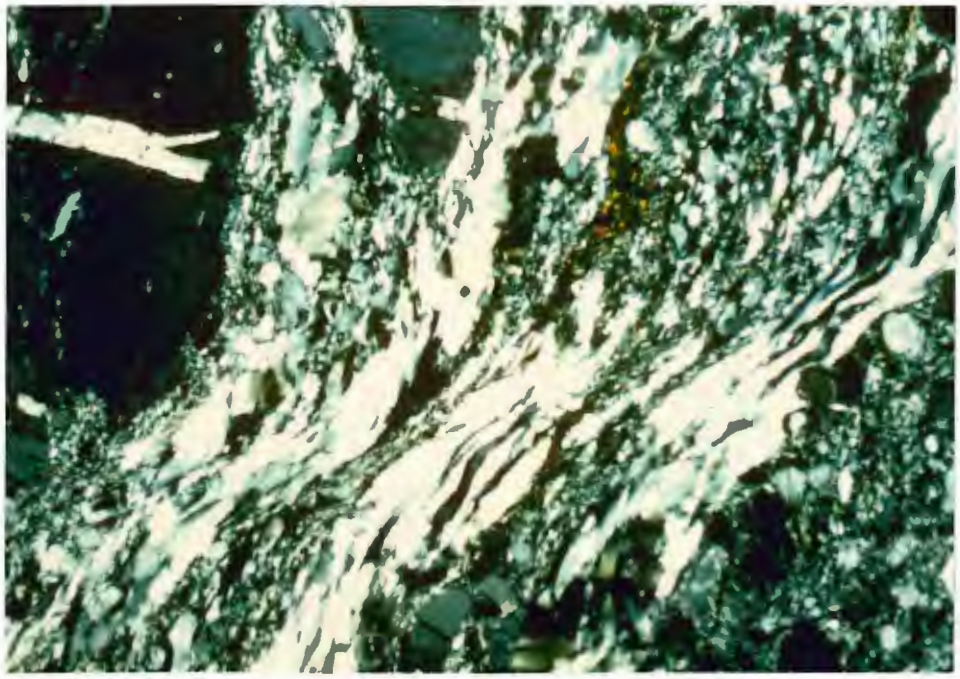

Fig. 40 Photomicrograph of graphic granite mylonite. Feldspars are rounded, recrystallized and fractured. Quartz exists as hightly deformed ribbons. Field of view is 5 mm. across, polars crossed. Sample F-40-3.

Quartz Syenite

Quartz syenite, recognized by its pink color, is easily distinguished from the granite and only crops out in the east-central part of section 10, forming the east flank of the ridge (Fig. 29). The intrusive contact relationship with the layered gneiss is clear, yet the foliation in the adjacent rock is subconcordant, indicating that both rock types were deformed together subsequent to intrusion and cooling.

The quartz syenite is K-feldspar porphyritic. Anhedral to subhedral plagioclase and quartz fill the interstices between euhedral K-feldspars that are several centimeters across. Alteration of the quartz syenite is minor, occuring principally as the alteration of plagioclase to sericite.

The quartz syenite acted like a competent clast in a less competent matrix of layered gneiss, the margin of the body much more deformed than the core. At the contact with the layered gneiss, porphyroclasts up to 4 cm. in diameter lie in a matrix of recrystallized quartz and mildy altered and deformed plagioclase. Away from the contact, two cross-cutting networks of planar ductile shear zones are present in the body. The older shear zones are associated with ductilely deformed feldspars. The younger shear zones are zones of intense alteration that cross-cut all earlier fabrics (Fig. 34).

Pegmatite

White tabular pegmatite veins and dikes up to 4 m. in width can be found throughout the study area. Pegmatites are most common in the vicinity of Francis Peak, and are fairly rare in the southern sections of the field area. In the least deformed gneiss, where contacts with the pegmatite are undistorted, layering is definitely cut by the intrusion. In the more deformed layered gneiss, pegmatite veins and dikes are subconcordant with layering. Highly deformed layered gneiss, with the layering disaggregated, will often contain tabular pegmatite bodies that are concordant and folded along with the gneissic layering. Put simply, the most deformed pegmatites have contacts that are most nearly concordant with the gneissic layering (Fig. 41).

The pegmatites were probably intruded along with the granites, as pegmatite veins do not penetrate the granites. The only xenoliths found in pegmatitic rock are amphibolite. There is no evidence to suggest that the gneisses were hot and ductile during the intrusion of the pegmatite. During the circa 1790 Ma intrusion, pegmatites probably formed by injection of granitic magma along fractures created by rising plutonic bodies. There is no obvious preferred orientation to the pegmatite dikes, therefore intrusion along a pre-existing fracture set can be ruled out.

The pegmatite consists primarily of K-feldspar, with lesser quartz and even lesser plagioclase. Euhedral garnets and books of muscovite, up to 3 cm. across, are not uncommon. Orthoclase occurs

as subhedral to euhedral crystals that average approximately 5 cm. across, and several tens of centimeters in length. Plagioclase grains are somewhat smaller than the average K-feldspar. Quartz, as in the granite and syenite, is intergranular and anhedral.

Deformed pegmatite bodies are locally fractured, folded, faulted and boudinaged. Fractures tend to be clean breaks rather than zones of brecciation. Faults, along which movement of several meters is common, are associated with narrow zones of cataclasis (Fig. 42). Boudinaged pegmatite bodies exhibit extreme deformation in necked zones and less intense deformation in the cores of the boudins.

Deformed pegmatite consists of flattened orthoclase, quartz and plagioclase grains, with or without thin (0.1 mm to 1 cm) films and folia of chlorite and sericite (Fig. 43). The orthoclase and plagioclase grains are fractured, flattened and disjointed. Angles between cleavages or crystal faces are distorted, and corners are more rounded than sharp. Boundaries between quartz and feldspars are commonly serrated and tortuous.

Quartz and feldspars have obviously responded differently to deformation. This difference is best observed in thin-section (Fig. 44). Large orthoclase grains have rounded and fractured margins with fine recrystallized orthoclase mixed with recrystallized quartz. Interiors of orthoclase grains may be riddled with fractures, along which new recrystallized grains have grown. Many types and widths of deformation bands occur in grain interiors, none of which transgress new grain boundaries. Microcline twinning on the peripheries of orthoclase grains is ubiquitous. Plagioclase is altered

Fig. 41 Mylonitic pegmatite in isoclinally folded, mylonitic layered gneiss. Contact between gneiss and pegmatite is subconcordant. Lens cap for scale (arrow). Location F-9.

Fig. 42 Pegmatite dike offset 1.2 m to the west by shallowly dipping fault. Foliation in gneiss (upper right) is at a high angle to contact between gneiss and pegmatite. Lens cap for scale just below fault (arrow). Location: S.E. 1/4 of section 9.

Fig. 43 Samples of highly deformed pegmatite (F-31-3 above, F-36 below) taken from contacts with layered gneiss. Note large porphyroclasts of orthoclase and plagioclase. Upper sample is mylonitic pegmatite in contact with layered gneiss above. Rims of some feldspars are more sodic.

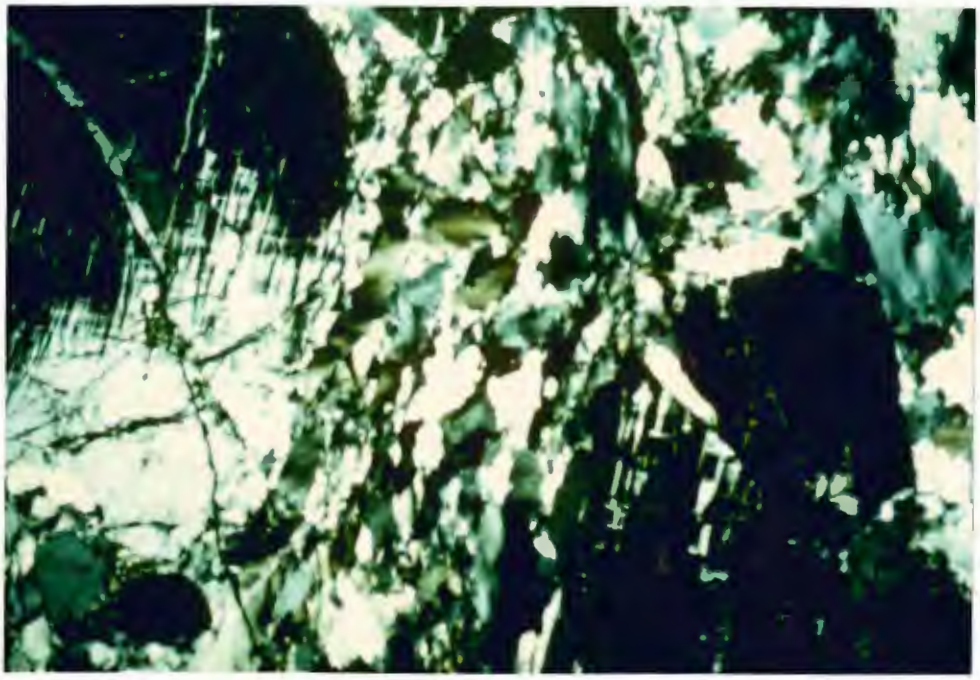

Fig. 44 Photomicrograph of a highly deformed pegmatite. Quartz is deformed and recrystallized, K-feldspar is fractured and inverted to microcline. Field of view is 5 mm. across, polars crossed. Sample F-2-3.

and disintegrated, even in the mildly deformed pegmatites. Quartz acts as a ductile enveloping matrix for fractured and separated blocks of orthoclase. Between blocks, ellipsiodal quartz grains are commonly alligned with long axes oblique to the orientation of the fracture.

The most intensely deformed pegmatite can be found at the margins of dikes (Fig. 45). Dike margins contain two characteristic structures. Infolded gneiss separates limbs of pegmatite. Rounded clasts of orthoclase or orthoclase/quartz aggregates isolated in a dark green mica matrix, or "gneiss", are found near the dike margin.

There are marked differences between the deformed pegmatites and the pegmatite mylonite (Fig. 46). In the latter, both quartz and K-feldspar occur as ribbons, and porphyroclasts of K-feldspar are 1 mm. or less in diameter, much smaller than those in the deformed pegmatite. Foliation in the deformed pegmatite is defined by crude layers of recrystallized quartz that envelop the porphyroclasts. Foliation in the pegmatite mylonite is continuous (Fig. 47), and may be traced for great distances.

Thin-sections of the pegmatite mylonite exhibit recrystallized quartz, relict K-feldspar, recrystallized K-feldspar and possibly recrystallized plagioclase (Fig. 48). Minor films of sericite and chlorite and granules of epidote commonly divide quartz layers from feldspar-rich layers. Quartz layers are composed of elongate, recrystallized quartz grains. Each layer is usually only several grains wide, the number of grains staying virtually constant along the layer. Quartz plus feldspar layers contain recrystallized quartz and feldspar

Fig. 45 Mylonitic pegmatite in mylonitic layered gneiss, looking along lineation. Pematite is rod-shaped perpendicular to page. Note intensity of deformation at margin of pegmatite. Chocolate bar is 12 cm long. Location: center of section 10.

Fig. 46 Outcrop of pegmatite mylonite (3 m. high). Pegmatite mylonite is light colored rock and layered gneiss mylonite is dark colored rock. Pencil for scale just above arrow. Location F-17.

Fig. 47 Samples of pegmatite ultra-mylonite. Light layers in bottom sample and light colored fold core in upper sample consist of recrystallized ribbons of feldspar and lesser quartz. Note pinch and swell of leucocratic vein in upper sample. Samples F-53.

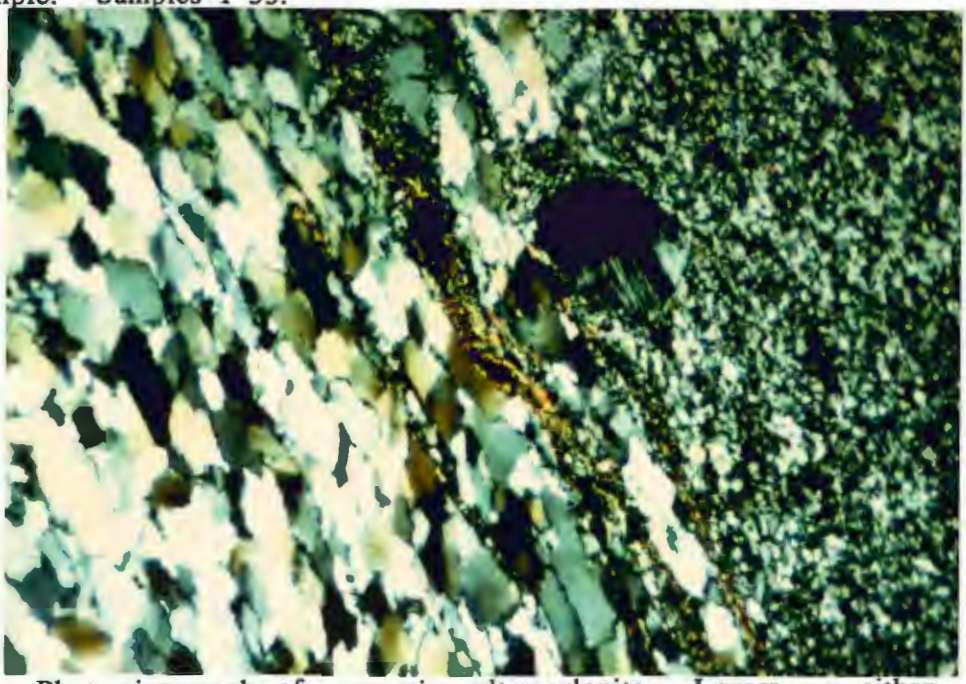

Fig. 48 Photomicrograph of pegmatite ultramylonite. Layers are either quartz-rich (large grains) or feldspar-rich (fine grains). Recrystallization is extensive and few original K-feldspars remain. Field of view is 3 mm. across, polars crossed. Sample F-9-1.

and porphyroclasts of K-feldspar. The quartz content in these layers is low, possibly around 5%. K-feldspar grains are generally finer than quartz grains, and they do not have clear grain boundaries (because the grains are around 30 or 40 microns thick). Porphyroclasts are well-rounded and flanked by pressure shadows of recrystallized K-feldspar that thin outward from the grain.

Metamorphism

There is evidence that at least three metamorphic events have affected the rocks of the Farmington Canyon Complex. A granulite facies metamorphism, of which no evidence was found by the present author, is postulated to have occurred at 2600 Ma (Hedge et al., 1983). The second event, an amphibolite facies metamorphism, is ubiquitous in the Farmington Complex. Syntectonic granites have been dated at 1790 Ma (Hedge et al. 1983). During the third event, the rocks were retrograded to greenschist facies assemblages along shear zones.

Bryant and Graff (1980) infer that a granulite facies event has affected the Farmington Canyon Complex, prior to the 1790 Ma amphibolite facies event, strictly on the basis of a few relict hypersthenes. Hedge and others (1983) concluded, on the basis of whole-rock Rb-Sr dating of the layered gneisses that the complex is as old as 2600 Ma. The Archean dates support the possibility that

the Farmington Canyon Complex was metamorphosed before the Proterozoic.

Farmington Canyon Complex rocks are largely of amphibolite facies, except along retrograde shear zones. Throughout the complex, prisms and fibrous masses of sillimanite have been found (Bryant, 1984). On Bountiful Peak, south of the present study area, the rocks contain upper amphibolite facies assemblages. These rocks are biotite-sillimanite gneiss, cordierite-garnet-biotite gneiss, hornblende-cummingtonite-garnet gneiss and cordierite-garnet-anthophyllite gneiss. The rocks on Francis Peak may once have been compositionally similar to those on Bountiful Peak. Francis Peak rocks are now so deformed and retrograded that only patchy evidence remains of the amphibolite facies mineralogy. Evidence, both concrete and indirect, has been found to support the idea that the rocks were of amphibolite facies prior to retrograde dynamic metamorphism. The only rocks on Francis Peak that are strictly amphibolite facies are the amphibolite gneisses, which are composed of hornblende, biotite, quartz, and feldspar.

The layered gneisses are intimately interlayered with the amphibolite gneiss. Though the layered gneisses contain retrograde metamorphic minerals they are considered to have been amphibolite grade by association with the amphibolite gneiss. Bryant (1984) mapped several types of layered, amphibolite facies, biotite gneiss in the Farmington Canyon Complex. He found hornblende-biotite quartz monzonite gneiss near Francis Peak, although none was found by the present author. Three compositional varieties of layered gneiss were

mapped on Francis Peak by the present author; biotite gneiss, garnet-biotite gneiss, and chlorite-epidote gneiss. The chlorite-epidote gneiss may be the equivalent of Bryant's hornblende gneiss.

Thin-section analysis confirms that the gneisses were once amphibolite facies and have since been retrograded to greenschist facies. The gneiss may contain two types of biotite, but commonly has only one or the other. The original, amphibolite facies brown biotite occurs as thin unaltered books a few millimeters long that have uniform optical properties (Fig. 8). In contrast, retrograde biotite is mottled green and brown, finer grained and has a dirty appearance (Fig. 20). The retrograde biotite is the product of either retrogression and recrystallization of original biotites in place or crystallization of new grains. Garnets in the biotite gneiss are either mildly altered to chlorite-biotite or completely altered to chlorite and epidote. Completely retrograded garnets often show excellent pseudomorphic outlines.

Common retrograde minerals, grouped according to association, are epidote, clinozoisite, allanite and sphene; biotite, chlorite, muscovite/sericite and magnetite. These minerals occur not only as alteration products of hornblende, biotite, feldspar and garnet, but also as vein minerals. Veins consist mostly of biotite and chlorite with lesser muscovite, epidote and sphene. These alteration veins are found in the deformed biotite gneisses as well as the deformed granitic rocks. The atomic constituents needed to crystallize biotite, chlorite, muscovite and epidote are readily available from the retrograded biotite, garnet and feldspars of the layered biotite

gneiss. Veins in the deformed amphibolite gneiss are usually rich in chlorite with lesser epidote and magnetite from the breakdown of hornblende.

Biotite, chlorite and muscovite usually occur together in the same folia in the deformed gneisses and granites. Muscovite is generally clean and undeformed. Chlorite is intergrown with the biotite as alternating cleavage flakes or rather amorphous patches. A submicroscopic intergrowth of biotite and chlorite is probably what makes the biotite look somewhat greenish and diseased.

Epidote and clinozoisite are common in the deformed layered gneisses and deformed amphibolite gneisses. The epidote occurs as euhedral blades and blocks that cross-cut foliation, riddle quartz grains, or replace Ca-rich minerals like garnet, hornblende and plagioclase. Some of the least deformed layered gneisses and granitic rocks have euhedral allanite crystals with overgrowths of epidote, the allanite being an original igneous mineral and the epidote a product of retrograde metamorphism. Sphene, also Ca-rich, is often associated with the epidote. Sphene appears as rounded diamond-shaped grains, occuring in trace amounts, scattered throughout alteration veins.

Structure of Francis Peak

The purpose of this section is to explain the meso and macrostructural elements of the Francis Peak field area. First, faults will be described, then folds, foliation, lineation, and cross-sections. Figures 49 through 60 record the field data, plotted according to domains of consistent structure.

Faults

The gneisses, granites and mylonites of Francis Peak are cut by systems of normal faults and ductile extensional faults (Plate 1). The study area is bisected by the Francis Peak normal fault zone (FPFZ). West of this zone, faults have a dominantly normal sense of movement. East of the FPFZ, faults show both thrust and normal movement. In the next chapter, a model for development of the faults is proposed.

A series of north-south, steeply dipping normal faults comprise the FPFZ (Plate 1). No ductile deformation is associated with these faults and cumulative movement on the faults is on the order of tenths of kilometers to kilometers. The faults were mapped as narrow outcrop-scale breccia zones or macroscopic, 100 m. wide zones of intense brecciation. The major faults follow valleys, or zones where the abundance of breccia is significant. The geometry and map traces of the fault zone are basically identical with that of

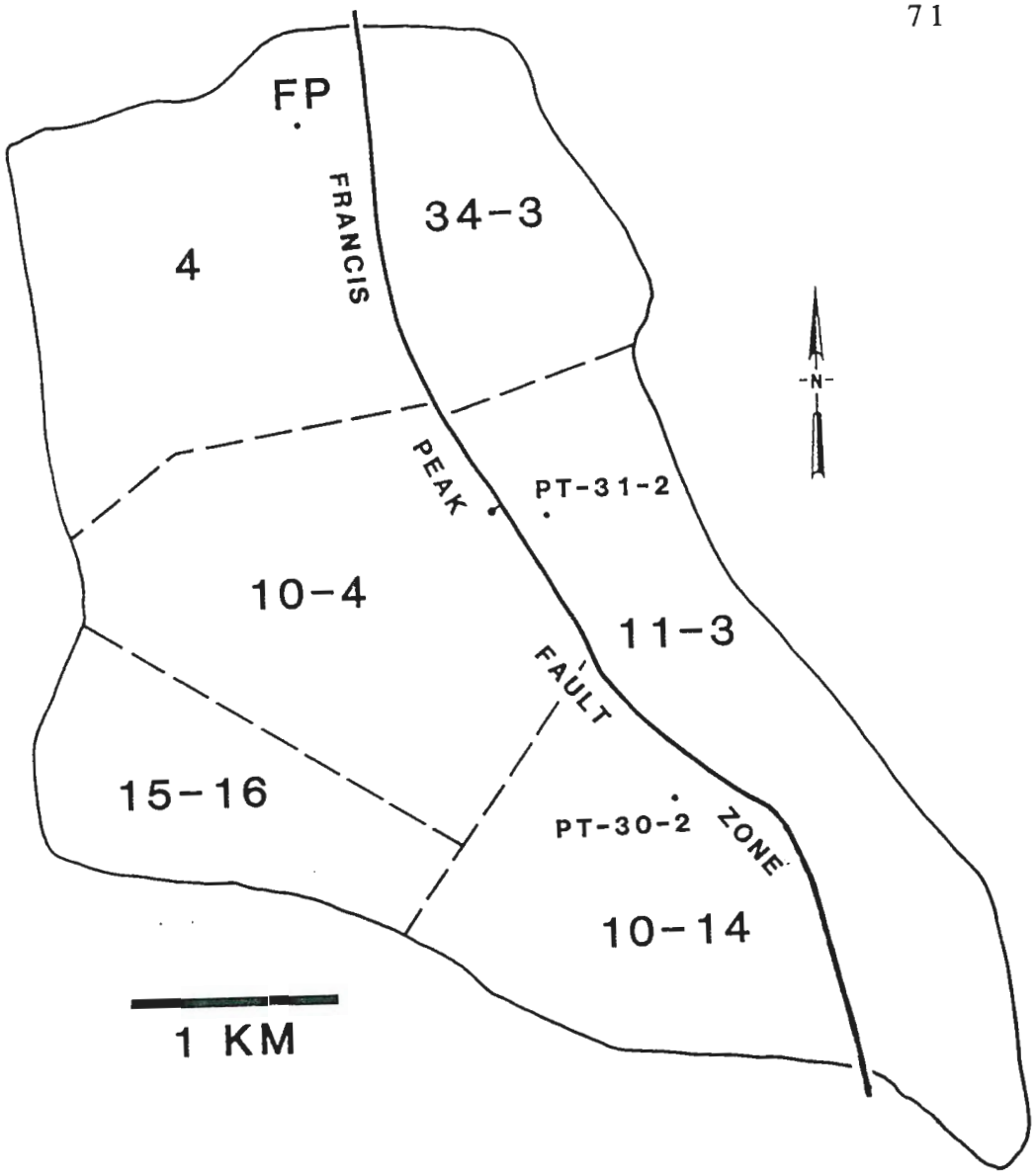

Fig. 49 Location map of field area divided into domains of similar structural geometry. Domain numbers refer to sections each domain covers in R1E, T2N and R1E, T3N of the Peterson and Bountiful 7 1/2 minute topographic quadrangles. Domain 10-4 falls mainly in sections 10 and 4. Points 30-2 and 31-2 are locations where detailed measurements were made.

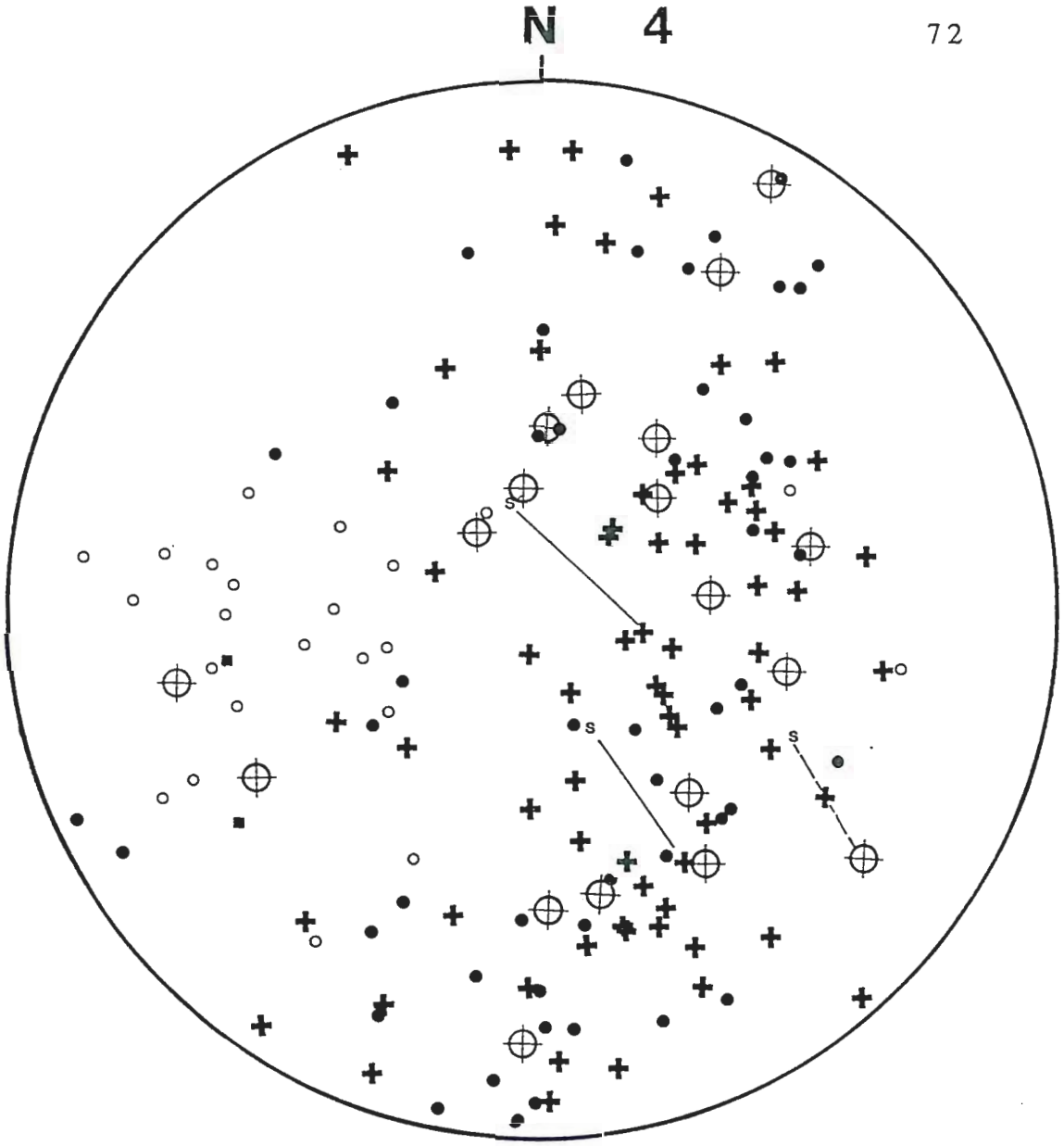

Fig. 50 Stereographic projection (Wulff net) of the structural data from domain 4. Lines are drawn between S-surfaces and corresponding foliation surfaces.

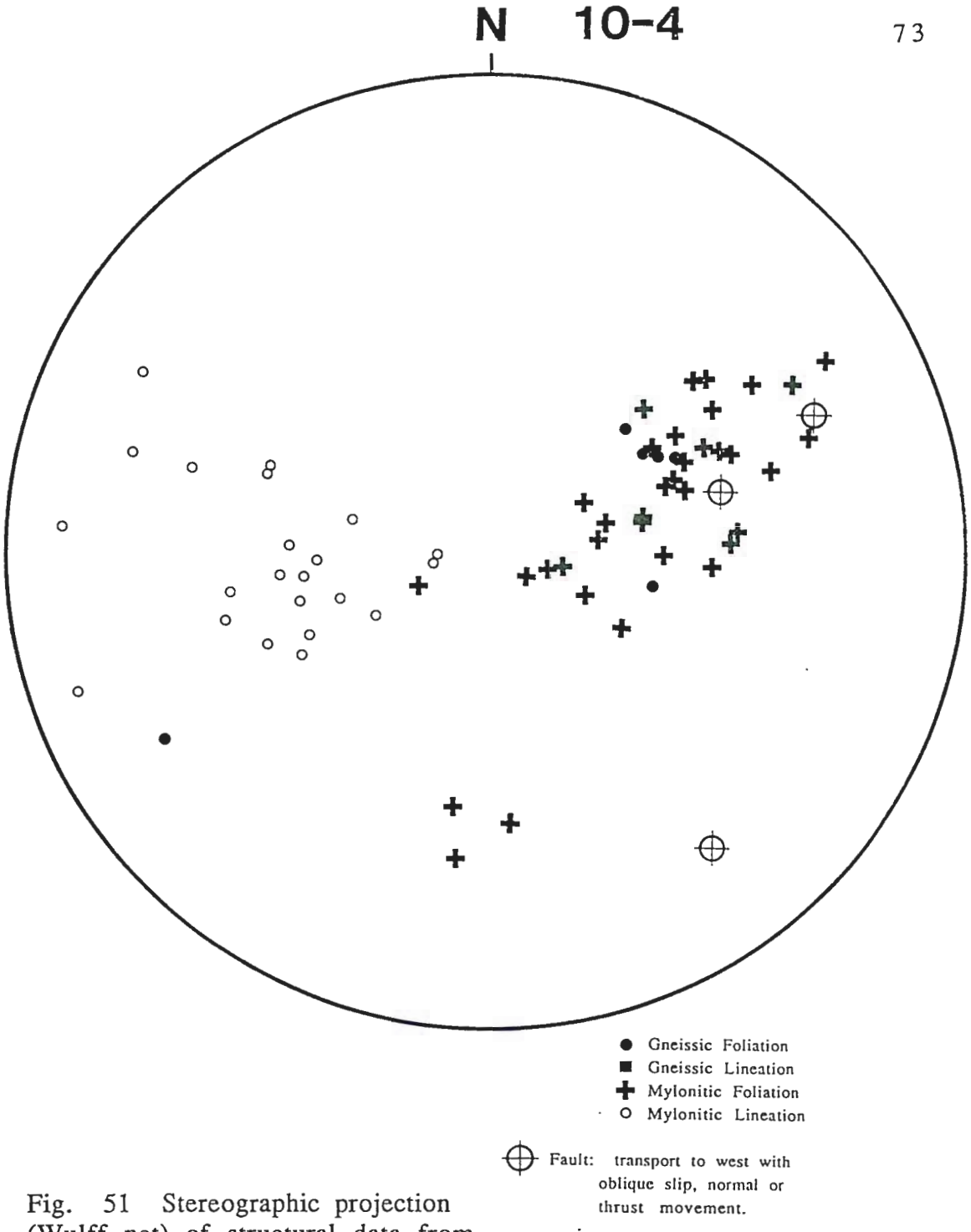

Fig. 51 Stereographic projection (Wulff net) of structural data from domain 10-4.

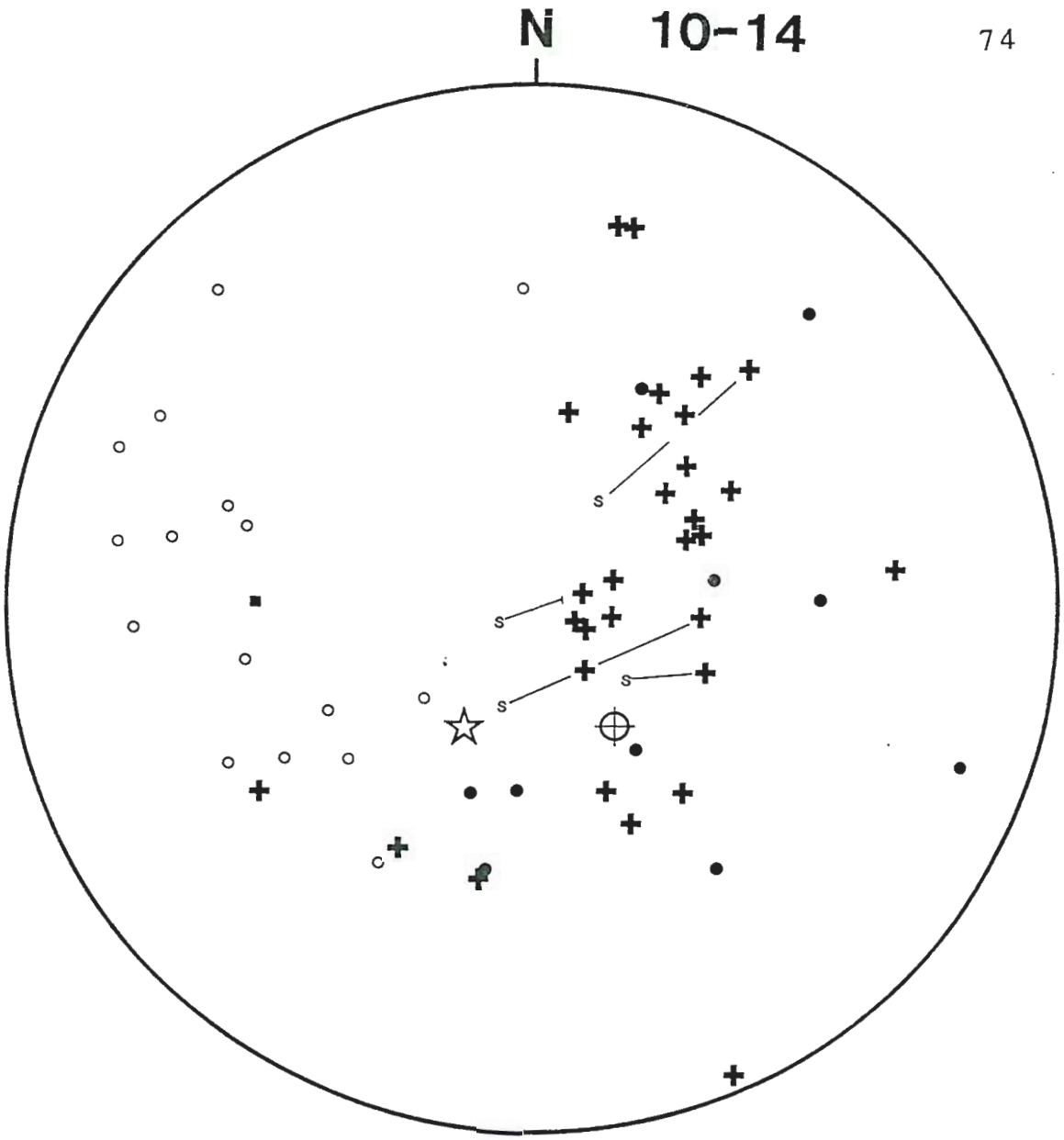

Fig. 52 Stereographic projection (Wulff net) of structural data from domain 10-14. Lines are drawn between S-surfaces and corresponding foliation surfaces.

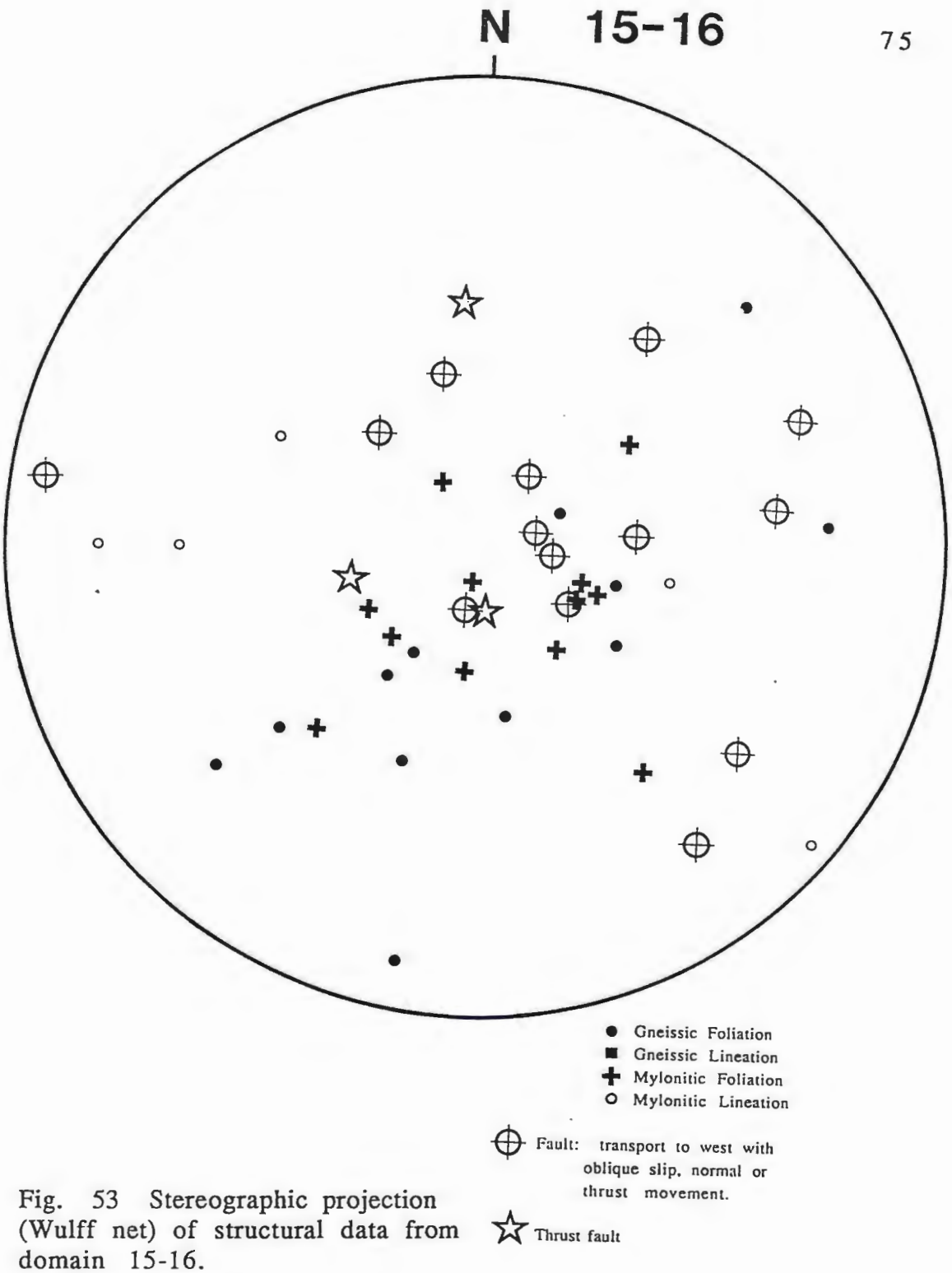

Fig. 53 Stereographic projection (Wulff net) of structural data from domain 15-16.

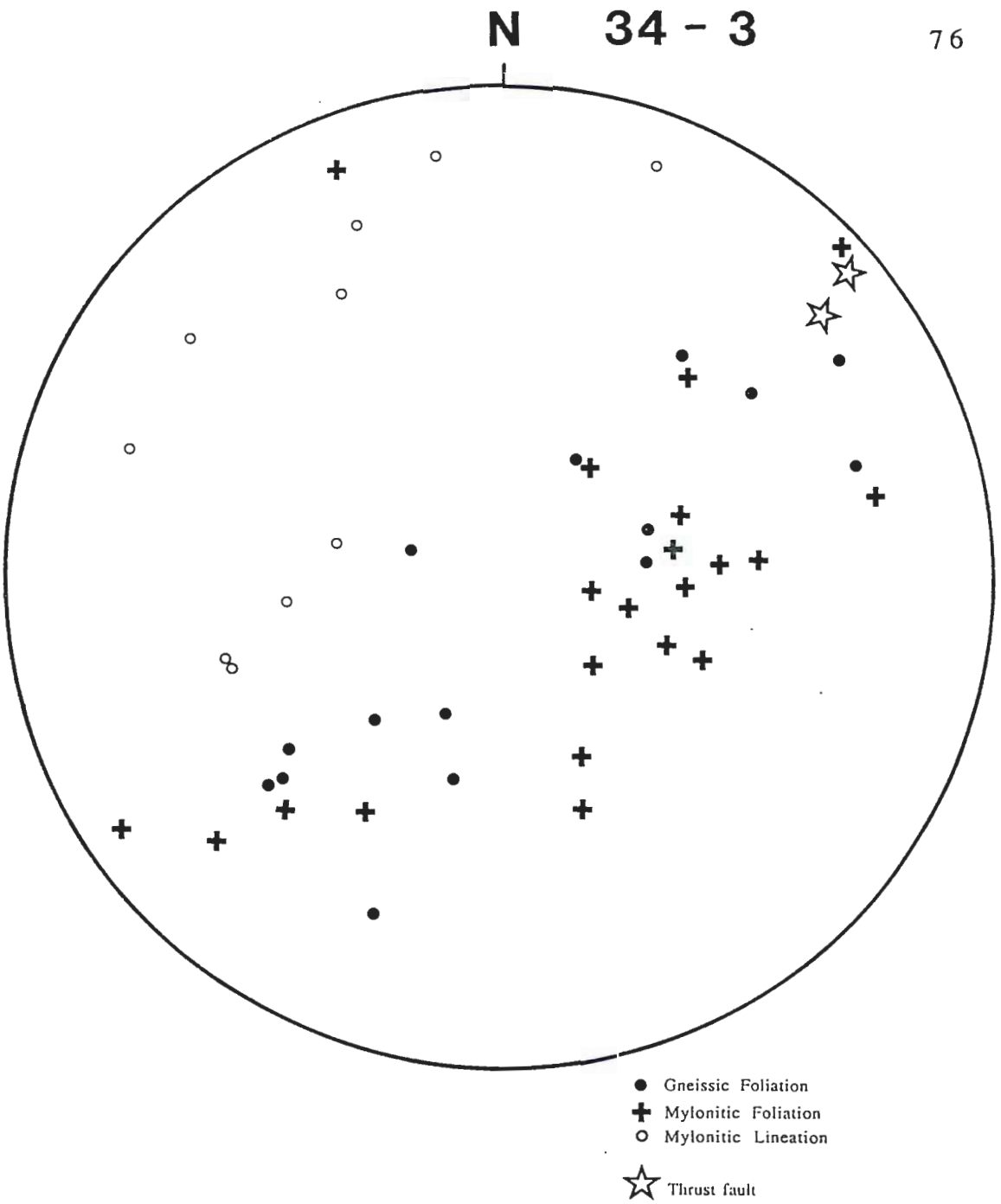

Fig. 54 Stereographic projection (Wulff net) of structural data from domain 34-3.

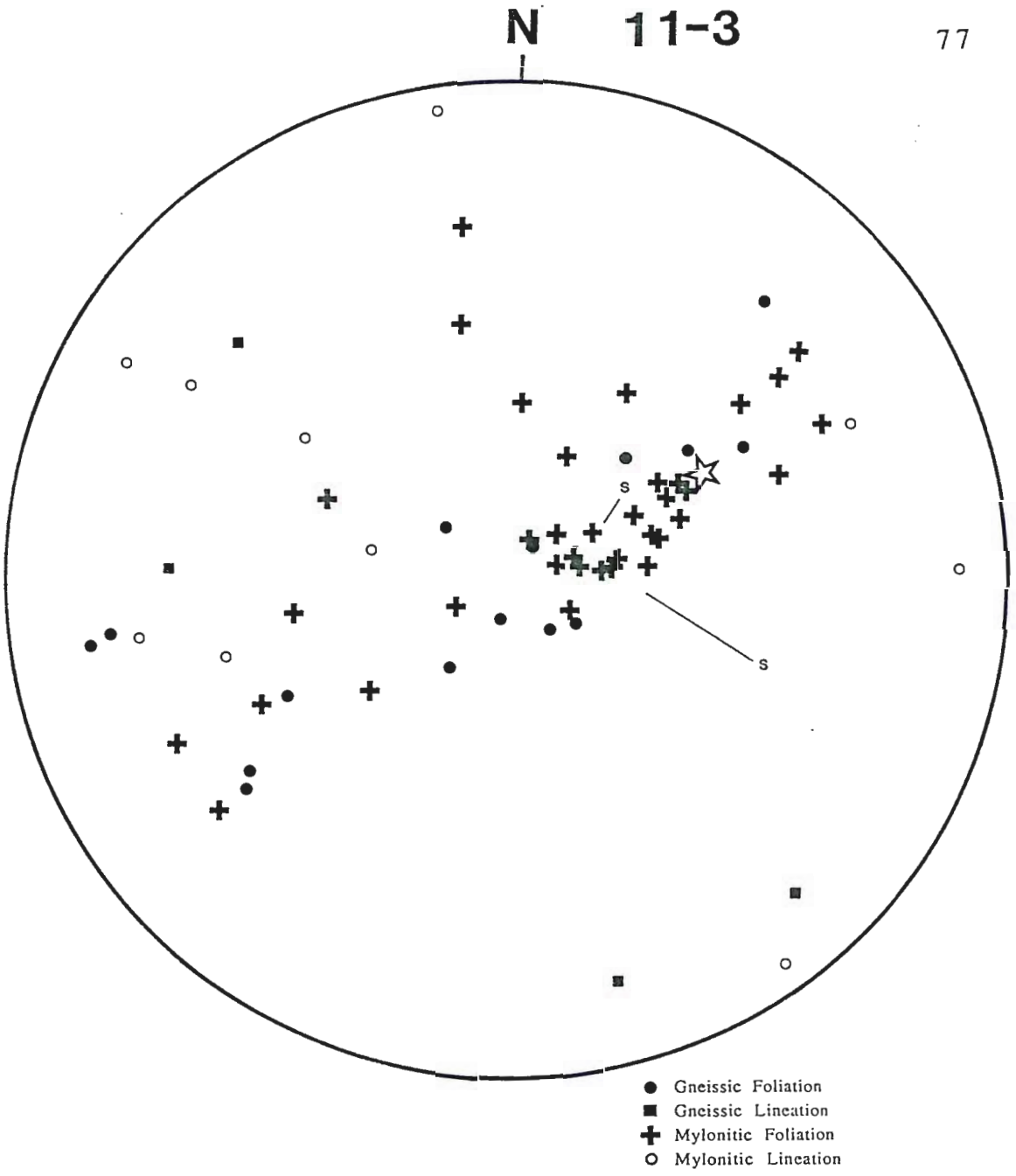

Fig. 55 Stereographic projection (Wulff net) of structural data from domain 11-3. Lines are drawn between S-surfaces and corresponding foliation surfaces.

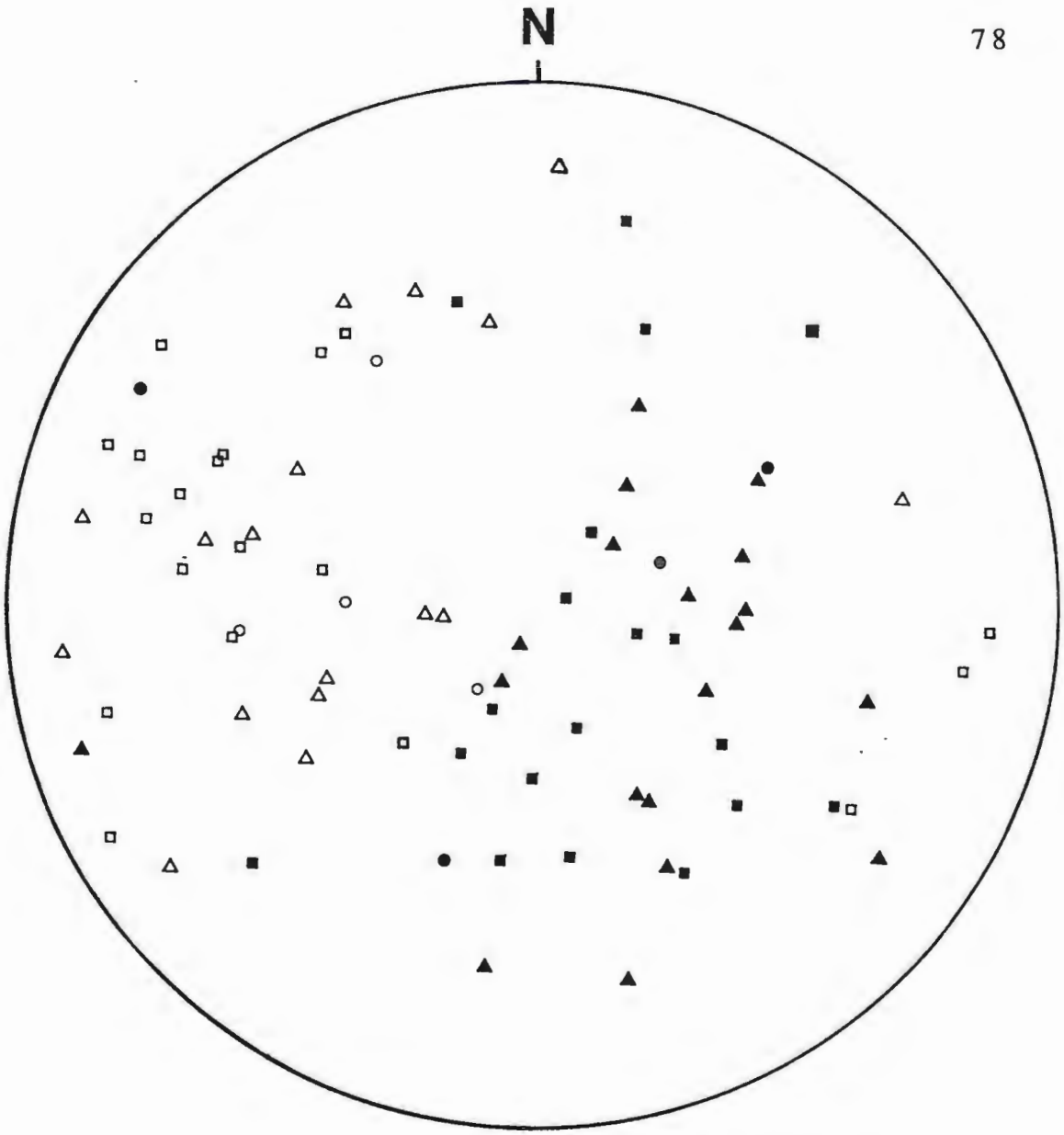

Fig. 56 Stereographic projection (Wulff net) of fold data from west of the FPFZ. Brittle folds are not plotted.

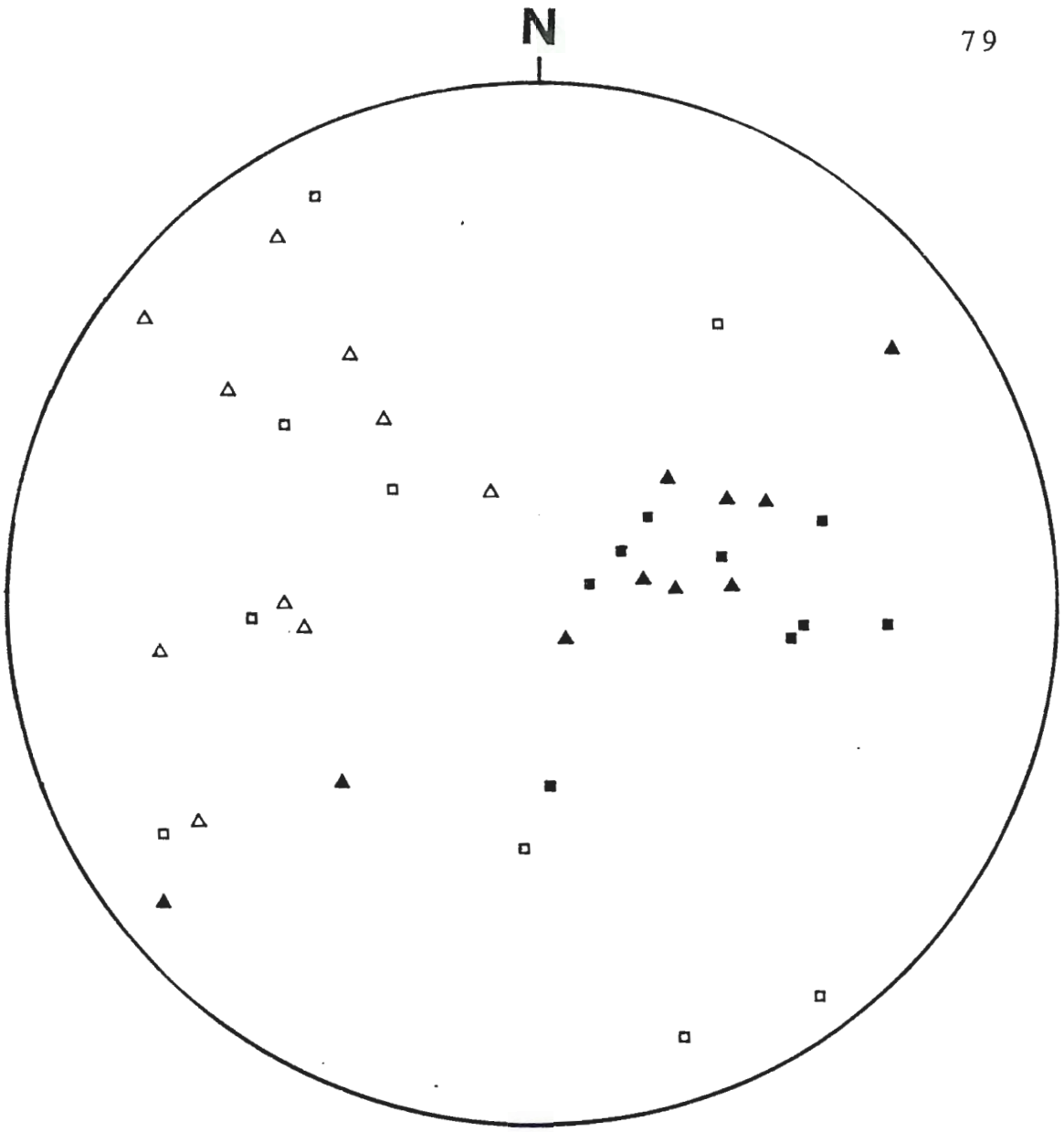

Fig. 57 Stereographic projection (Wulff net) of fold data from **east** of the FPFZ.

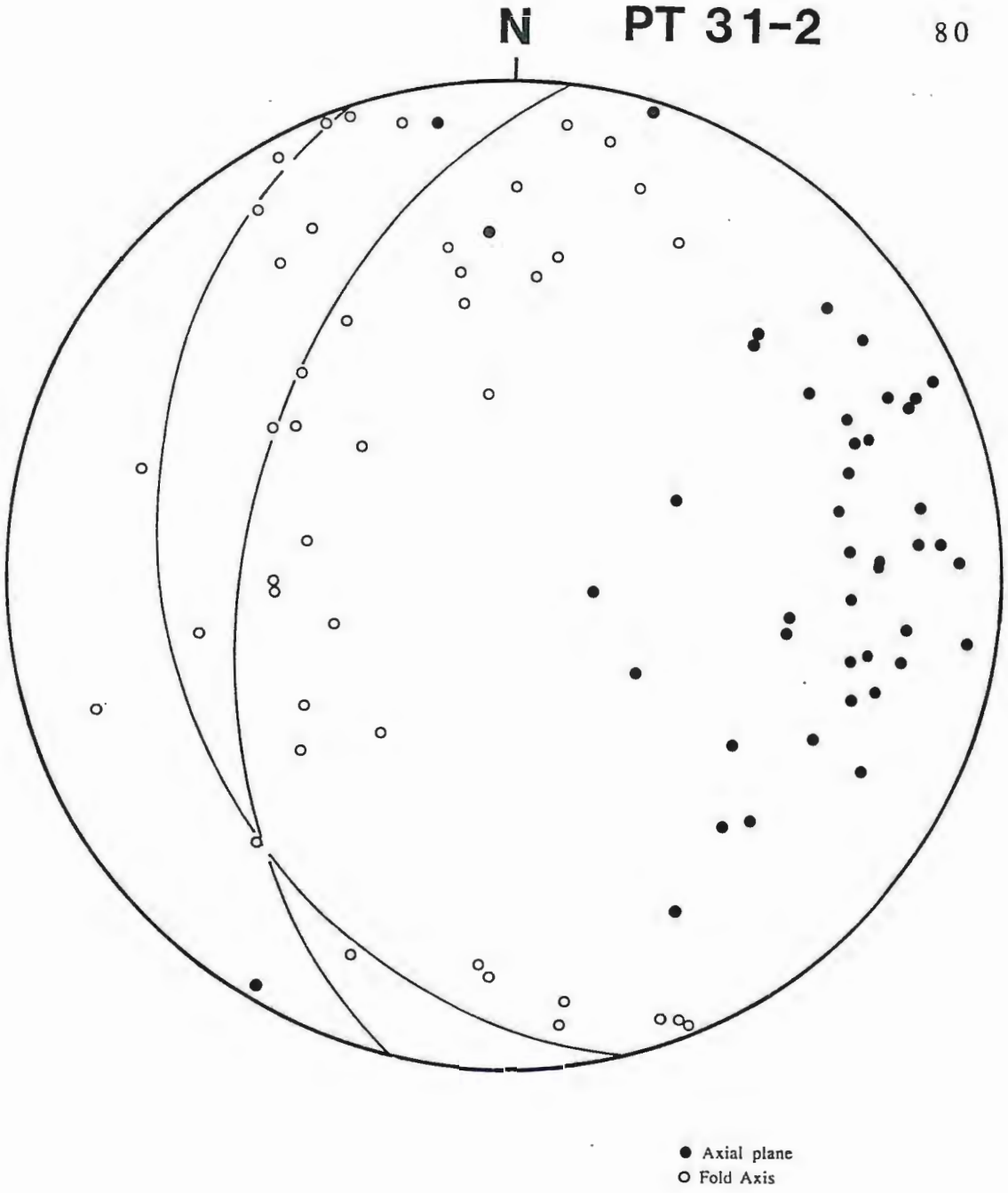

Fig. 58 Stereographic projection (Wulff net) of fold data from PT-31-2.

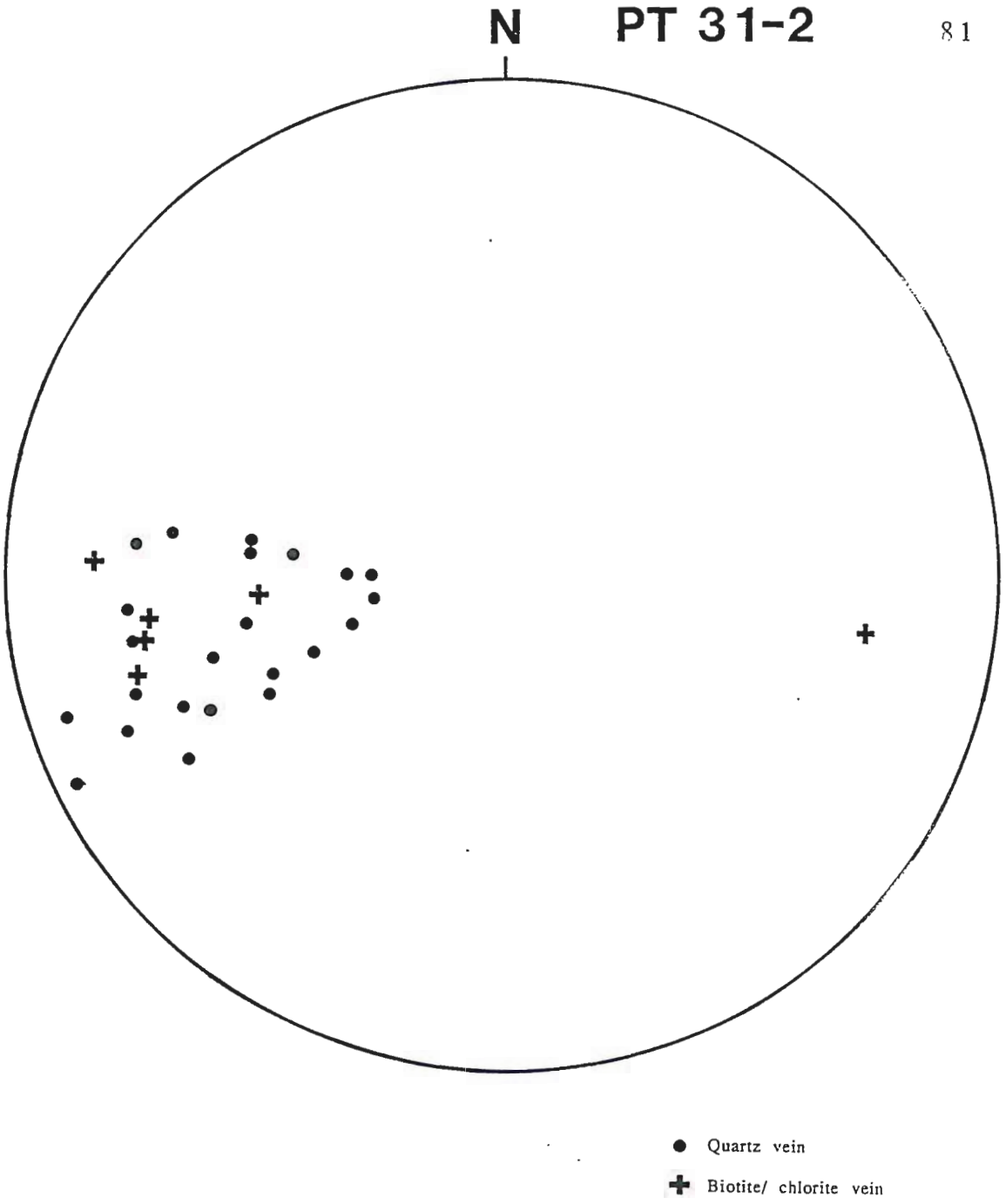

Fig. 59 Stereographic projection (Wulff net) of tension gash data from PT-31-2 located in south-central section 3.

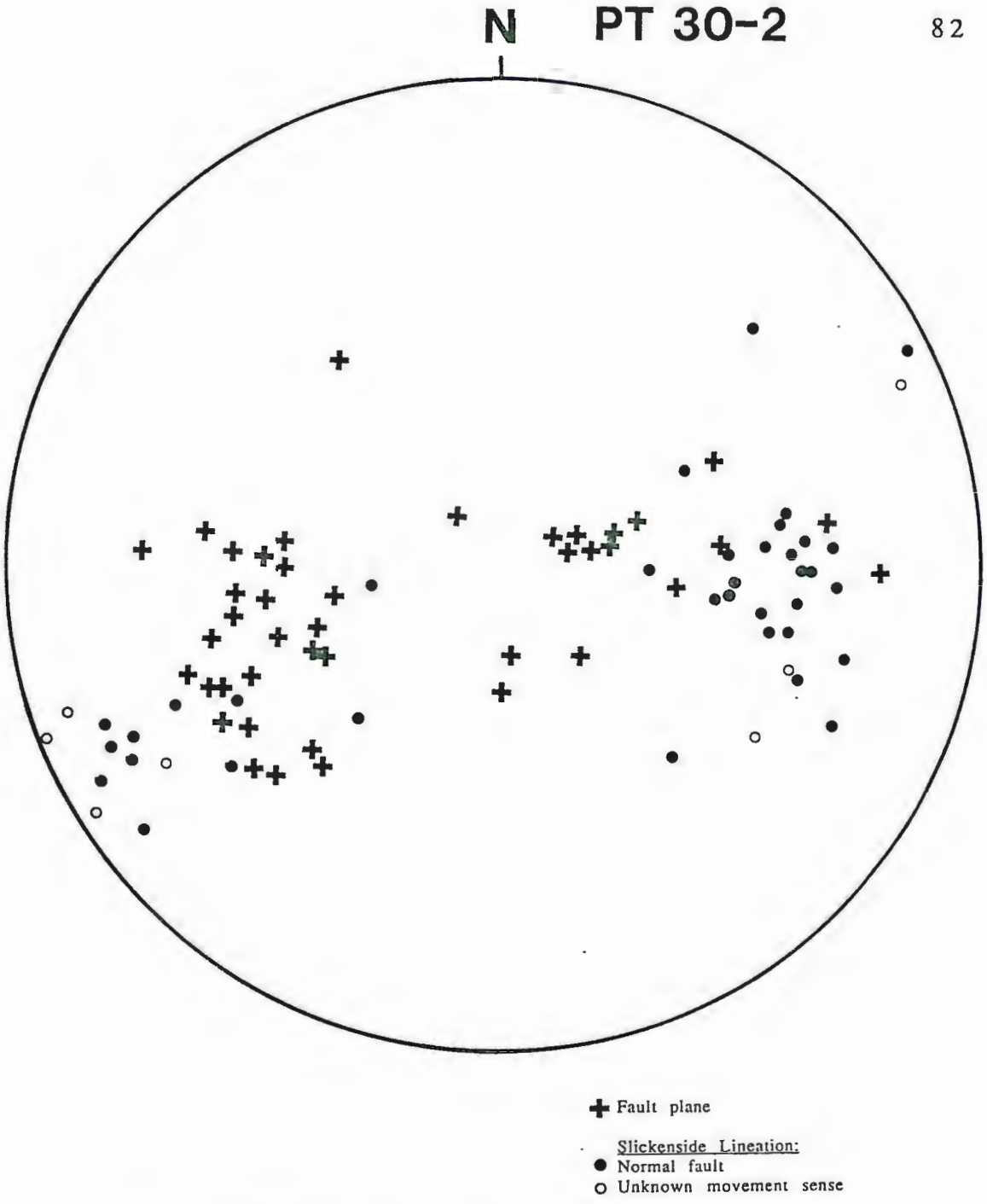

Fig. 60 Stereographic projection (Wulff net) of fault plane data from PT-30-2.

Bryant (1984). In accord with Bryant (1984) and Naesser and Bryant (1983), the present author believes Francis Peak rocks to be down thrown to the west, because the western block is capped by Tertiary Wasatch Formation near Bountiful campground. The FPFZ is believed to be Tertiary in age and related to Basin-and-Range normal faulting.

Another fault system, of large-scale normal faults, striking roughly north-south and dipping to the west, was mapped on Francis Peak and the ridge to the south (Plate 1). These faults are associated with intense ductile deformation. The strike of these faults is generally north-south, except in section 4 on the western side of the FPFZ where the faults tend to strike NE to E. This change in structural style is corroborated by a comparison between plate 1 and figures 50 and 51. Although the faults are not traceable across the FPFZ, they are traceable along strike for up to two miles. These faults vary widely in attitude, thus making reliable cross-sections difficult to construct.

At only a few locations could major fault surfaces actually be seen. Exposed surfaces tend to be minor faults, associated with zones less than a meter wide, and not traceable for more than 200 m. Large-scale faults were identified by either a change in the attitude of foliation across the fault or the coincidence of mylonitic foliation with topography (Fig. 61).

Despite the change in attitude of foliation across major faults, meso-scale cylindrical folds were not observed due to poor exposure. Cylindrical folds were, however, found on the outcrop scale. There is

no evidence for fault-bend folds (Suppe, 1983) or frontal ramps. Most faults are planar and laterally continuous as can be demonstrated with strike lines on plate 1 on faults east of the FPFZ. In general, movement on the major faults failed to fold the rocks.

Populations of meso-scale ductile normal faults are associated with the large-scale faults. In transverse (normal to lineation) cross-section (Fig. 62), these faults bound horses (Boyer and Elliot, 1982) of rock that are eye shaped. Most of these normal faults have an asymmetric fabric adjacent to them that indicates sense of shear. Poles to these faults plot in the midst of poles to gneissic and mylonitic foliation, all three sets of structures dipping to the west. This geometry suggests that the faults formed on surfaces subparallel to foliation, and may have nucleated as foliation plane detatchments.

A system of minor ductile extensional faults cuts the rocks of Francis Peak. These faults are probably associated with the meso-scale faults that bound the horses. They are generally shallowly dipping to subhorizontal and are not associated with brecciation of the rocks: they are single surfaces of detachment. Figures 50 through 53 show poles to fault planes not designated thrusts. These faults may be thrust, normal or oblique slip faults. They exhibit some evidence for movement direction, such as rotation of fabric, step-like slickensides or off-set pegmatite dikes and veins. Collectively, the faults show dominant movement of hanging wall rocks toward the west (Fig. 63). It is important to note that these faults are located exclusively on the western side of the FPFZ.

Fig. 61 Looking south at 250 m. face in southcentral part of section 3. At top of cliff lies 5-20 m. of phyllonite and mylonite. Layered gneisses at base of face were little affected by mylonitization.

Fig. 63 Minor west directed thrust in phyllonitic layered gneiss. Pen lies parallel with foliation in lower part of outcrop. Detachment surface essentially follows border of shadow. Location F-35.

Fig. 62 View to the west of small horses bound by minor faults. Small pine tree is 4 m high. Below is a line drawing of the photo showing location of the faults (dashed lines). Located at bend in Whipple creek in center of section 10.

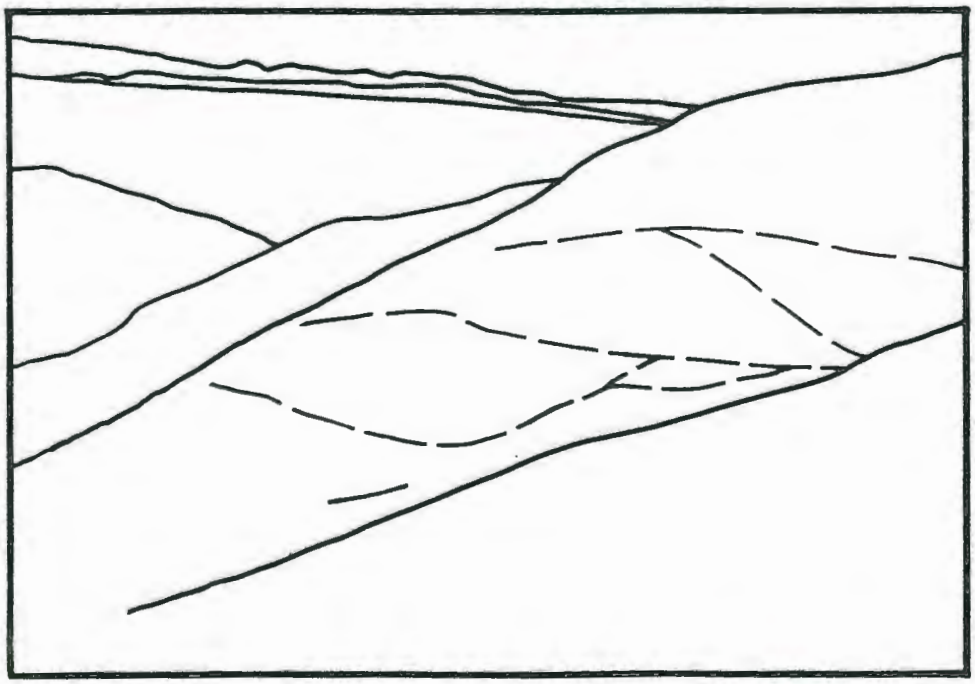

These minor ductile extensional faults were studied in detail (Fig. 60 and 60B below) at an outcrop, just west of the FPFZ, Pt 30-2 (see fig. 49 for location). On figure 60 there is two sets of faults, one subhorizontal set and one east-dipping set. Though almost all of the faults are normal faults, the subhorizontal set generally exhibits large displacements parallel to foliation. The east-dipping faults exhibit only small displacements and generally cut the foliation. Movement of hanging wall rocks on the subhorizontal faults is to the west, and that on the east-dipping faults is to the east. Movement was determined from step-like, quartz-mica slickensides exposed on almost every fault surface. East-plunging slickensides curve asymptotically toward the subhorizontal fault surfaces, suggesting that west-directed shear on the subhorizontal faults has deformed the east-plunging slickensides. It seems that both sets of faults and associated shear fabric were generated during one event, which involved bulk westward-directed noncoaxial shear, with layer parallel extension of the material taking place on the east dipping faults and westward transport taking place on the subhorizontal faults.

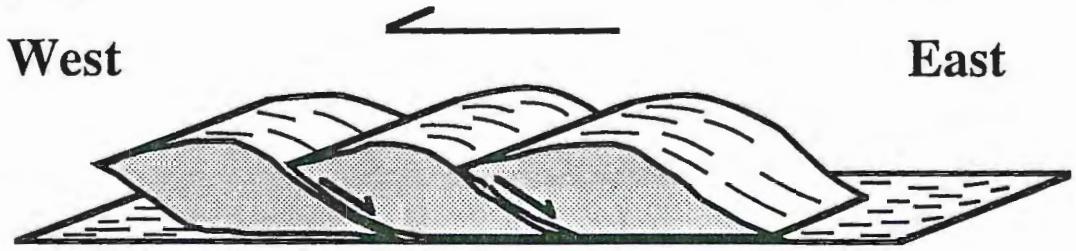

Figure 60B

Folds

There are two sets of folds in the rocks of the Farmington Canyon Complex, those in the gneisses and those in the mylonites. The folds exist on the macro, meso, and micro-scales, but only macro and meso-scale folds will be addressed here. First, the relationship between the macro-scale folds of Francis Peak and the rest of the Farmington Canyon Complex will be explained. Second, folds in the layered gneisses and mylonites will be described and contrasted. Finally, detailed analysis of an exposure of folds in mylonite, from the east side of the FPFZ will be presented.

One large-scale fold was found on Bountiful Peak by Eardley and Hatch (1940). The two folds may be related, but this is not apparent as their attitudes differ widely. No other folds of this scale have been reported in the Farmington Complex, though a detailed study and adequate reconnaisance mapping have been done (Hollet, 1979; Bryant, 1984).

Meso-scale, open to isoclinal folds are common in the layered gneisses (Fig. 6 and 64). These folds are essentially cylindrical and harmonic. Folds in the deformed layered gneiss, on the other hand, are rather disharmonic. This is probably because of the inhomogeneous nature of deformation associated with mylonitization. Isoclinal folds seem to grade into tight and open folds in adjacent outcrops.

Axial planes dip and fold axes plunge gently to the west in the folded gneiss (Figs. 56, 57). On the stereonets, though the data are

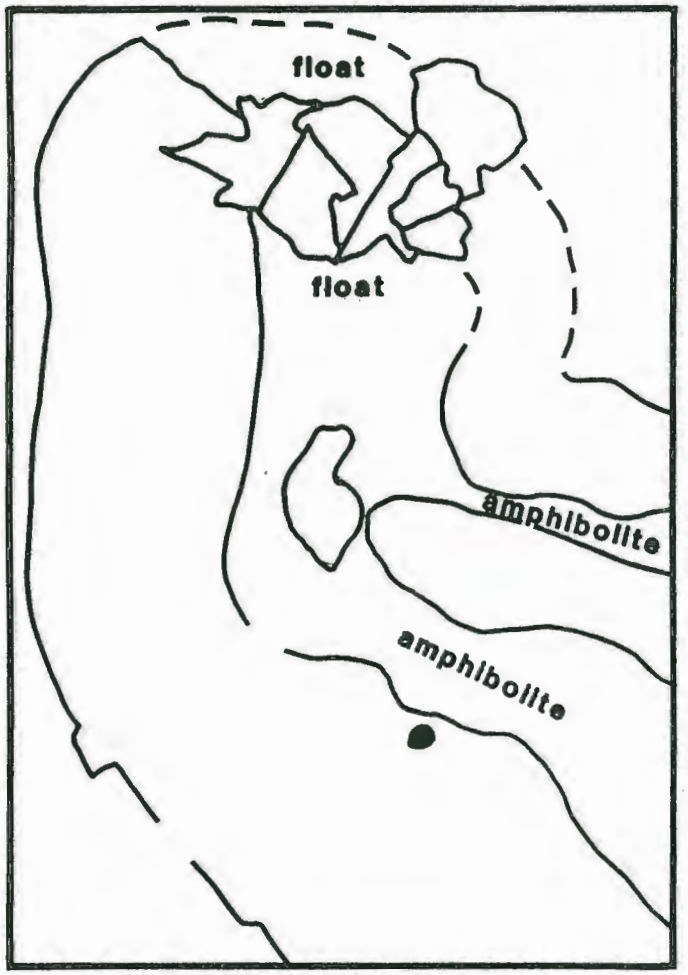

Fig. 64 Large fold in layered gneiss with amphibolite gneiss wrapping around hinge. Lense cap is 52 mm. At left is a line drawing of the same fold, lines dashed where inferred. Location F-34.

limited, axial planes of open folds are indistinguishable from those of tight to isoclinal folds. This suggests that the folds are of one generation. Indeed, axial planes of folds from east of the FPFZ are well clustered, though the fold axes are quite variable in orientation. Poles to axial planes west of the FPFZ describe a rough great circle arc. These axial planes may have been folded on an axis that trends N 56 W and plunges 30 W, however, the girdle is rather weak.

Folds in the mylonites are ubiquitous, but differ in style from those in other Farmington Canyon Complex rocks (Fig. 65). Folds in the gneisses are usually cylindrical and symmetrical and can be classified as parallel folds (Class 1B of Ramsay,1967). Folds in the mylonites, on the other hand, are usually isoclinal or tight, mostly disharmonic and can be classified as similar folds (Class 2 of Ramsay, 1967). Folds in the mylonites are defined by ribbons of pure recrystallized quartz and feldspar. Lineation on the surface of quartz-rich layers is folded, suggesting that the lineation was present before folding (Fig. 66). The intensity of folding (and deformation) in the mylonites increases toward faults. Asymmetric fold trains usually indicate the sense of shear on the faults.

The orientation of folds in the mylonite is consistent throughout the study area, however, folds from the west side of the FPFZ are in contrast with folds from the east side (Figs. 56, 57). Overall, folds in the mylonite have axial planes that dip west and fold axis lineations that plunge west. Axial planes from folds in the west (Fig. 56) define a great circle girdle similar that of axial planes from the layered gneiss. The rocks were undoubtedly folded together, for it is

Fig. 65 Typical folds in the mylonites at F-50. Folds can be open, isoclinal or isoclinal and highly disharmonic.

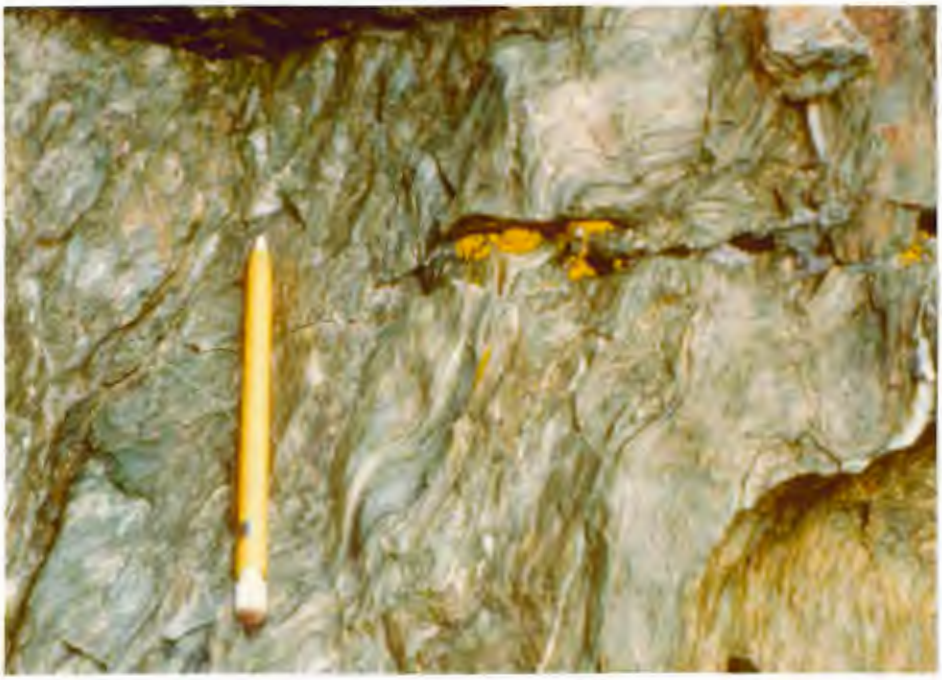

Fig. 66 Lineation in this mylonite is folded. Pencil lies subparallel with fold axes. Location F-46.

impossible to distinguish axial planes, or folds axes, of folds in the mylonite from those in the layered gneiss. Poles to axial planes from the east side of the FPFZ (Fig. 57) delineate a distinct maxima and perhaps a weak girdle striking N 53 W. Fold axis lineations have a more northwesterly trend, and again the data for folds in the gneiss are inseparable from those from the mylonite. A comparison between figures 56 and 57 reveals that the geometry of the data is similar, though quite distinct, in that poles to axial planes in the east are well clustered and those in the west are not.

Some folds seemed to have formed under more brittle conditions than others. In these folds, quartz ribbons are commonly fractured at the hinge, making the fold chevron-like (Fig. 67). Alternatively, the hinge area may be brecciated altogether (Fig. 68). In fractured folds, quartzofeldspathic material tends to be fractured and micaceous material generally flows and fills or recrystallizes in the fractures.

Detailed measurement of brittle folds in the mylonite was conducted on the ridge in the south-central portion of section 3 at PT-31-2 (Fig. 58). These rocks lie just below a major west-dipping fault and in a zone of intense ductile deformation. Axial planes of these folds dip steeply west and form a diffuse maximum on figure 58. Note that vergence of all the folds is to the east; that is, axial planes dip more steeply to the west than the foliation surfaces (great circles). Fold axis lineations describe a distinct girdle that dips more steeply than the average mylonitic foliation plane. The attitudes of many quartz or mica filled tension gashes were also measured at PT-

Fig. 67 View looking south at brittle chevron folds in mylonite that have snapped hinges. Asymmetry of folds suggests transport to the east. Rocks located on east side of FPFZ.

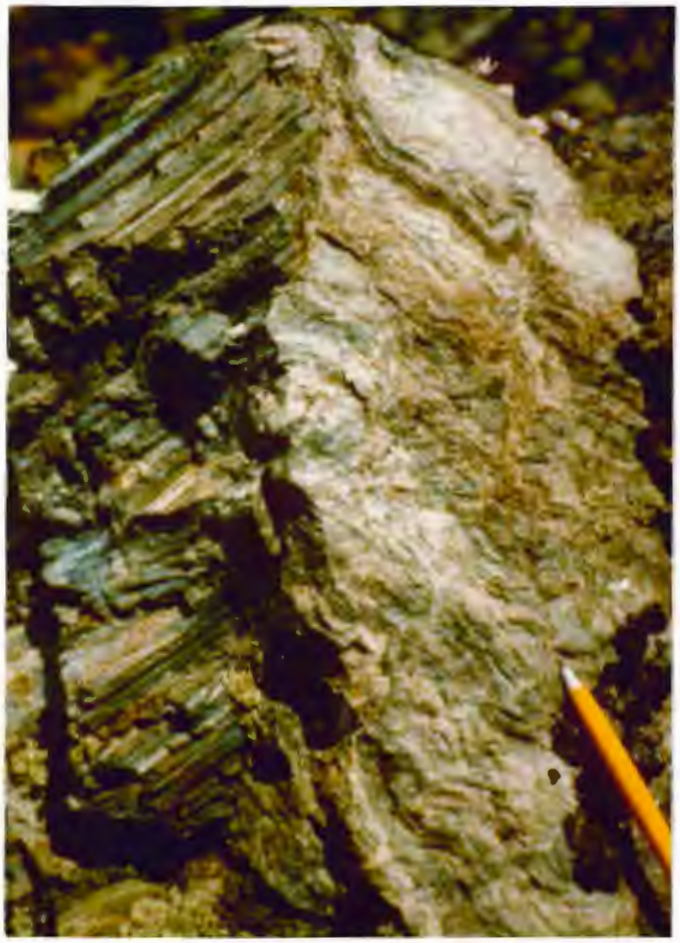

Fig. 68 View looking north at shattered hinge of fold in ultra-mylonite. Rocks are located on east side of FPFZ at PT-31-2. Assymetry of fold suggests transport to east during brittle deformation.

31-2 (Fig. 59). Quartz or mica planes may represent the Y-Z plane of the strain increment during fracture. These planes lie subperpendicular to the average mylonitic foliation plane and they were probably rotated on an E-W axis after their formation. The most deformed tension gashes have poles that plot nearly horizontal suggesting a top to the east sense of shear. These tension gashes are probably related to the same semi-brittle deformation that fractured the hinges of the folds.

Fabric

The purpose of this section is to describe the meso and macroscopic planar and linear fabrics of Farmington Canyon Complex protoliths and mylonites.

The stereonets from the west side of the FPFZ, figures 50-53 will be considered first, starting with the highest topographic level and moving down the ridge to the south. Figure 50, from domain 4, shows that foliation in the layered gneiss and the mylonite generally dips to the west, and may have been folded as shown by the girdle of gneissic foliation poles. Lineation in both the layered gneiss and the mylonite plunges moderately to the west. The foliation and lineation in the layered gneisses are nearly identical with those in the mylonites. In no other portion of the study area, east or west of the FPFZ, is their such a fanning of data as that on figure 50. Figure 51, from domain 10-4, has an excellent cluster of west-dipping mylonitic

and gneissic foliation planes, corresponding to a west-plunging cluster of linear elements from the mylonites. These data were obtained from a package of minor sheets that lie above a major fault (Plate 1). The north-dipping mylonitic planes are from the boundary between domains 4 and 10-4, and may define a transition from the structural style of domain 4 to that of domain 10-4. The structure of domain 10-14 (Fig. 52) is similar to that of domain 10-4, though some fanning of the data is evident. Figure 53 is from data obtained in Farmington Canyon, domain 15-16, at a much lower topographic level than the other data (Plate 1). Mylonitic and gneissic foliation, as well as fault planes, are much more horizontal compared to other domains in the study area.

Data from the east side of the FPFZ are shown in figures 54 and 55. These data sets are almost identical, suggesting great consistency in structural geometry along strike east of the FPFZ. In general, poles to gneissic and mylonitic foliation planes plot amidst each other and form a girdle that strikes NE-SW, suggesting folding of the foliation on a northwesterly axis. Most mineral lineations plunge to the northwest.

A comparison between data from the east side of the FPFZ (Fig. 54, 55) with that from the west side (Figs. 50-53) reveals two important differences. Structural data from east of the FPFZ is extremely consistent along strike, whereas the data from the west side of the FPFZ varies greatly from one domain to another. Another difference is that on the east side of the FPFZ, mylonitic and gneissic lineation plunge more toward the NW than the W. A 40°

anticlockwise rotation on a vertical axis of the data from the east side would bring the two data sets, east and west, into close allignment. A general comparison between the structural data from east and west of the FPFZ leaves little doubt that there is a significant structural discontinuity across the FPFZ.

To summarize the stereonets, mylonitic and gneissic foliations dip to the west and lineations plunge to the west throughout the study area. Since the data sets from east and west of the FPFZ are grossly similar it is reasonable to suggest that both sets of structures are subsets of the same large scale fault system. However, structural data from east of the FPFZ appears to be rotated with respect to the data from west of the FPFZ. Perhaps the structures on the east side of the FPFZ formed at a different structural level from those on the west.

In the deformed rocks of Francis Peak there are many surfaces that are not included on the stereonets, discussed below, along which deformation took place. These surfaces are either anastamosing or planar, or rather consistently oblique to the main foliation. The oblique fabrics in the mylonites yielded especially valuable structural data.

S-surfaces (Berthe et al., 1979) were found in the phyllonites and mylonites (Fig. 16, 69). The phyllonites are usually anastamosing in three dimensions, but some s-c phyllonites were found. S-surfaces are usually penetrative, bounded by C-surfaces (Berthe et al., 1979) or mylonitic foliation surfaces, making an angle of 25-30 degrees with the C-surfaces. The intersection of foliation

Fig. 69 View north of S-surfaces in a phyllonite that are truncated by C-surfaces that are spaced. Found in rocks on west side of FPFZ and suggests transport to the west. Location F-3.

and S-surface is a line that is perpendicular to lineation, and in the foliation plane. S-surfaces verge in the direction of tectonic transport and should not to be confused with a transposed foliation, although they both indicate the same sense of shear. Several examples of S-surfaces that showed a consistent sense of shear are plotted on figures 50, 52, and 55. Note that movement on upper plate rocks containing these structures is from + (foliation surface) to S (S-surface), on the diagrams. The sense of movement in each part of the study area is consistent. Over the area as a whole, however, sense of movement is strongly divergent (Plate 1). Sense of shear on the west side of the FPFZ is either to the NW or SW and that on the east side of the FPFZ is both east and west. These observations concern the development of the structures on Francis Peak and will be interpreted in the next chapter

Shear bands (Simpson, 1986) are quite common in the mylonites of Francis Peak (not plotted on stereonets). These bands are only a few centimeters long and 2-3 mm. in width. The intersection between mylonitic foliation and shear bands defines a line perpendicular to lineation. The angle between the two planes is approximately 20-45 degrees and the shear band verges in the direction <u>opposite</u> that of tectonic transport. Simpson (1986) claims that the sense of shear on the band is sympathetic with that of the zone as a whole, and thus can be used to determine sense of shear.

Cross-sections

Three cross-sections have been drawn through the Francis Peak field area (Figs. 70 A,B,C). These sections have been drawn on roughly E-W lines, nearly perpendicular to the lineation and major faults (Plate 1). All three sections cross the FPFZ, at which there is marked structural discontinuity. Note that the line of section A-A' changes azimuth at the FPFZ.

The FPFZ is downthrown to the west as evidenced by Tertiary Wasatch Formation capping the western block (Bryant, 1984; and pers. comm.) and fission track ages of apatites from the gneisses of the complex (Naesser and Bryant, 1983). Fission track ages are determined by quantifying the density of fission tracks. The greater the density of tracks, the longer it has been since the rock passed through the apatite annealing temperature. In general, rocks on the west side of the FPFZ yield older ages, indicating that higher level rocks have been downdropped to the west.

Sections A-A', B-B', and C-C' are from progressively lower and more southerly elevations (plate 1), and were drawn through areas that differ in structural style. Sections B-B' and C-C' are quite similar, though they are from different topographic levels. The strike of the structures on section A-A' deviate markedly from that on sections B-B' and C-C'. Each section shows that there is a stack of horses bound by mylonites to the west of the FPFZ. Ductilely deformed zones of similar dip lie across the FPFZ to the east. These zones do not show the consistency of movement sense that was

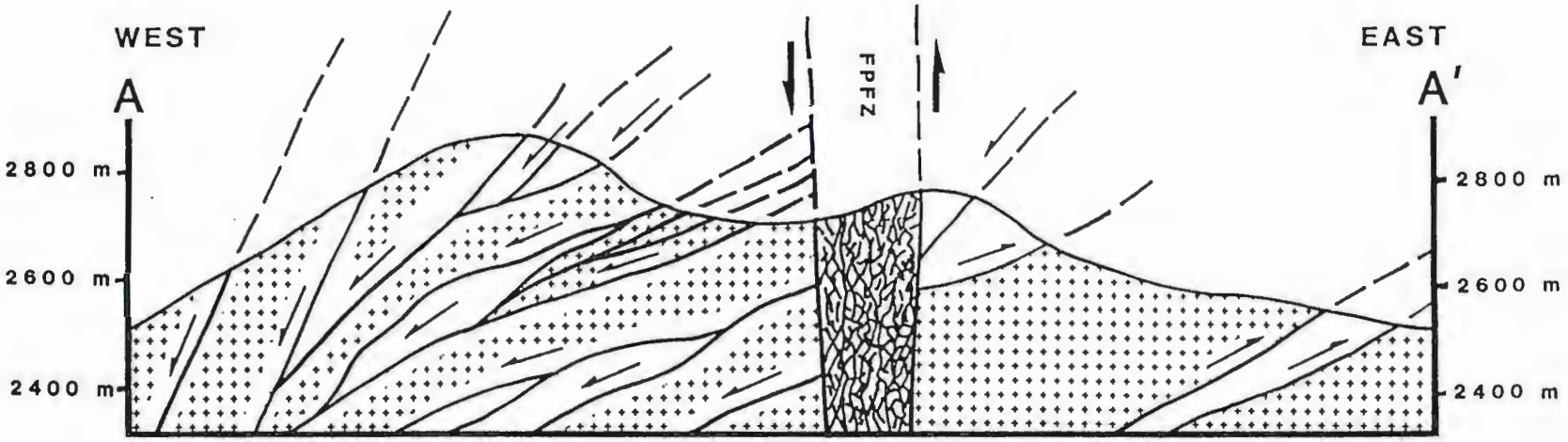

Fig. 70A Cross-section A-A' through the northern portion of the study area (see plate 1 for location of section line). FPFZ is down-thrown to the west. Ductile zone east of FPFZ exhibits both east and west senses of shear. Patterned rock is unmylonitized gneiss, unpatterned rock mylonitized gneiss. Vertical scale = horizontal scale.

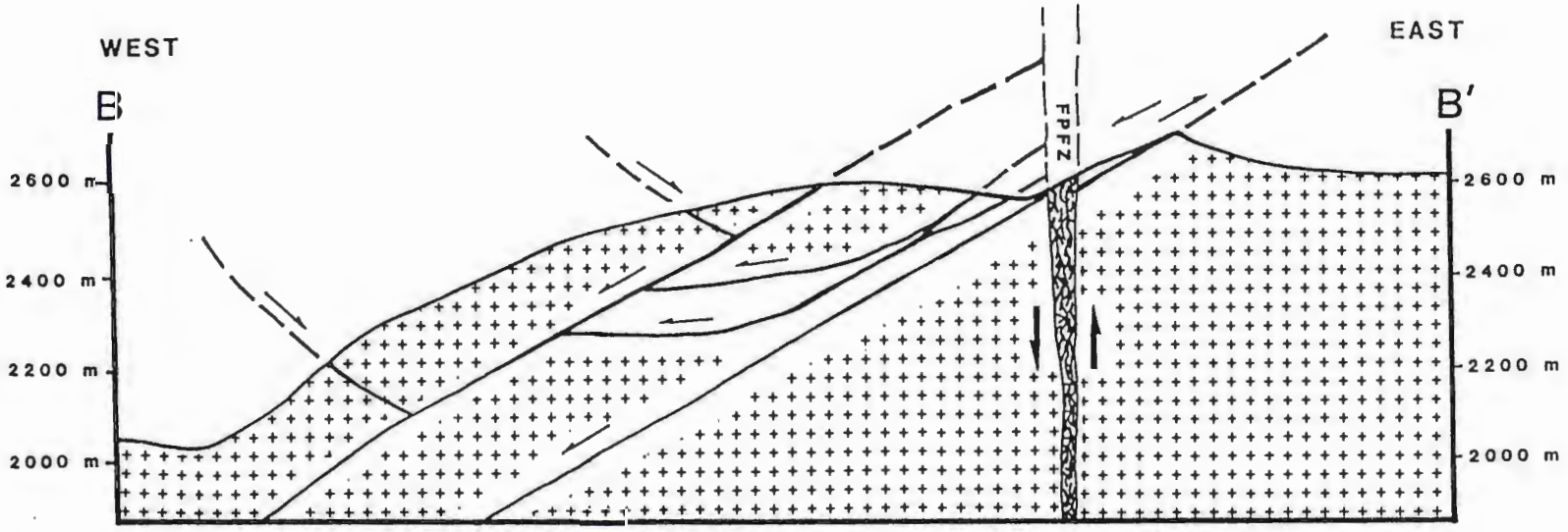

Fig. 70B Cross-section B-B' through the central portion of the study area. Ductile zone east of FPFZ exhibits both east and west senses of shear. Patterned rock is unmylonitized gneiss, unpatterned rock mylonitized gneiss. Vertical scale = horizontal scale.

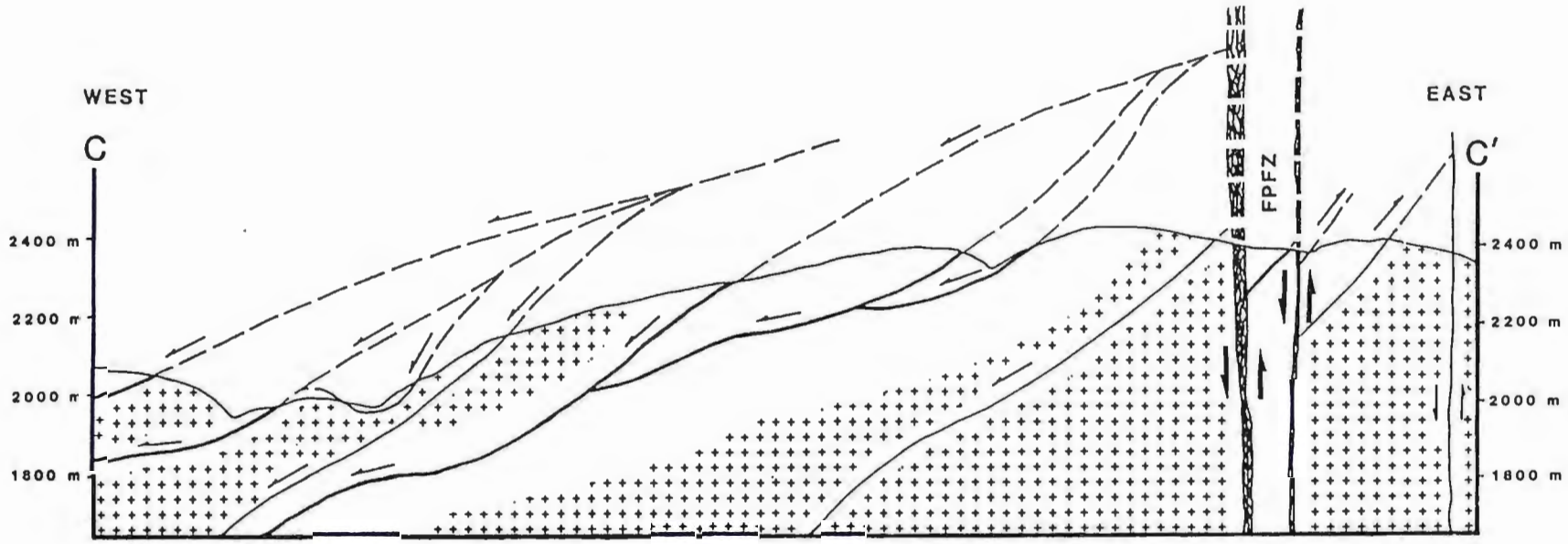

Fig. 70C Cross-section C-C' through the southern portion of the study area. Patterned rock is unmylonitized gneiss, unpatterned rock mylonitized gneiss. Vertical scale = horizontal scale.

observed west of the FPFZ. Rocks on the east side show dominantly up-dip movement, though down-dip movement sense indicators are found.

Faults and mylonitic rocks shown on the cross-sections are only the prominent ones. Minor thrusts are the rule rather than the exception. Thrusts on the scale of figure 63 bound small horses, and may have only a few meters of movement on them. Normal faults are also common away from the FPFZ, though offsets again are on the order of meters and they have had little effect on the larger-scale structures shown on figures 70 A,B,C. The major faults may have had several hundreds of meters of movement on them, and can thus be depicted on cross-sections of the scale of figures 70 A,B,C. Mylonites with thicknesses of less than about 10 cm. have been largely ignored in the construction of the sections. Several meters or tens of meters of either phyllonite or mylonite lie above and below the major faults.

A Comparison Between the Structures of Francis Peak and Bountiful Peak

Bountiful Peak and Francis Peak represent the same present-day topographic level. Whether the two peaks are of the same structural level is another question. Rismeyer (1980) plotted poles to axial planes, from the gneisses of Bountiful Peak, and found a girdle of points (Figs. 71 A,B). This girdle strikes N 48 E and has a normal plotting at N 42 W, 12 W. This normal corresponds nicely with his

maximum of fold axes at N 51 W, 15 NW (Fig.71C). He believes that early folds were refolded about this axis. Axial plane data from Francis Peak (Figs. 56 and 57) define difuse girdles. Fold axes from folds in the layered gneisses trend WNW-ESE and plunge approximately 30 degrees to the WNW. Again note that data from the west of the FPFZ appears to be rotated anticlockwise, on a vertical axis, from the data on the east. Rismeyer's data appears to match the data plot of figure 57, from east of the FPFZ. Perhaps the two areas were folded on W to NW fold axes during the same event.

Stereoplots of gneissic foliation and lineation from Bountiful Peak (Figs. 71 D,E; Rismeyer, 1981) have a striking similarity to the data from Francis Peak. In general, foliations dip and lineations plunge to the west or northwest on both Francis and Bountiful Peaks.

Gneissic foliation on Bountiful Peak has been folded, like the axial planes of folds, on a northwesterly axis. Stereoplots of mylonitic and gneissic foliation from the east side of the FPFZ, figures 54 and 55 show girdles with northwesterly plunging poles. Girdles on figs. 50 and 52, from domains 4 and 10-14 from the west side of the FPFZ, strike essentially N-S. Girdles of poles to foliation from both Francis and Bountiful Peaks strike N to NE and dip steeply E to SE. This suggests that Francis Peak and Bountiful Peak were folded on northwesterly axes during the same event.

Lineations on Bountiful Peak also have orientations similar to those on Francis Peak (Fig. 71 C,D). Lineations from Francis Peak, be they from the mylonites or the gneisses, trend approximately W to NW and plunge 10-50 degrees west. A simple anticlockwise rotation

of the lineation data from Bountiful Peak would bring them into allignment with the majority of data from Francis Peak.

To summarize, it appears that both Francis Peak and Bountiful Peak are at the same topographic and structural level. Axial planes of folds and compositional layering in both areas have been folded on W to NW trending fold axes. An anticlockwise rotation of Bountiful Peak structural data leads to stereoplots similar to those for Francis Peak.

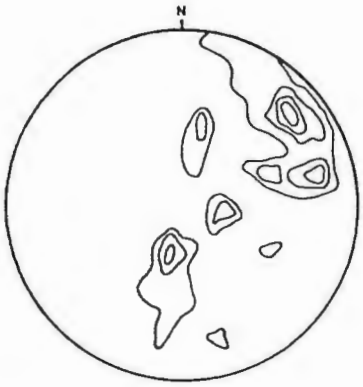

Fig. 71A Poles to axial planes.
Two main maxima at:
1) N. 40 W., 68 S.W.
2) N. 64 W., 20 N.E.
Contours 3-6-9-12% per 1% area.
(36 meas.)

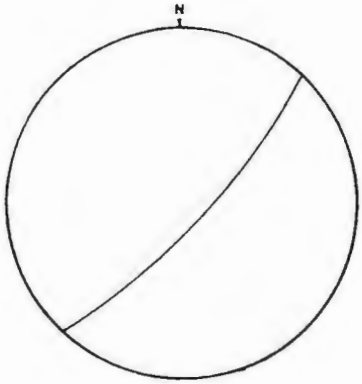

Fig. 71B Girdle of poles to axial planes implies folding on an axis: N. 42 W., 12 N.W.

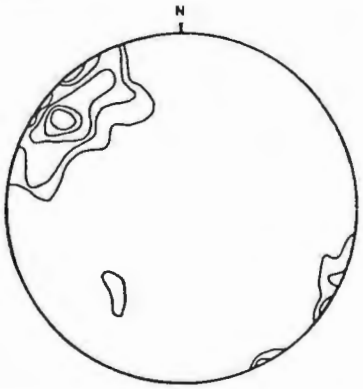

Fig. 71C Stereonet of fold axes with two main maxima:
1) N. 51 W., 15 N.W.
2) S. 40 W., 40 S.W.
Contours 2-4-6-8-12-16% per 1% area. (62 meas.)

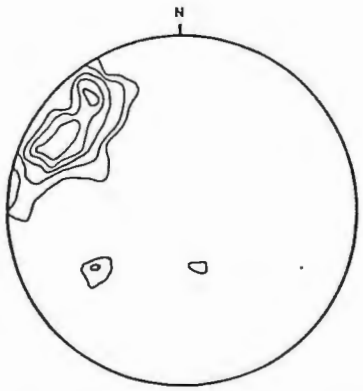

Fig. 71D Stereonet of all lineations with two maxima at:
1) N. 59 W., 22 N.W.
2) N. 39 W., 17 N.W.
Contours 2-4-6-8-12-16% per 1% area. (50 meas.)

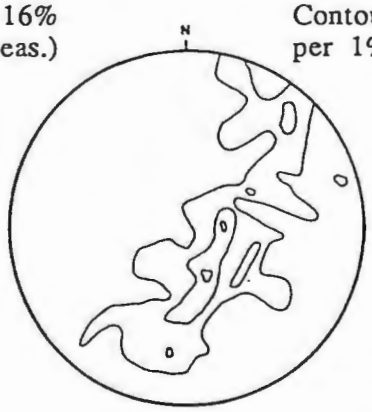

Fig. 71E Poles to foliation and compositional layering with major fold axis at N. 65 W., 13-20 N.W. Contours 2-4-6% per 1% area. (94 meas., after Rismeyer, 1981)

CHAPTER FOUR

DEVELOPMENT OF STRUCTURES

The purpose of this chapter is to **interpret** the development of structures found in Farmington Canyon Complex rocks on Francis Peak. Since the focus of the thesis is on the mylonitization of the rocks, the structures that developed prior to and after the mylonitization will be mentioned only briefly. Premylonitic structures are layering, lineation and folds in the gneisses. Brittle normal faults were active after mylonitization, so only their geometry is important here.

The development of gneissic layering, lineation, folds, and amphibolite facies assemblages in the gneisses may have begun more than 2600 m.y. ago, but was completed during the 1790 Ma metamorphism. Deformation and metamorphism of igneous rocks and layered sediments resulted in multiply folded gneisses (Rismeyer, 1981). The folds and mineral lineations associated with the 1790 Ma event dominate in the gneisses, with older linear structures being completely overprinted. The mylonites cut these gneisses and are therefore younger than 1790 Ma.

Normal faults of the Francis Peak Fault Zone, FPFZ, were active during the Neogene (Naeser et al., 1983). These normal faults brecciate the mylonites of Francis Peak, which means that mylonitization occurred before 24 Ma. The mylonites were not produced during movement on these normal faults because clasts of

Farmington Canyon Complex gneisses were deposited prior to the Neogene, in the Eocene Wasatch Formation to the east in Morgan Valley. This implies that the rocks were at a depth of around 2 km. or less and were too cold to deform plastically. The Wasatch fault and the normal faults bounding the complex to the east have moved anywhere from 3.7 km. to 11 km. (Parry and Bruhn, 1987), displacing Farmington Canyon Complex rocks relatively upward.

Several structures associated with the mylonitization will be discussed with regard to their development during progressive deformation. These structures are 1) foliation, 2) lineation, 3) folds, 4) S-C structures, 5) shear sense indicators and 6) faults. Finally a model will be presented that will attempt to relate the structures and shear sense indicators to regional tectonics.

There are two deformations that could have produced the mylonites. On Antelope Island there are ductile shear zones that deform the Archean gneisses, yet are unconformably overlain by a late Proterozoic diamictite (Bryant and Graff, 1980; Bryant pers. comm. 1987). The mylonites on Francis Peak may be the same age as those on Antelope island. A much more widely recognized deformation is associated with the Sevier Orogeny, active from the late Cretaceous through the Eocene. However, little mylonite has been found on or associated with the thrusts of the Sevier Belt (Armstrong, 1968). The mylonites on Francis Peak were probably brought to the surface by both Cretaceous thrusting (Royse et al., 1975) and Neogene normal faulting and erosion.

Mylonitic Layering

Layering in the mylonites has arisen by a complicated process involving mechanical breakdown, progressive rotation of gneissic layering, recrystallization and metamorphic reaction. Mechanical dissection of gneissic layers during the early stages of mylonitization may lead to a rock composed of thin, stretched lenses of quartz and feldspar with long axes subparallel to that of the finite strain ellipsoid. Whether dissection occurs or not, rotation of early fabric, or transposition (Myers, 1978), into parallelism with the protomylonitic layering occurs. As strain increases, the amount of rotation that fabric elements experience is progressively smaller. Early foliations become indistinguishable from the mylonitic foliation. At high strains, a complete transformation of the protolith has been accomplished. While dissection and rotation becomes less important at higher strains (except for rotation on the grain scale), recrystallization becomes pronounced (Vernon, 1976). Recrystallization during non-laminar flow (Lister & Snoke, 1984) facilitates the extreme changes in grain shape that accompany formation of the mylonitic layering. Metamorphic segregation, primarily by the diffusion of silica may, in part, be responsible for the pure quartz ribbons found in mylonites, according to Robin (1979). Silica may diffuse faster than chemical components of the phyllosilicates in response to stress-induced pressure gradients. This leads to the formation of pure quartz ribbons by growth similar to that observed in pressure shadows.

Layering in the granitic and amphibolitic mylonites is formed by the same processes cited above, though rotation of original layering is probably not important to the development of the fabric. The granitic rocks and the amphibolite gneiss were essentially compositionally isotropic.

Lineation

The mineral lineation in the mylonites, defined by elongate masses of aphanitic recrystallized quartz or feldspar, developed by a different mechanism from the foliation, as shown by thin-section analysis of approximately fifty mylonites. These lineations were not oriented by rotation as rigid bodies because they were not elongate before the deformation. Recrystallization of quartz or feldspar is the primary mechanism by which the lineation arises (Hobbs et al. 1976). Pressure solution of quartz in domains of high stress, and subsequent deposition in low stress domains like the tail of a growing quartz ribbon, may be significant (Robin, 1979). Individual lineations are probably the result of deformation of single grains or monomineralic aggregates of grains. The lineation is therefore sub-parallel with the long axis of the finite strain ellipsoid at high strains (Hobbs et al., 1976).

Lineations in mylonites adjacent to thrust faults usually form in the direction of movement (Bryant et al., 1969, Hobbs et al., 1976), though examples from less deformed rocks in the Himalaya (Brun et

al., 1985) and central Australia (Dunlap, 1988) show that lineations can form at a high angle to the direction of movement on the fault. Since thrust faults usually move contemporaneously with, but may predate, or even postdate (Johnson, 1970) mylonite formation, it is likely that any set of lineations lies only subparallel with the direction of thrusting. Indeed, lineations on Francis Peak fan about 20° or more in outcrop. This fanning is either 1) the result of lineations forming during different phases of mylonitization or 2) the lineations forming simultaneously, but recording only local movement directions.

Folds

An interpretation of the folds must account for the fact that folds in the mylonite are virtually indistinguishable from those in the deformed layered gneiss (Figs. 56, 57). Folds in the mylonite form with axes in the foliation plane and at some angle to lineation (Fig. 66). As deformation progresses, folds become tighter and fold axes rotate into parallelism with the mylonitic lineation. A cursory look at the stereonets of the field data reveals that fold axes in the mylonite lie roughly parallel with the mylonitic lineation. As deformation of the gneiss progresses, fold axes and mineral lineations tend to rotate toward the new mylonitic lineation. Given this interpretaion, it is reasonable that fold axes and mineral lineations in the gneisses and mylonites now plot in the same part

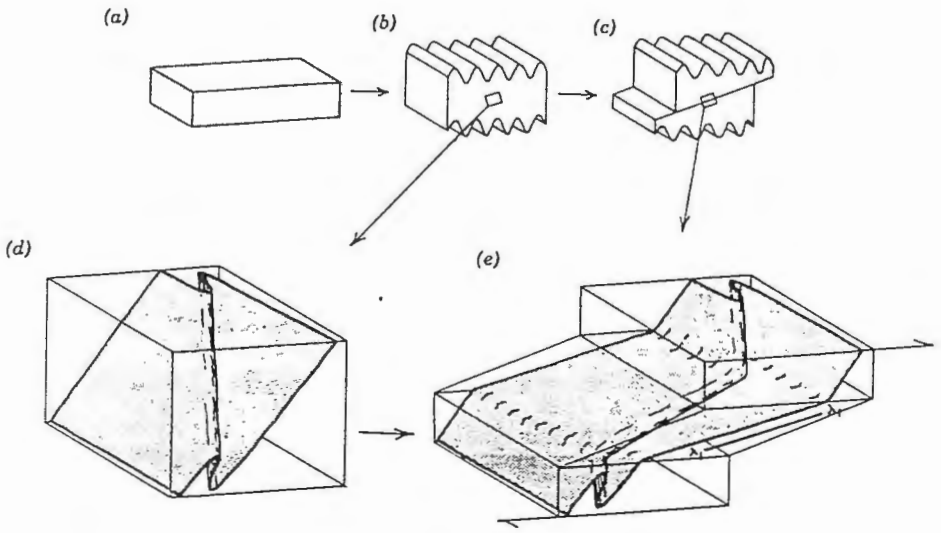

Fig. 72 Diagram showing how early fold hinge lines may be rotated, within a zone of intense deformation, toward parallelism with the direction of thrusting. Parts (a)-(c) show how the crust may be shortened first by folding and then extended by thrusting. Parts (d) and (e) show what is happening on a smaller scale (note that in these diagrams it is assumed that, due to local variation in fold plunge, the hinge line of the fold is not parallel to the thrust, this of course will be true in general). The thrusting is assumed to be achieved solely by ductile deformation concentrated in a narrow zone and the strain is assumed to be simple shear. Since the strain is plane, the principal axis of extension, for the front face of the block (heavy line marked λ_1), is the three-dimensional, principal axis of extension for the deformed zone. As shear is increased both this axis and the fold hinge line will rotate toward parallellism with the direction of thrusting or transport, as indicated by the single barbed arrows in (e). Note that in this environment, where the thrusting may be measurable in tens of kilometers and the shear zone may be only tens of meters thick, the possible shear strains are enormous. (from Hobbs et al., 1976)

of the stereonets. This rotation of pretectonic and syntectonic structures is shown in figure 72.

Folds in the mylonites can sometimes be used as mesoscopic indicators of bulk shear sense (Simpson, 1986). The vergence and asymmetry of folds indicates the direction they have been sheared (fig. 63), though caution should be exercised as folds of opposing vergence are not uncommon. Folds have been used as shear sense indicators to deduce the movement of upper plate rocks in the field area (see next two sections).

S-C structures

Occurrences of an oblique foliation called S surfaces (Berthe' et al., 1979) were found in the mylonites of Francis Peak. These S surfaces are similar to the schistosity surfaces described by Ramsay and Graham (1970), and they are assumed to approximate the x-y plane of the finite strain ellipsoid. Berthe' et al. (1979) coined the term S surface (for shistosity) in their description of mylonitic orthogneisses of the South Armorican shear zone. S surfaces are bound on the top and bottom by C surfaces (for cisaillement), bands of more intense shear strain. S surfaces are pervasive mylonitic folia that have been deformed into a sigmoidal shape by deformation on C surfaces (Fig. 73).

Lister and Snoke (1984) have defined two types of S-C mylonites. Type I S-C mylonites are common in mylonitic

granitoids. They contain abundant mesoscopic S surfaces that envelop feldspar porphyroclasts and are truncated by regularly-spaced shear bands or C surfaces. The rocks studied by Berthe' et al., (1979) are of this type. Type II S-C mylonites form predominantly in quartz-mica rocks. Asymmetric mica "fish" or an oblique fabric defined by elongate recrystallized quartz grains define the S surfaces. All the S surfaces studied by Berthe' et al. (1979) and Lister and Snoke (1984) give the same sense of shear as that shown in figure 73.

One example (Fig. 11) of a possible S surface was found in the ultramylonites at location 53 (Plate 1). This mylonite may be a type I S-C mylonite, but there are two problems with this idea. Type I S-C mylonites typically have a pervasive system of both S and C surfaces, like that shown in figure 73. Also, the S surfaces in figure 11 lie at a small angle to the bulk foliation, and grade into it laterally. This geometry is extraordinary and may better be explained as the sheared-out hinge of an isoclinal fold.

Eight type II S surfaces were found in the phyllonites (Fig. 25, note sinistral sense of shear in lower left sample). These S surfaces were difficult to measure because the C surfaces are anastomosing and truncate the S surfaces in three dimensions instead of two. The S surfaces were only measured in well-developed S-C phyllonites where the sense of shear was unmistakable.

S surfaces and associated C surfaces were plotted on the stereonets of chapter 3. Movement sense determined from S surfaces is consistent with the bulk sense of the zone (Simpson,

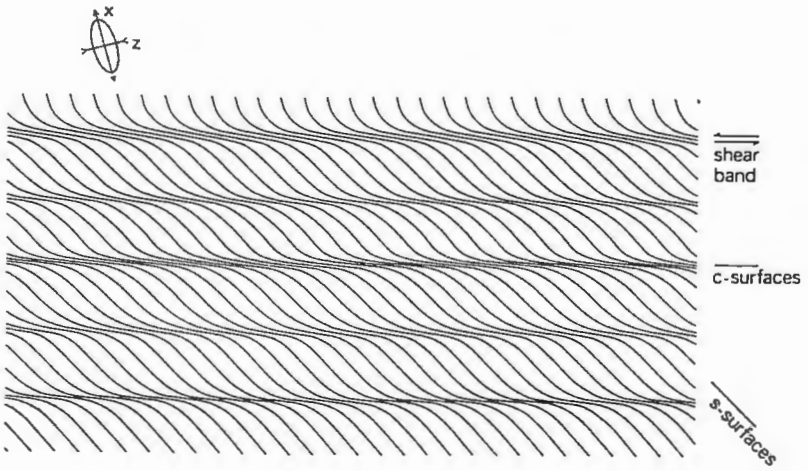

Fig. 73 Trajectories for the axis of principal finite extension in a type I S-C mylonite. Microstructures are characterized by shear bands transecting a mylonitic foliation. The S- and C-surfaces are shown. (Lister and Snoke, 1984)

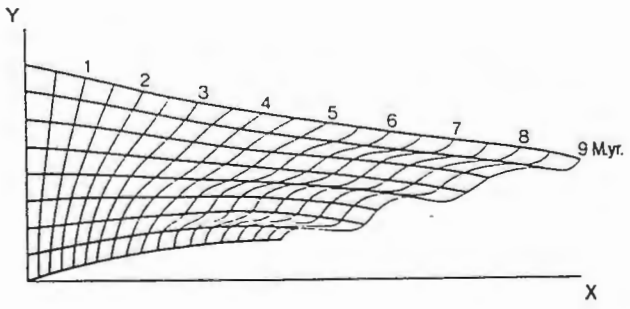

Fig. 74 A non-coaxial laminar flow that degenerates with time into narrow zones in which intense strains accumulate. Initially the strain is penetratively distributed. X-Y coordinates of points initially on the Y-axis are shown at different times. Heavy lines show trajectories of the poionts initially on the Y-axis. (Lister and Snoke, 1984)

1986). Note that movement sense on upper plate rocks is to the west on the west side of the FPFZ (from + to S on the diagrams) and to the east on the east side.

If the S and C surfaces found in the field area are indeed type II structures, then they developed in a manner similar to the structures described by Lister and Snoke (1984). Lister and Snoke (1984) believe that S-C mylonites form by the degeneration of non-coaxial laminar flow over time (Fig. 74). In this scenario, the S and C surfaces form during the latter part of a progressive deformation.

Shear sense indicators and results of thin-section analysis

Many microscopic structures in mylonites can be used to determine the sense of shear (Berthe' et al., 1979; Brunel, 1980; Schmid et al., 1981; Simpson and Schmid, 1983; Simpson,1981, 1986). The structures, which have been categorized by Simpson (1986), are asymmetric σ and δ porphyroclasts (see Simpson, 1986, Fig. 7), microscopic S and C surfaces, obliquely oriented, elongate, recrystallized quartz grains, mica "fish", micro-folds, shear bands and fractured and rotated porphyroclasts. All of these structures have been found in the mylonites of Francis Peak. The vast majority of shear sense indicators in the mylonites are obliquely oriented, elongate, recrystallized quartz grains.

Obliquely oriented, elongate, recrystallized quartz grains are common in the mylonites that are relatively poor in mica and have

not experienced secondary, static recrystallization. These grains form in the incremental plane of flattening, the x-y plane of the incremental strain ellipsoid (Simpson and Schmid, 1983). The orientation of the long axis of the grains is approximately 45° to the mylonitic foliation, just after recrystallization. Continued deformation results in rotation of the new grain toward the mylonitic folation plane. Progressively smaller new grains form, again at 45° to foliation, as mylonitization progresses, so that several generations of recrystallized grains may be present in any one thin-section (Fig. 75). Quartz recrystallizes relatively easily and these oblique foliations probably only represent the last increment of deformation in the mylonites (Simpson, 1986). Folding a quartz ribbon may induce recrystallization in an axial planar orientation (Fig. 76). Recrystallization in hinge zones of folded quartz ribbons is favored due to the local increase in strain (Fig. 77), whereas the limbs of the fold may or may not be affected.

Extreme care must be taken when interpreting oblique quartz foliations. One always looks for the long dimension of the recrystallized grains. Some optical fabrics appear as though they are formed by elongate quartz grains, but their obliquity is antithetic to elongate quartz grains (Fig. 78). These fabrics are probably related to crystallization fronts (Teyssier, pers. comm., 1987) that migrate through quartz ribbons and systematically recrystallize new grains. The present author believes that these fronts were initially alligned with the y-z plane of the incremental strain ellipsoid.

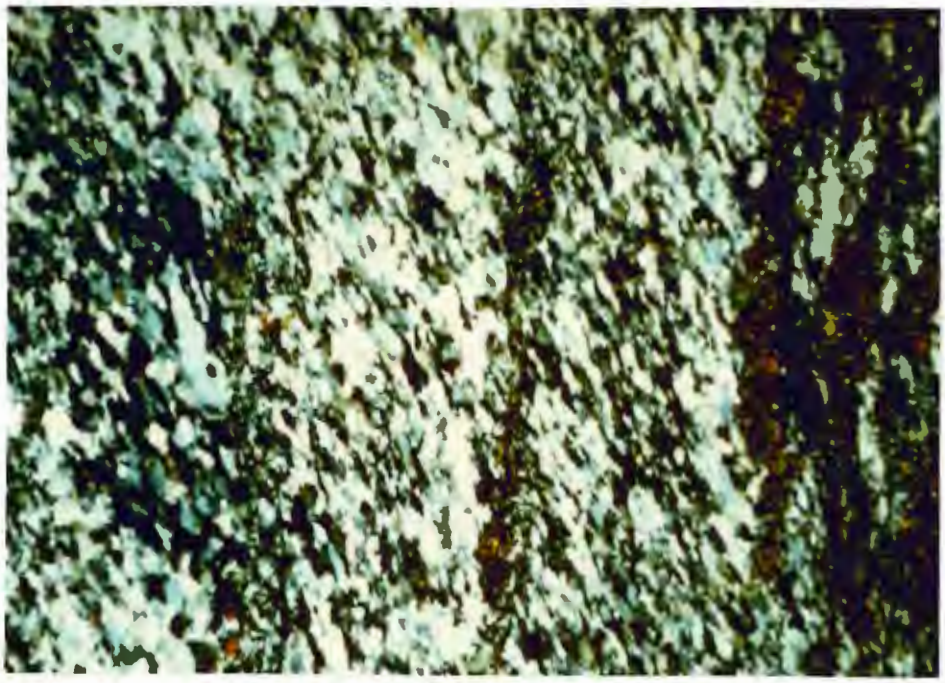

Fig. 75 Ultramylonite with two foliations. Mesoscopic foliation defined by layers rich in quartz or epidote. Oblique foliation of elongate, recrystallized quartz grains lies at about 45° to main foliation. Some larger grains are at a lower angle to foliation and may represent an earlier generation of recrystallization grains. Field of view is 3 mm. across, polars crossed.

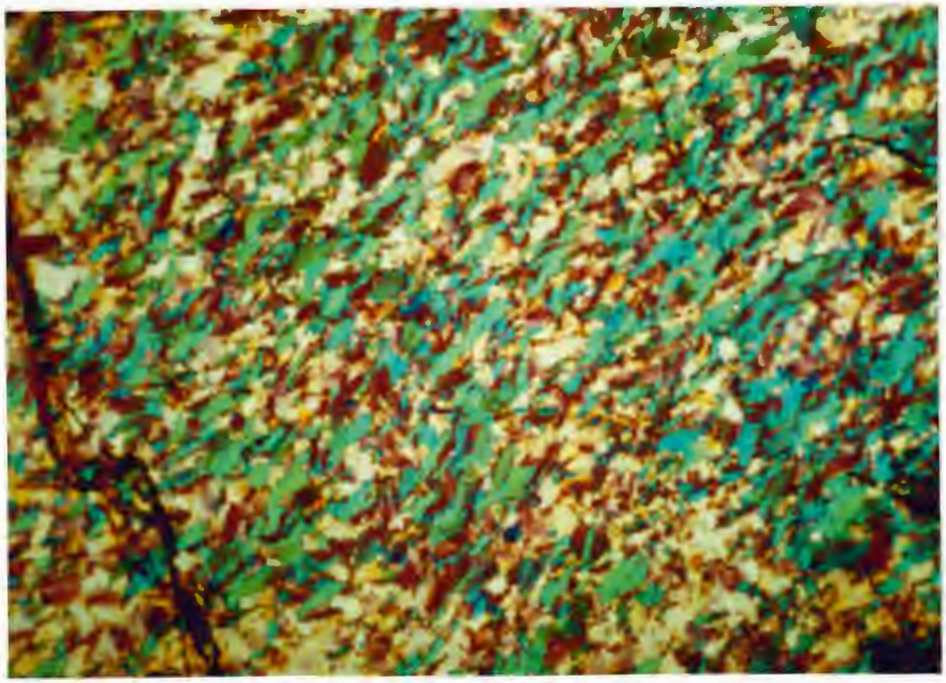

Fig. 76 Quartz ribbon in mylonite shows multiple optical orientations and two foliations. Axial planar foliation defined by long axis of grains with green or red interference colors. Grains with yellow interference colors are remnant grains that were less affected by folding. Field of view is 3 mm. across, polars crossed and quartz plate in.

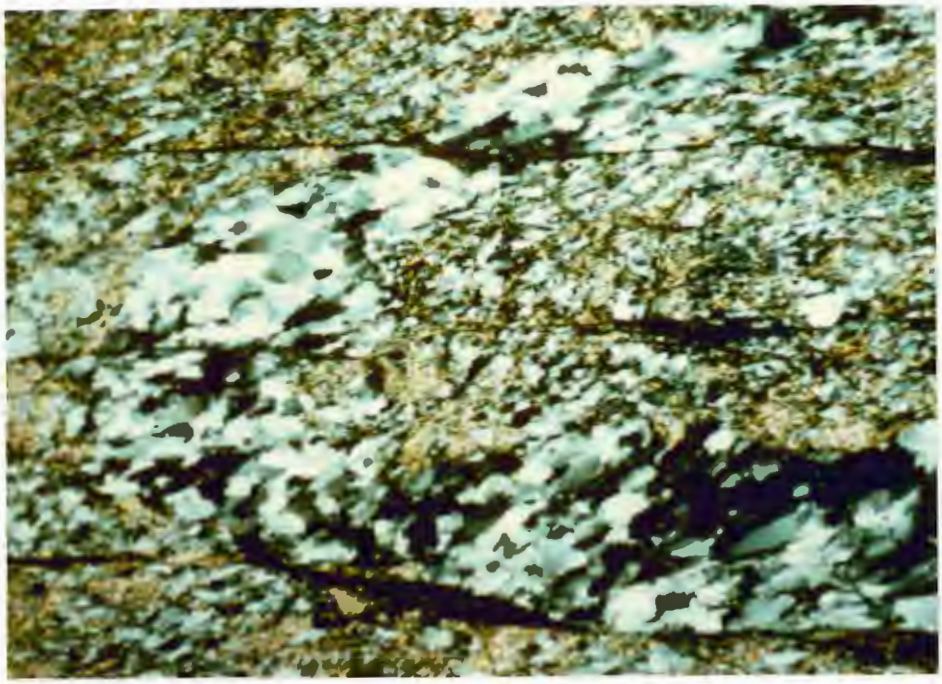

Fig. 77 Photomicrograph of folded quartz ribbon in a layered gneiss mylonite. Quartz grains are oriented with long axes 45° to foliation in lower limb, axial planar in hinge zone, and both axial planar and oblique (sympathetic with lower limb) in upper limb. Field of view is 5 mm. across, polars crossed.

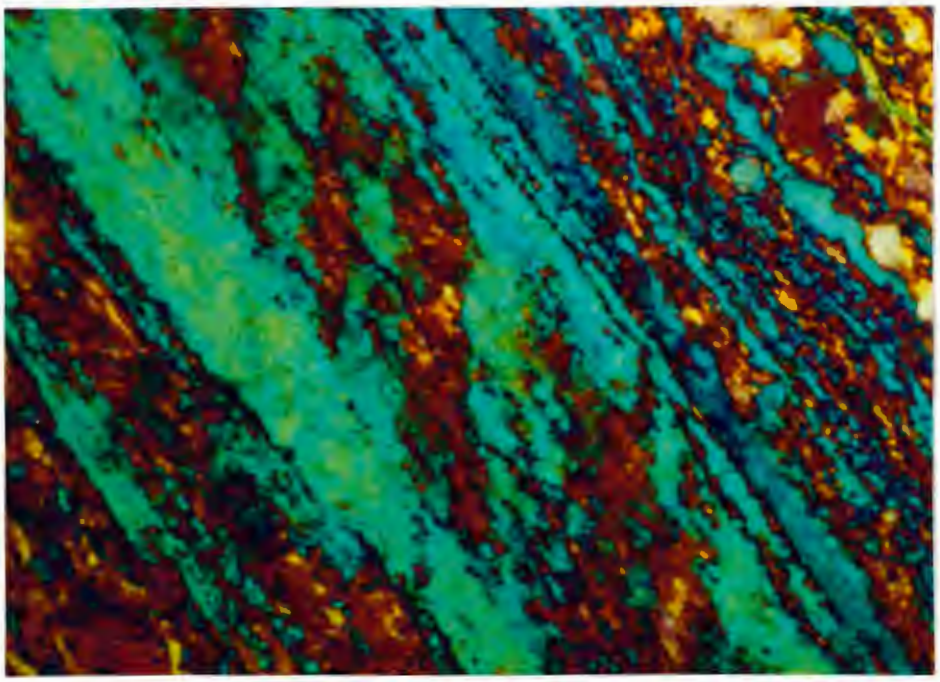

Fig. 78 Optical fabric in ultramylonite is antithetic to long axes of recrystallized quartz grains defining oblique (right lateral) foliation. These are crystallization fronts that form in the Y-Z plane of the incremental strain ellipsoid. Field of view is 1 mm., polars crossed and quartz plate in.

The S and C surfaces of the type I S-C mylonites (Lister and Snoke, 1984) are not abundant on the microscale. The S surfaces occur as sets of surfaces and the C surfaces are single surfaces that bound the S sets (Fig. 79). The S-C sets appear to have nucleated on or near quartz and feldspar knots or remnant pegmatite veins. The rheologic anisotropy has thus facilitated the degeneration of non-coaxial laminar flow (Lister and Snoke, 1984).

C surfaces sometimes occur alone, without an adjacent S surface, in which case the stuctures are simply called shear bands (Simpson, 1986). These shear bands are the microscopic equivalent of the shear bands described previously (Fig. 80). Layering is usually warped by the band and may be truncated, but the sense of shear is exactly the same.

Mica "fish" (type II S-C structures of Lister and Snoke,1984) are absent in the ultramylonites and mylonites, but may be found in the phyllonites of Francis Peak. The asymmetry of the fish and their oblique orientation with respect to foliation dictate the sense of shear (Fig. 81). Bulk shear sense is consistent with that of the fish (Lister and Snoke, 1984). The fish look like S surfaces and are bound by shear bands along which displacement has occurred.

Asymmetric porphyroclasts are useful in interpreting the bulk shear sense in mylonite (Simpson and Schmid 1983; Simpson,1986). The mylonites of Francis Peak contain numerous porphyroclasts of feldspar, usually K-feldspar, that have mica tails. Most of the porphyroclasts are symmetric (orthorhombic symmetry of Simpson, 1986) or not sufficiently asymmetric to give a definite sense of

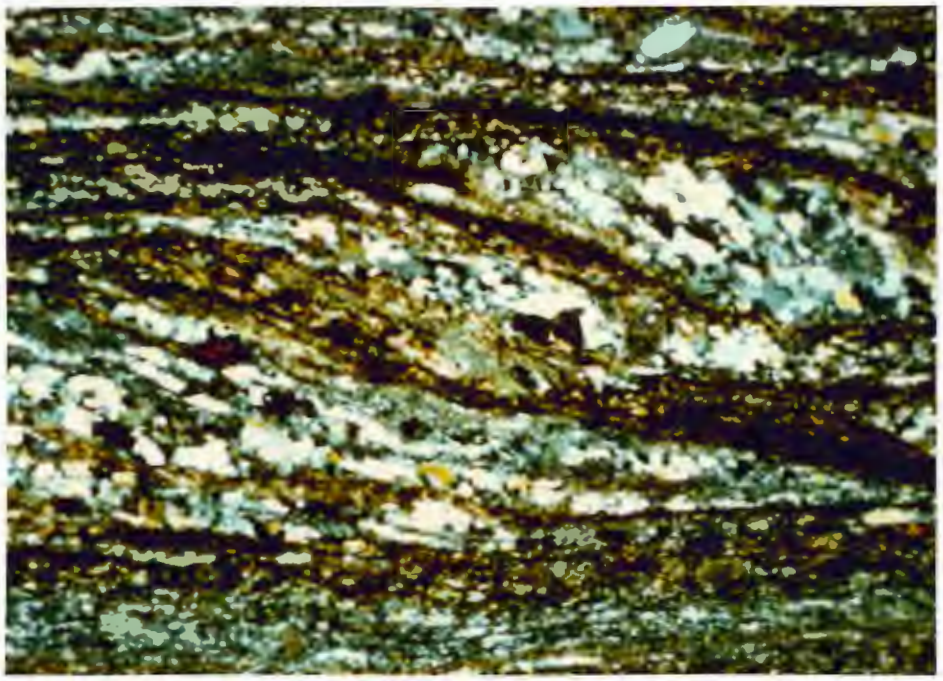

Fig. 79 Set of S-surfaces that curve into the main foliation or C-surfaces. Note the obliquity of quartz grains between the S-surfaces. Sense of shear is sinistral. Field of view is 5 mm. across, polars crossed.

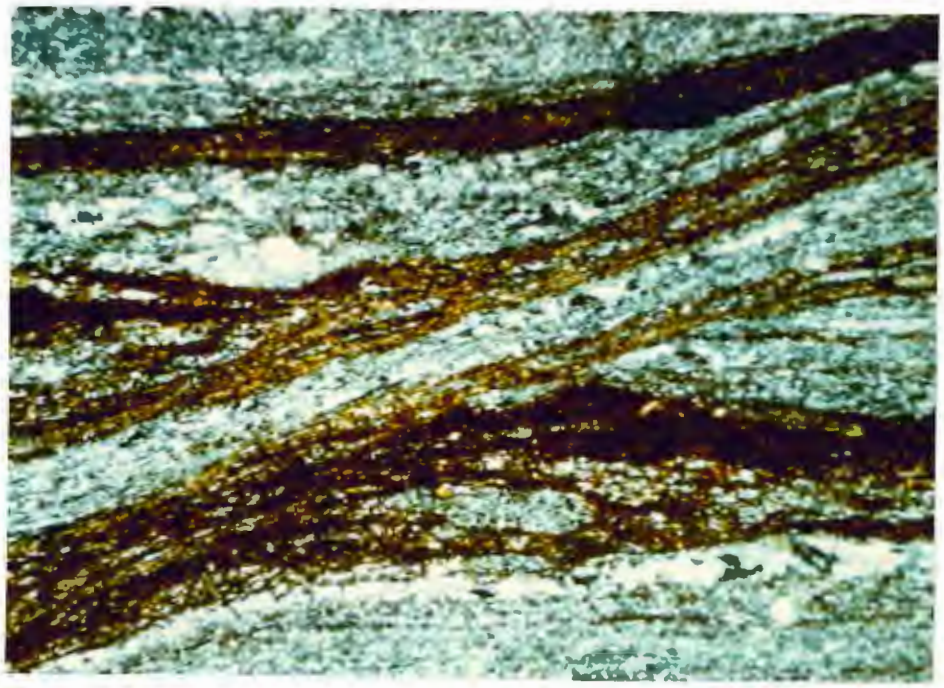

Fig. 80 Structure called a C-surface when it occurs with an S-surface, otherwise called a shear band. Sense is sinistral. Band truncates and warps layering. Long edge of picture parallel with main foliation. Field of view is 5 mm across, polars crossed.

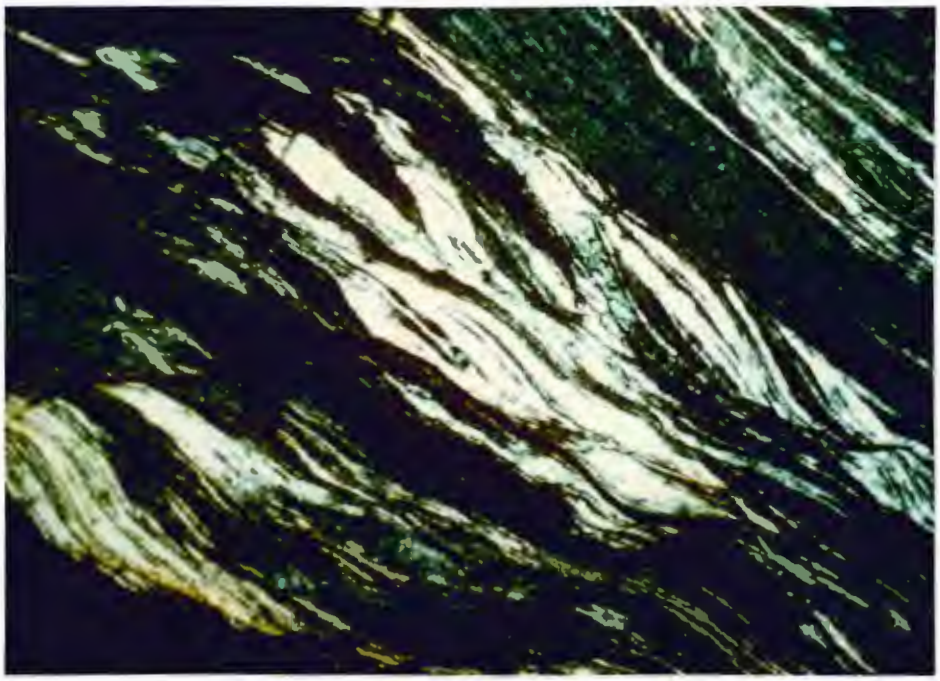

Fig. 81 Asymmetric muscovite "fish" lie oblque to phyllonitic foliation. Sinistral shear bands, or zones of higher strain, truncate and warp the tails of fish. Field of view is 5 mm. across, polars crossed.

Fig. 82 Asymmetric K-feldspar porphyroclast with mica tails. σ–type symmetry indicates sinistral shear sense, compatible with oblique fabric in quartz ribbon. Field of view is 5 mm. across, polars crossed.

shear. The porphyroclast in figure 82 is a δ-type (Simpson, 1986), with tails that cross the foliation plane of clast symmetry. Bulk shear sense in this mylonite is sinistral, sympathetic with the oblique foliation in the quartz ribbon.

Fractured porphyroclasts can also be used as shear sense indicators (Simpson, 1986). These structures may develop at any time in the deformation history, depending on when the porphyroclast fractures. The angle, in relation to foliation, at which the clast fractures determines the sense of movement (Simpson, 1986, fig. 10). A common analogy is one of books falling dominoe-style, where shear sense between adjacent parts of the fractured porphyroclast is opposite that of the bulk rock (Fig. 83). Other less common geometries have a sympathetic shear sense in adjacent parts of the porphyroclast.

Asymmetric microfolds are valuable indicators of shear sense in mylonites. Simpson (1986) believes that the folds amplify in local perturbations in the flow and, thus, represent late stage structures. The vergence of the folds may indicate shear sense, the axial planes verging in the direction of shear, however, axial planes may also verge in the direction opposite that of bulk shear sense, depending on the amount of strain and the initial orientation of the layer. Microfolds in the Francis Peak mylonites are common, but few possess the symmetry that is helpful in determining shear sense.

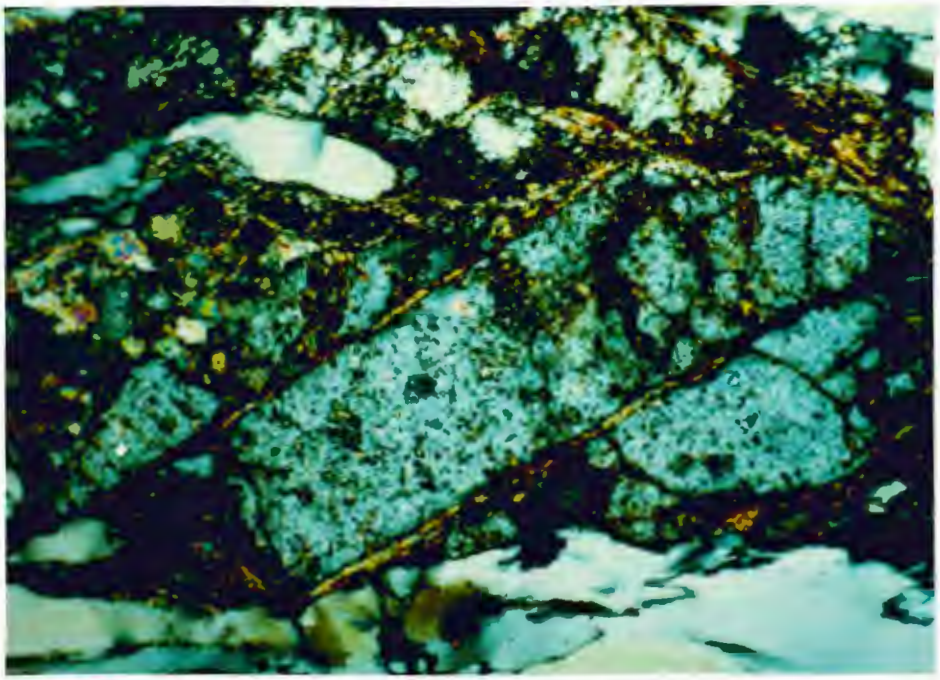

Fig. 83 A fractured and rotated porphyroclast of orthoclase. Blocks have acted like falling books. Sense of shear between blocks is sinistral and that in the rock is dextral. Field of view is 5 mm. across, polars crossed.

Kinematic study

Shear sense indicators have been found to be consistent along strike in the field area, and markedly different across the FPFZ. Simpson (1986) claims that in most mylonite zones all shear sense indicators will show sympathetic senses as a whole, and that bulk shear sense can therefore be predicted with a high degree of certainty. Movement indicators from all available criteria, microstructures as well as mesostructures, have been synthesized and plotted as two dimensional vectors on plate 1. Movement has taken place on upper plate rocks in the direction of the arrow and in the mylonitic foliation plane. Large volumes of rock have moved in the same direction along zones of mylonite that are continuous for up to 3 km.

West of the FPFZ, two domains of differing shear sense are evident. In section 4, movement of upper plate rocks has been down dip toward the NW. South of section 4, movement is still down dip, but toward the WSW. Between these two domains lies a thick zone of mylonitization that dips steeply north, strikes E-W and shows thrust motion to the SW. The stereonets of chapter 3 show that section 4 has a structure different from that of the rocks to the south, the change in structure taking place across the E-W zone of mylonitization. The change in the azimuth of movement indicators correlates well with this change in structure.

The movement history of upper plate rocks east of the FPFZ has been more complex. Shear sense indicators show that the rocks

have been normal faulted down to the west and then thrusted to the east (Plate 1). Indicators that show westward movement are from tens of meters of ultramylonite. Indicators of eastward movement are late brittle structures like those in figures 67 and 68. Shear sense indicators and field data suggest that all the rocks east of the FPFZ have experienced the same kinematic history.

To summarize, the shear sense indicators show that rocks to the east of the FPFZ have experienced a different kinematic history than those to the west. This relationship is further evidenced by a comparison between Plate 1 and the field data plotted in figures 49-60.

Faults associated with the mylonites

A network of faults related to mylonite genesis was mapped in the field. It is evident that these faults are **normal** faults, according to the shear sense indicators. The history of these faults since their formation is rather uncertain, but it is likely that the faults and associated mylonites are remnants of an ancient mid-crustal, extensional or compressional fault system.

The major faults are zones of intense deformation and discontinuity. In the adjacent less deformed rocks, minor faults occur as swarms that decrease in frequency away from the mylonites and major faults. These minor faults lie at small to

moderate angles to mylonitic foliation, and have small displacements (less than a meter).

Fault systems with a geometry similar to the one discussed above have been studied by Wojtal and Mitra (1986). They found that displacement of large sheets of rock is partially accomplished on a thick zone of minor faults adjacent to the main fault. Blocks bound by the minor faults also deform, which adds to displacement on the fault zone. Wojtal and Mitra (1986) believe that the blocks are displaced past one another in a kind of mesoscopic "grain boundary sliding".

As the faults formed, individual fractures spread laterally, linking to form larger faults which continued to propagate (Dunlap and Ellis, 1986; Ellis and Dunlap, 1988). The largest or most extensive faults linked to form the faults shown on plate 1. The smaller faults also linked, forming horses on the outcrop scale. Movement on these faults has facilitated the internal deformation of the horses during deformation.

Model for the structural development of Francis Peak

A model for the structural development of Francis Peak must account for the observed changes in structure across the FPFZ, the large-scale geometry of the fault system, the systematic changes in sense shear and the kinematic history of the rocks. The main structural features of the area are shown schematically in figure 84.

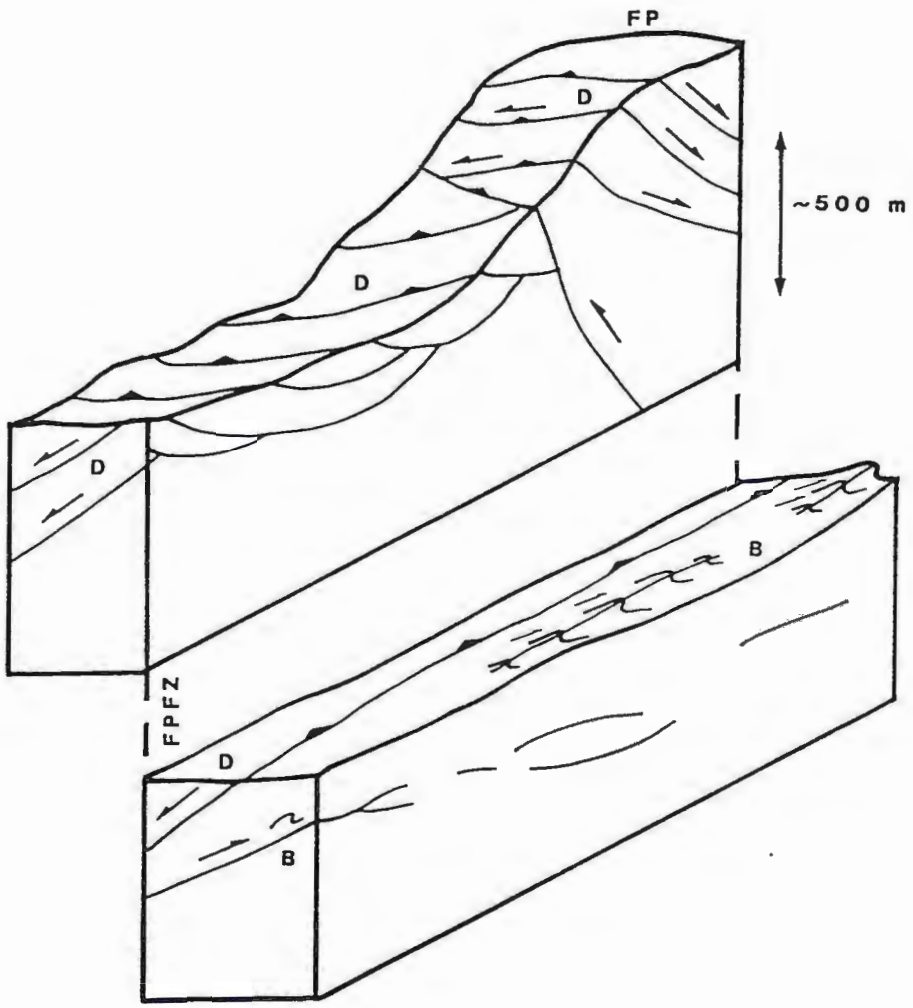

Fig. 84 Schematic block diagram of the field area. Displacement on the FPFZ has been reversed so that the pre-faulting relationship of the blocks is approximated. View is to the NNW. Early ductile structures marked by D and late brittle structures marked by B. Scale is only approximate.

Mylonitization of the gneisses, possibly during the late phases of amphibolite facies metamorphism, produced the majority of structures in the field area. The most conspicuous evidence for this deformation is the thick sequence of west-dipping mylonites that show down dip movement toward the west. Indicators of bulk shear sense such as asymmetric porphyroclasts are compatible with westward movement. Indicators of late phase movement like S surfaces, shear bands and oblique quartz fabrics are also compatible with westward movement. The thick mylonites that top the less deformed rocks east of the FPFZ all show westard movement, though they are probably from a deeper structural level.

The last phase of deformation was dominated by brittle behavior. Structures that formed during this late phase are found on the east side of the FPFZ and below the mylonites. Evidence for this phase of deformation includes overturned chevron folds and some brecciated, overturned folds at the base of the mylonites. The vergence of these structures indicates that upper plate rocks were transported to the east, 180 degrees from movement directions in the mylonites.

A model has been developed to account for the structure of Francis Peak. This model infers a relationship between the mylonites of Francis Peak and the Proterozoic shear zones in the gneisses of Antelope Island. The model also relates static retrogression of the rocks and contemporaneous brittle structures to the Cretaceous Sevier Orogeny.

Considering the fact that most of the structures on Francis Peak indicate movement westward and down dip, it may be untenable to try and relate these structures to eastward thrusting (Dunlap, 1988). Armstrong (1968) has studied the whole Sevier belt and has noted a distinct lack of mylonite. Bryant believes that Francis Peak mylonites are related to an older deformation (pers. comm., 1987). Shear zones on Antelope Island are oriented NE-SW and are truncated by an erosional surface that is topped by late Proterozoic diamictite (Bryant and Graff, 1980). These shear zones probably originated between 1790 Ma and the time of deposition of the diamictite. Perhaps the mylonites on Francis Peak formed during the same deformation that is responsible for the mylonites on Antelope Island. Since the rocks of both Antelope Island and Francis Peak were located at the continental margin in the Proterozoic (Stewart, 1976), the possibility that the Francis Peak mylonites are late Precambrian cannot be ruled out.

Large sheets of rocks, including the Farmington Canyon Complex (Royse et al., 1975), were thrust eastward on low-angle detachments, like the Weber Canyon thrusts, during the late Cretaceous Sevier Orogeny. The complex is now steeply overturned to the east, as evidenced by the Cambrian Tintic quarzite that rims and is in unconformable contact with the gneisses (Bryant, 1984). The Willard thrust sheet has possibly overridden Farmington Complex rocks, and the hinterland extension of the Absaroka thrust may dip below Farmington rocks (Royse et al., 1975). The preserved pre-late Cretaceous sedimentary section to the south in

Parley's Canyon suggests that Farmington Complex rocks were at about 8 km. depth prior to thrusting (Naeser et al., 1983). Fission track dating (Naeser et al.,1983) indicates that the complex was at around 2 km. depth by 55 Ma. Since Farmington rocks were thrust up from a depth of only about 8 km., it is unreasonable to infer that mylonitization and ductile deformation of feldspar took place in Francis Peak rocks during the Sevier Orogeny.

The brittle structures and associated east-directed shear sense indicators of Francis Peak probably developed during the late Cretaceous Sevier Orogeny. Massive retrogression along old shear zones is associated with the brittle thrusting. Dynamic microstructures in the old, west-directed mylonites are commonly completely destroyed by static retrogression and alteration of recrystallized feldspar to muscovite, sericite and chlorite (Fig. 13). As the thrusts carried rocks closer to the surface, deformation became more brittle and retrogressive fluids along old shear zones overprinted the older structures. Before movement on the thrusts seized, east-verging folds formed in footwall rocks. Some cores of these folds even shattered during this final brittle phase of deformation.

Conclusions

1) Before deformation, the rocks of Francis Peak consisted of "undeformed", amphibolite facies gneisses and granites.
2) The formation of foliation and lineation in mylonites was brought about by dynamic recrystallization of quartz and feldspars.
3) Fold axes, foliation and lineation in the gneisses were rotated toward parallelism with the same mylonitic structures during deformation.
4) Mesoscopic and microscopic movement sense indicators show that there are zones of consistent movement sense in the area, as well as a two stage kinematic history.
5) Structural data from Bountiful Peak show good correlation with that from Francis Peak. A simple rotation of the data on a near- vertical axis gives a good match between the data sets.
6) Faults have linked to form horses of rocks that are least deformed in their interiors.

In summary, the proposed model of ductile deformation and extension of Farmington Complex rocks during the Proterozoic followed by eastward thrusting, brittle deformation and retrogression during the late Cretaceous Sevier Orogeny accounts for all the observed structures on Francis Peak.

CHAPTER 5

PROGRESSIVE DEFORMATION OF THREE COMMON ROCK TYPES

Introduction

The protoliths, layered gneiss, amphibolite gneiss and granite and their deformed equivalents have been described in detail in chapter 3. The purpose of this chapter is to describe and interpret the textural changes that take place during progressive mylonitization of these protoliths. Two or three stages of textural evolution will be discussed for each of the protoliths. These stages are deformed, mylonitic, and ultramylonitic rock. Deformed protoliths resemble their undeformed counterparts, yet distortion of grains, subgrain development, minor dynamic recrystallization and development of a new fabric distinguishes the onset of deformation (Bell and Etheridge, 1973). Mylonites are characterized by at least 50% dynamically recrystallized grains (Sibson, 1977), highly deformed and kinked or fractured porphyroclasts or porphyroliths, and relatively pure ribbons of recrystallized grains. Ultramylonites contain over 90% dynamically recrystallized grains (Sibson, 1977), are typically very finely laminated with pure, uniform ribbons of one or more mineral species, and have few small porphyroclasts.

After analyzing over one-hundred thin sections it has become apparent that there are hundreds of textures that arise during mylonitization. For the sake of brevity only the most common

textures will be described, and only textures in the granite will be illustrated. These textures include; shape changes associated with deformation, recrystallization textures especially in quartz and feldspar, and fractures, kinks, inversion textures, and deformation twinning in feldspars. A couple of uncommon textures will be discussed and analyzed with respect to the mechanisms that govern the formation of their more common textural counterparts.

Deformed Layered Gneiss

The deformed layered gneiss exhibits textures that vary with the amount of mica present (Fig. 9). Layers in the gneiss that were initially biotite-rich before deformation are now dominated by an anastomosing matrix of fine-grained biotite-chlorite intergrowths that define the new fabric and envelop lenses of quartz-feldspar aggregates, or porphyroliths. This mica-rich rock posseses a dissected texture, in that the original gneissic layering has become disaggregated on microfaults (Fig. 9, top). Deformation of the quartz- and feldspar-rich gneiss leads to a texture different from that of the mica-rich gneiss. This rock is less strained overall and is virtually devoid of anastomosing faults. Deformation and new fabric development is accomplished primarily by the straining of grains of quartz and feldspar.

In the deformed mica-rich layered gneiss, lenses of quartz and feldspar have been displaced on an anastomosing system of

microfaults that lie everywhere parallel with the basal plates of the micas. Movement on these microfaults is about 0.1 mm. to several cm., those with the most displacement associated with the most intensely deformed gneiss. The displacement is accomplished by a process analogous to "grain boundary sliding" (Wojtal and Mitra, 1986). In this situation, slices of rock slide past one another instead of individual grains, and the "grain boundaries" are the microfaults themselves. The microfaults envelop lenses of rock that are composed dominantly of quartz and feldspar. Within the lenses, internal deformation of grains and grain boundary sliding works to extend the clast and break it apart. The long axes of quartz and feldspar grains rotate with increasing strain and end up making a small angle with the foliation plane. Displaced grain boundaries may merge with microfault tips and, once linked, continue to slide, thus propagating the microfault and dismembering the porphyrolith.

Deformation of the quartz- and feldspar-rich layered gneiss involves more extreme deformation and recrystallization of the quartz and feldspar, yet less bulk strain due to the paucity of microfaults. Intergranular slip, therefore, is probably controlled by recrystallization and dislocation movement rather than by microfault displacement as in the mica-rich gneiss. Grain boundary sliding takes place because dislocations pile up and concentrate stress at the boundary (Vernon, 1976). Grain boundaries become somewhat disorganized and serrated as intracrystalline deformation

progresses. Recrystallized grains occur at or near the edges of grains and are more common at triple junctions.

Strain in the layered gneiss is accomodated not only by microfaulting and grain boundary sliding, but also by intracrystalline deformation and recrystallization. Recrystallization in the deformed layered gneiss is minor overall, yet may be extensive in quartz grains. Deformation of grains occurs by movement on a network of discontinuities, even smaller than the microfaults, called crystal lattice dislocations (Vernon, 1976). Quartz changes its shape as thousands of dislocations propogate across the grain. These dislocations may become tangled, lending the grain a wavy extinction or strain shadowed appearance. If the dislocations become organized such that cumulative displacement leads to a systematic misorientation of the lattice, the grain will take on a mottled appearance due to subgrain or new grain formation (Vernon, 1976). Subgrains are optically visible, though rather indistinct, and bound by low angle boundaries (mismatch < or = to 7°, see Bell and Etheridge, 1973) or walls (Vernon, 1976). New grains are optically distinct, strain free, bound by high angle boundaries (mismatch > or = to 7°) and mark the completion of recrystallization.

Fracturing, kinking, warping and twinning of feldspars, rather than recrystallization, is common at this stage of textural evolution. Thus, it appears that feldspars have acted more rigidly than quartz, the feldspars tending to form porphyroclasts and quartz the recrystallized matrix. Though recrystalliation in the feldspars is

absent, polygonization or subgrain formation may be present in K-feldspar in the more deformed gneiss. Fracturing of the feldspars is by far the most common mechanism of deformation. Fracturing usually takes place along cleavage planes, but may cut across crystallographic planes.

The composition of the layered gneiss does change somewhat during this first phase of deformation. Biotite is retrograded to an intergrowth of biotite and chlorite and plagioclase is more or less sericitized. Wholesale redistribution of Fe, Mg, Ca, Na, and K, and the influx of large amounts of water, is to be expected in shear zones (Beach, 1980). The result of the retrograde reactions and the influx of water is that the nature of the deformation changes from one of strain hardening to one of strain softening (Beach, 1976). The onset of strain softening results strain localization and anomalously strained zones in the mica-rich gneiss. The state of strain in the undeformed gneiss is relatively close to that in the deformed gneiss, but there is a quantum leap in strain from the deformed gneiss to the mica-rich deformed gneiss. Strain softening, initiated by retrogressive metamorphism, may be the mechanism responsible for the textural transition from the quartz- and feldspar-rich deformed gneiss to the mica-rich deformed gneiss.

Layered Gneiss Mylonite

Layers that were once either richer or poorer in biotite are still recognizable as such in the layered gneiss mylonite. Quartz- and feldspar-rich layers now appear as sets of lightly colored ribbons. Layers once rich in biotite now appear as dark colored layers that have minor ribbons of quartz.

Since the gneiss is so fine grained to begin with, it is not surprising that the layered gneiss mylonite is much less common than the layered gneiss ultramylonite. With such fine grained feldspars, only small amounts of deformation are required to completely recrystallize the porphyroclasts and thus the entire rock. Another reason for the dearth of layered gneiss mylonites is that the rocks contain relatively more plagioclase and biotite, minerals that tend to retrograde and deform. Granitic rocks tend to form mylonites rather than ultramylonites, as they initially contain a smaller volume percent of minerals that retrograde, like plagioclase, and the grains are so much bigger that extensive recrystallization is required to transform the rock into an ultramylonite.

Thin-section analysis show that layered gneiss mylonite forms from deformed layered gneiss predominantly by recrystallization processes. Microfaulting appears not to be involved, and previous microfaults from the early stages of deformation are probably completely overprinted. Quartz exhibits extreme ductility in the layered gneiss mylonite, but feldspars do not. Quartz has recrystallized into long continuous ribbons. Feldspars, on the other

hand, may form minor ribbons, but usually form microscopic porphyroclasts that constitute over 10% of the rock. As deformation progresses, polygonization and serration of grain boundaries is followed by recrystallization and formation of new, strain free grains. This recrystallization facilitates the change in shape of the grains from ellipsoidal to shapes with extreme eccentricity. The recrystallization process is cyclic, each cycle reducing the grain size of the quartz and feldspar further than the last cycle. After several cycles of recrystallization, the original grains have recrystallized all the way to the core, and the grain size becomes very small.

K-feldspar acted more rigidly than quartz during the deformation, yet it does exhibit the full range of recrystallization textures in the layered gneiss mylonites, from mildly deformed original grains to fine recrystallized new grains. Plagioclase retrograded very easily to sericite and was not involved in recrystallization. Some porphyroclasts of K-feldspar show extensive polygonization where the subgrains have gradational boundaries (as opposed to the sharp boundaries seen in quartz). Others show little or no internal deformation, but have well-rounded margins, as though the clast has been abraided in a cataclastic manner. The recrystallized K-feldspar of the matrix appears to have reached an equilibrium grain size (Kerrich, 1977), one which is always smaller than that of quartz.

Layered Gneiss Ultramylonite

The layered gneiss ultramylonites differ from the mylonites in two ways. First the quartz ribbons in the ultramylonites can be much thicker and noticably purer than those in the mylonites. The increased purity of the bands may be a product of metamorphic differentiation (Robin, 1979), with diffusion of silica, a major mechanism of mass transfer, into quartz ribbons from more mica-rich domains. This differentiation is accomplished by the pressure solution and redeposition of quartz during deformation, where silica is transported in solution along grain boundaries (Ruter, 1976).

The second difference is that the feldspars now exhibit extreme ductility. Complete recrystallization of initially fine grained feldspars has fascillitated the formation of long ribbons, exactly like those composed of quartz, though finer grained. Recrystallization is now the dominant deformation mechanism in the feldspars rather than more brittle processes.

Deformed Amphibolite Gneiss

The response of the amphibolite gneiss to deformation depends largely on the amount of quartz and feldspars present, and on the extent of retrogression that took place before and during deformation. Deformation usually leads to a chlorite or epidote phyllonite. Since the deformed amphibolite gneiss is quite variable

in composition, only progressions that grade into the best mylonites will be discussed.

A weak retrograde foliation of chlorite and epidote forms around porphyroclasts of hornblende. Some of the foliation surfaces are better developed than others. These define a weak anastomosing fabric across which small offsets in veins can be seen. The surfaces are obviously small faults developed subparallel with foliation. A close association exists between these faults and the larger-scale faults seen in outcrop. Thin-section analysis indicates that the most important aid to deformation in the amphibolite gneisses was the influx of water. The least retrograded hornblende grains have lost 30% of their volume to chlorite and epidote.

Textural evolution from undeformed to deformed amphibolite gneiss was the result not only of retrogression, but also of straining, recrystallization, and fracturing of grains. Quartz and plagioclase take on an new, ellipsoidal shape when subjected to deformation. Plagioclase is almost completely retrograded to an extremely fine grained sericite matrix, which has flowed in response to deformation, and that forms ellipsoids. Quartz was the only mineral to accumulate strain energy and recrystallize during deformation. Large strain free grain aggregates have replaced single large grains, due to static recrystallization probably aided by abundant water. This is a most common phenomenon in rocks that consist of 50% or more hydrous minerals. Recrystallization was never observed in plagioclase or hornblende, because these grains acted brittlely or altered to hydrous minerals readily during deformation (Fig. 24).

Hornblende deformed primarily by fracturing. Fractures would form, more often than not, parallel to mineral cleavage and sheets of hornblende would deform like a stack of cards. Fracture flow was aided by films of chlorite that formed along cleavage. In this way, the hornblende deformed into oblate shapes by a kind of intragranular grain boundary sliding.

Amphibolite Gneiss Mylonite

Only one satisfactory progression from amphibolite gneiss to mylonite was found (Figs. 23-26). Why don't the amphibolite gneisses seem to form good mylonites? Hornblende was apparently very susceptible to retrogression and more likely to deform brittlely under the P-T conditions that prevailed during deformation. Much of the retrogression in the study area may have taken place during the early stages of deformation, leaving the amphibolite gneisses as chlorite schists prior to deformation.

The amphibolite mylonite consists of ribbons of quartz and chlorite-epidote. The foliation defined by the ribbons is probably not a remnant of the original gneissic foliation because the amphibolite gneiss is poorly foliated to begin with. All that remains of the hornblende is layers of chlorite-epidote. Plagioclase was probably also replaced early in the deformation by epidote and possibly sericite. Subsequent deformation of this quartz-chlorite-epidote rock led to nicely segregated layers of quartz and chlorite-

epidote, with segregation of the quartz accomplished by the processes discussed previously. The lineation is defined by stringers of chlorite-epidote which replaced the hornblendes during deformation.

Thin-section analysis shows that recrystallization is the dominant process by which the deformed amphibolite gneiss becomes amphibolite mylonite. Quartz ribbons are virtually devoid of impurities. Patchy extinction in epidote blocks suggests that recrystallization was active in the chlorite-epidote ribbons as well. Chlorite and fine, granular epidote form pressure shadows around porphyroclasts of epidote. Quartz also exists as large flattened masses of variable grain size, strain free recrystallized grains that show evidence of having been recrystallized several times. The recrystallized grains have not reached an equilibrium grain size and do not define a uniform fabric. This may be due to pronounced static grain growth under wetter conditions. Whether intermitant periods of static grain growth are responsible for the large grain size or not, some of the quartz is much coarser grained than that in the layered gneiss mylonite, suggesting that fluid content in the deforming amphibolite gneiss was higher.

Deformed Granitic Rocks

The three types of granitic rocks, granite, quartz syenite, and granitic pegmatite have all behaved differently during deformation. The differences are so marked that the three protoliths can be distinguished even after deformation, due to the compositional and textural differences between them. Recrystallization rarely affects the innermost cores of large feldspar grains, which means that intrafeldspar textures that survive deformation can be used to help determine the rock type. As long as extensive alteration is absent, or restricted to certain layers, the composition of recrystallized ribbons can also be used to determine the protolith.

During the early stages of deformation, igneous textures are not altered enough to mask their origin. For example, coarse pegmatite crystals have become warped but have not disintegrated. Graphic textures are still easily recognizable in hand sample. Feldspars in the equigranular granites become rounded with only mild deformation, yet the texture is still equigranular. K-feldspar crystals in the quartz syenite become disected into systems of eye-shaped slices that have the same crystallographic orientation.

Deformation microtextures are best observed in the granitic rocks, because of their coarse grain size, and hence these rocks give excellent clues as to the mechanisms active during progressive mylonitization. Layered gneiss and amphibolite gneiss do not exhibit the textures described below, at least on the microscale,

however, they may on the submicroscopic scale. Other textures arise only from preexisting igneous textures.

Quartz commonly exhibits the full range of deformation and recrystallization textures in the deformed granitic rocks, including wavy extinction, deformation bands, polygonization, serration of grain boundaries, recrystallization and secondary, static recrystallization. Fig. 85 shows one deformed original grain of quartz that consists of recrystallized grains that have been mildly polygonized, heavily strain shadowed, and highly serrated at grain boundaries. Some boundaries are so convoluted that grains have actually detached from the parent recrystallized grain. Secondary growth under static conditions results in polygonal, strain-free grains.

Feldspars in the granitic rocks react differently than quartz during deformation, and tend to deform by brittle mechanisms. The deformation mechanisms active in plagioclase during deformation can be seperated from those active in K-feldspar. Plagioclase tends to kink or fault, warp, or retwin, while K-feldspar tends to brecciate, recrystallize or invert to microcline (Debat, 1978). Figure 86 shows a porphyroclast of plagioclase that has deformed by kinking and sliding on a system of dislocations that have culminated into faults. Fig. 87 shows a porphyroclast of plagioclase that has two sets of twins. The large set is original and has been misoriented by deformation and the small set has grown in an orientation determined by stresses that were probably normal (Debat, 1978) to the new twin plane. The disintegrated K-feldspar in figure 88 has

Fig. 85 Large grain of quartz (top) and large sericitized feldspar (bottom) in a deformed granite. Quartz grain has been recrystallized into new grains which show subgrains and detached lobes along serated grain boundary. Field of view 5 mm. across, polars crossed.

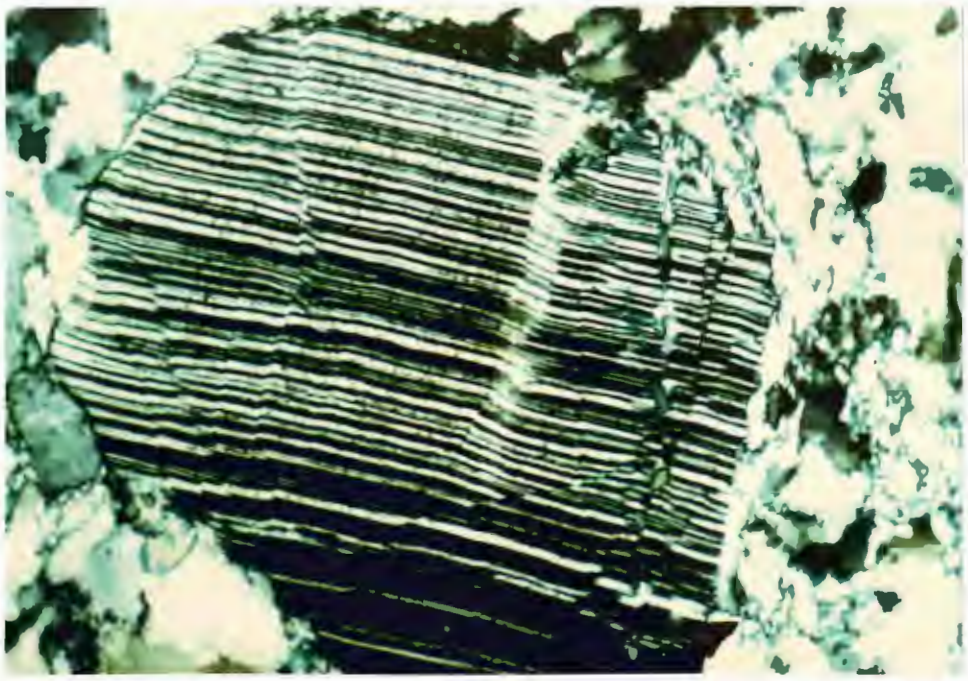

Fig. 86 Large porphyroclast of plagioclase in a deformed granite. Note that kink bands have culminated into fractures, fascilitating deformation of the grain. Field of view 5 mm. across, polars crossed.

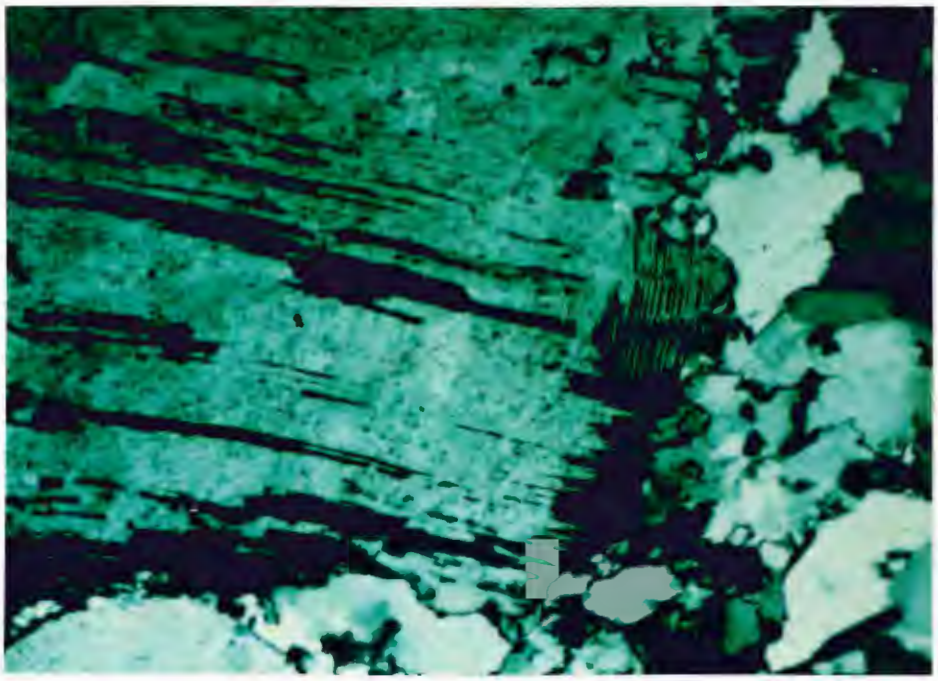

Fig. 87 Large plagioclase grain in a deformed granite has retwinned in response to deformation. Horizontal twins are original and vertical twins on edge of grain are deformation induced. Field of view is 5 mm. across, polars crossed.

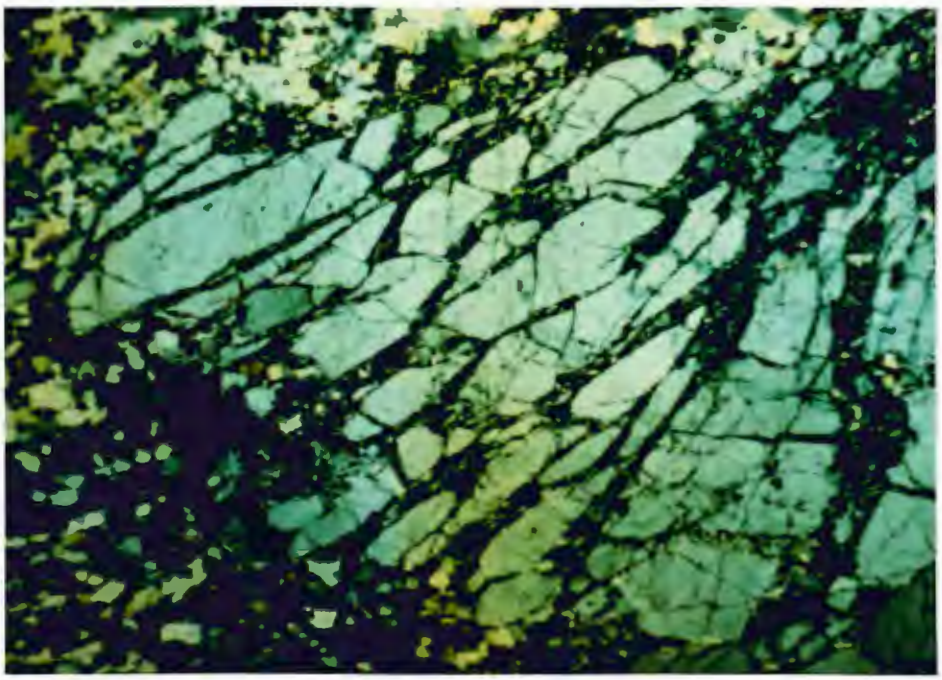

Fig. 88 Large porphyroclast of K-feldspar has shattered, primarily along cleavage, and expanded during deformation. Field of view is 5 mm. across, polars crossed.

been cut by fractures that formed mostly parallel to cleavage. Figure 89 shows orthoclase grains with undeformed interiors and rims that have inverted to microcline. Exsolution also occurs in response to deformation. Figure 90 shows a large dark grain of plagioclase that has patches of exsolved microcline and patchy subgrains, and a large light grain of K-feldspar that has started to exsolve pale lamellae of plagioclase. The result of deformation here is antiperthitic and perthitic textures from originally homogeneous crystals.

There are several textures that occur exclusively in the granitic rocks, two of which will be described here. Graphic granites deform by ductile flow on quartz planes. Blocks of K-feldspar rotate and impinge on one another as the quartz matrix flows. The quartz recrystallizes oblique to the grain boundaries and indicates a local sense of shear compatible with the rotation of the K-feldspar blocks. More deformed, remnant porphyroclasts may consist of two hemispherical orthoclase grains in optical continuity separated by a deformed quartz plane. This texture is the result of disection of a single orthoclase grain. As the grain deforms, dislocations culminate into fractures and the grain begins to flow plastically. The result of deformation is a dismembered set of orthoclase micro-horses that are still in optical continuity.

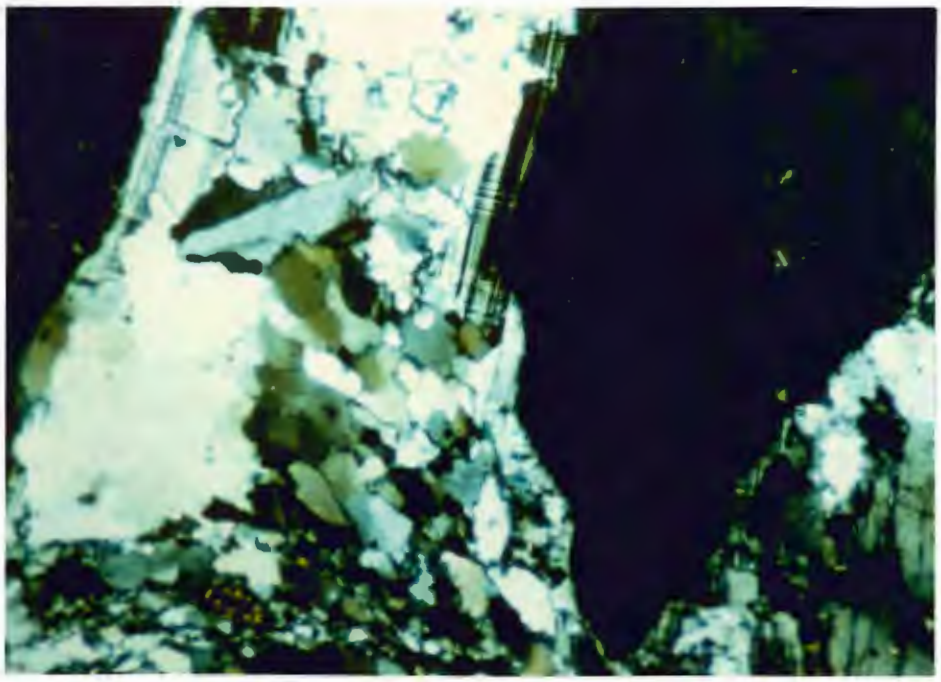

Fig. 89 Orthoclase in a deformed granite has inverted to microcline along its edges in response to deformation. Field of view is 5 mm. across, polars crossed.

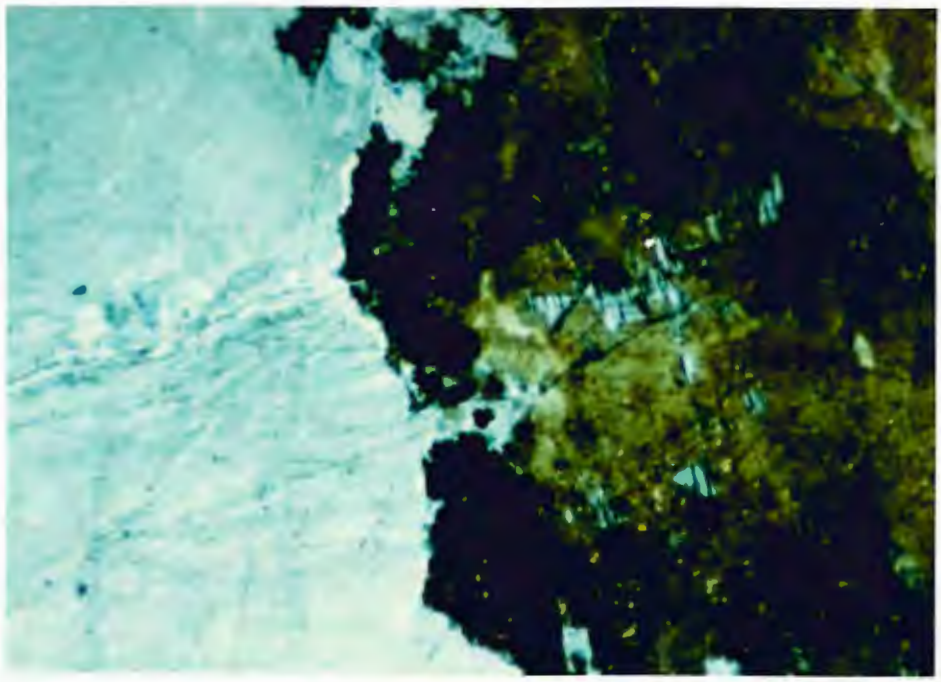

Fig. 90 Plagioclase on right has exsolved microcline, and orthoclase on right has exsolved plagioclase lamellae during deformation. Field of view is 5 mm. across, polars crossed.

Granitic Mylonite

Granite mylonites are characterized by ductile ribbons of quartz, minor ribbons of feldspar, and large well-rounded porphyroclasts of feldspar. Samples of deformed granite can be distinguished from the mylonite in that original quartz grains can no longer be discerned with any certainty in the mylonite. Quartz is so extensively recrystallized that ribbons extend for many tens of centimeters. Recrystallization in the feldspars is minor, yet results in creamy colored, relatively Na-rich pressure shadows around porphyroclasts.

Thin-section analysis confirms that quartz is extensively recrystallized and that feldspars have not only acted brittlely, but ductilely as well. A view parallel to lineation and perpendicular to foliation shows both brittle and dutile features (Fig. 91). Quartz can no longer be referred to as "original grains", and exists as rods that are flattened. Recrystallization and diffusion form these pure, fine-grained rods. Orthoclase and plagioclase exist as either brittlely deformed porphyroclasts or fine recrystallized grains. Feldspar-rich layers consist of broken and abraided porphyroclasts enveloped in a sea of fine recrystallized feldspar and quartz. Brecciation, in addition to recrystallization, appears to be an efficient means of distributing feldspar in the granite mylonites. This juxtapostion of brittle and ductile features in the feldspars is generally not found in the deformed granites or the granite ultramylonites.

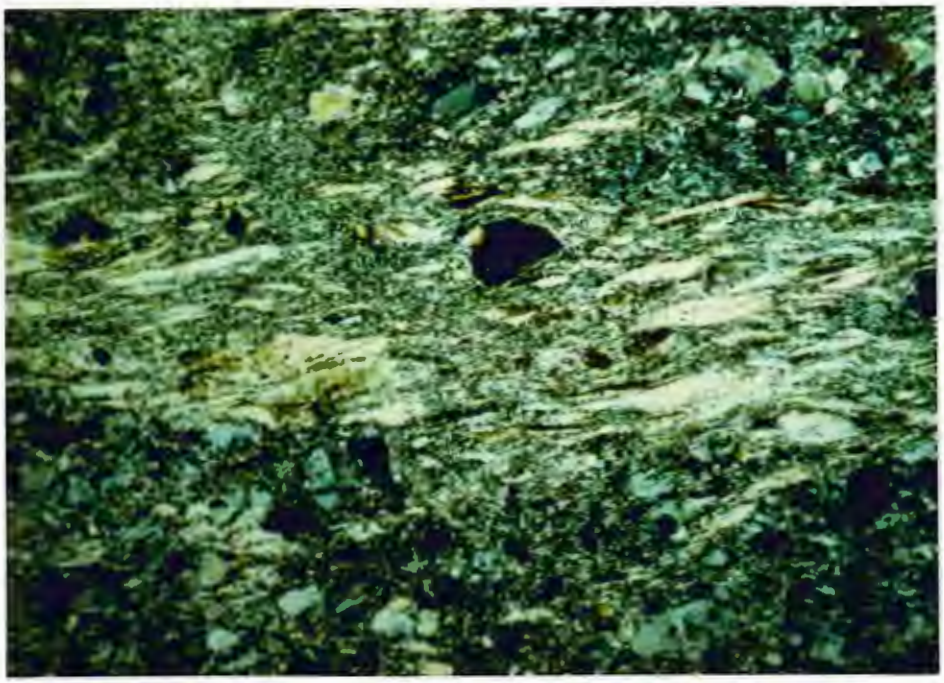

Fig. 91. Photomicrograph of a deformed granite cut perpendicular to foliation and lineation. Note flattened quartz and brecciated and recrystallized feldspar. Field or view 5 mm across, polars crossed.

Granite Ultramylonites

Granite ultramylonites are recognized by their bright color and their ribbons of recrystallized quartz and feldspar. The feldspar ribbons are wider than any of those in the layered gneisses. This suggests that the width of the ribbons is proportional to the protolith grain size (Fig. 39). Some ribbons look remarkably like flattened grains that may have been several centimeters across (see pink sample in Fig. 39). This observation suggests that recrystallization is 1) the dominant mechanism by which the ultramylonites form and 2) the most efficient means of distributing fine feldspar into ribbon-like forms. The implication is that diffusion is a minor process even in the ultramylonites.

Thin-sections of granite ultramylonite show a texture that is consistent from one ultramylonite to the next. This texture is defined by very pure ribbons of feldspar that have an average grain size of around 20 microns and ribbons of quartz with an average grain size of around 100 microns. The only original grains that remain are small porphyroclasts less than 1 mm. in diameter. These represent the unrecrystallized core of the most resistant grains. The most recently recrystallized feldspar resides in the pressure shadow near the grain. The porphyroclast may not show evidence of being strained, which means that the porphyroclasts may have attained an equilibrium grain size. The fine-grained matrix of recrystallized feldspar has also probably attained an equilibrium grain size (Kerrich, 1977).

Conclusions

Each of the protoliths exhibits textures in the deformed state that are characteristic of the protolith rock type. The layered gneisses have two characteristic textures, one the dissected texture where the mica-rich rock has been dismembered on a network of faults, and the other where the quartz- and feldspar-rich rock has been strained enough to create an oblique fabric. Deformed amphibolite gneiss is heavily retrogressed and ribbons in the mylonite are formed from retrograde minerals. The granitic rocks are little retrogressed, and they deform into mylonites with very thick ribbons. They must be extensively recrystallized in order to form mylonites, due to the coarse grained nature of the feldspars.

The mylonites of Francis Peak apparently formed under conditions where the quartz deformed entirely by ductile mechanisms and the feldspar by both brittle and ductile mechanisms. The textural transition in feldspar from mylonite to ultramylonite is coincident with the appearance of feldspar ribbons and with the change in deformation style from one of brittle-ductile to one of ductile flow only. The transition in the response of rock to deformation from brittle to ductile takes place at around 10 km. depth and at a temperature of around 300 °C (Sibson, 1977) under a normal geothermal gradient of 30° per km. The rocks of Francis Peak were therefore deformed at a depth greater than 10 km. in order to produce the ultramylonites that contain recrystallized feldspar.

References

Allmendinger, R.W. and Jordan, T.E., 1981, Mesozoic evolution hinterland of the Sevier Orogenic belt: Geology, v. 9, p. 308-313.

Arabasz, W.B., Smith, R.B. and Richins, W.D. 1980, Earthquake studies along the Wasatch Front, Utah: Network monitoring, seismicity and seismic hazards: Bulletin of the Seismological Society of America, v. 70, #5, p. 1479-1499.

Armstrong, F.C. and Oriel, S.S., 1965, Tectonic development of the Idaho-Wyoming thrust belt: A.A.P.G. Bulletin, v. 49, p. 1847-1866.

Armstrong, R.L., 1968, Sevier orogenic belt in Nevada and Utah: Geological Society of America Bulletin, v. 79, p. 429-458.

Armstrong, R.L., 1972, Low-angle (denudation) faults hinterland of the Sevier Orogenic belt, eastern Nevada and western Utah: Geological Society of America Bulletin, v. 83, p. 1729-1754.

Beach, A., 1976, The interrelations of fluid transport, deformation, geochemistry and heat flow in early Proterozoic shear zones in the Lewisian complex: Philosophical Transactions of the Royal Society of London, v. A280, p. 569-604.

Beach, A., 1980, Retrogressive metamorphic processes in shear zones with special reference to the Lewisian complex: Journal of Structural Geology, v. 2, # 1/2, p. 257-263.

Beck, S.L. and Bruhn, R.L., 1983, Ductile deformation and basement involvement contemporaneous with a Mesozoic thrust fault, in the Sevier orogenic belt, northern Utah: Geological Society of America, abs. progs., v. 15, p. 377.

Bell, T.H., and Etheridge, M.A., 1973, Microstructure of mylonites and their descriptive terminology: Lithos, v. 6, p. 337-348.

Berthe', D., Choukroune, P. and Jegouzo, P., 1979, Orthogneiss, mylonites and non-coaxial deformation of granites: the example of the South Armorican Shear Zone: Journal of Structural Geology, v. 1(1), p. 31-42.

Blackstone, F.L., 1977, The overthrust belt salient of the cordilleran fold belt: Wyoming Geological Ass., 29th annual field conference, guidebook, p. 367-384.

Boyer, S. E. and Elliot, D., 1982, Thrust systems: A. A. P. G. Bulletin, v. 66(2), p. 1196-1230.

Bruhn, R.L., 1984, Continental-ocean transect C-1; geology and structure of the eastern Great Basin and middle Rocky Mountains, Utah: Geological Society of America, abs. progs., v. 16, p. 457.

Bruhn, R.L. and Beck, S.L., 1981, Mechanics of thrust faulting in crystalline basement, Sevier orogenic belt, Utah: Geology, v. 9, p. 200-204.

Bruhn, R.L. and Smith, R.B., 1984, Extensional tectonics of eastern Basin-Range/overthrust belt; inferences on structural style from reflection data, surface geology, and rheologic models: A.A.P.G. Bulletin, Rocky Mountain section meeting abstract, v. 68, p. 933.

Brun, J-P, Burg, J-P, and Guo Ming, C., 1985, Strain trajectories above the Main Central Thrust (Himalaya) in southern Tibet: Nature, v. 313, #6001, p. 388-390.

Brunel, M., 1980, Quartz fabrics in shear-zone mylonites: Evidence for a major imprint due to late strain increments: Tectonophysics, v. 64, p. T33-T44.

Bryant, B., 1978, Farmington Canyon Complex, Wasatch Mountains, Utah: Geological Society of America, abs. progs., v. 10(5), p. 211.

Bryant, B., 1984, Reconnaissance geologic map of the Precambrian Farmington Canyon Complex and surrounding rocks in the Wasatch Mountains between Ogden and Bountiful, Utah: U.S.G.S. miscellaneous investigation series, map I-1447.

Bryant, B. and Reed, J.C., Jr., 1969, Significance of lineations and minor folds in the southern Appalachians and the British and Norwegian Caledonides: Geological Magazine, v. 106, p. 412-429.

Bryant, B. and Graff, P., 1980, Metaigneous rocks on Antelope Island: Geological Society of America, abs. progs., v. 12(6), p. 269.

Crittenden, M.D., 1972, Willard thrust and Cache Creek allochthon, Utah: Geological Society of America Bulletin, v. 83, p. 2871-2880.

Debat, P., Soula, J.-C., Kubin, L. and Vidal, J.-L., 1978, Optical studies of natural deformation microstructures in feldspars (gneiss and pegmatite from Occitania, southern France): Lithos, v. 11, p. 133-145.

Deer, W.A., Howie, R.A. and Zussman, F, 1966, An introduction to the rock forming minerals: Halsted Press, 528 p.

Dunlap, W.J. and Ellis, M.A., 1986, Fault nucleation and propagation: Evidence from thrust displacement analyses: Geological Society of America abs. progs., v. 18(6), p. 590.

Dunlap, W.J., 1988, Progressive reorientation of orogen-parallel stretching lineations is a ductile duplex, Arltunga Nappe Complex, central Australia: Geological Society of America abs. progs., v. 20, north-central section.

Dunlap, W.J., 1988, Ruby Gap duplex, central Australia: A model of continental megathrust development: Geological Society of America abs. progs., v. 20, #7, p. A396.

Ellis, M.A. and Dunlap, W.J., 1987, Displacement distribution along thrust faults: implications and speculations: Tectonic Studies Group Annual Meeting abs. prog., p. 12.

Ellis, M.A and Dunlap, W.J., 1988, Displacement variation along thrust faults: Implications for the development of large faults: Journal of Structural Geology, v. 10, #2, p. 183-192.

Eardley, A.J. and Hatch, R.A., 1940, Precambrian crystalline rocks of north-central Utah: Journal of Geology, v. 48(1), p. 58-72.

Eardley, A.J., 1969, Willard thrust and the Cache uplift: Geological Society of America Bulletin, v. 86, p. 669-680.

Hedge, C.E., Stacey, J.S., and Bryant, B., 1983, Geology of the Farmington Canyon Complex, Wasatch Mountains, Utah: Geological Society of America Memoir #157, p. 37-44.

Hintze, L.F., 1973, Geologic history of Utah: Brigham Young University Geology Studies, v. 20, Pt. 3, 181 p.

Hintze, L.F., 1975, Geological Highway Map of Utah: Department of Geology, Brigham Young University.

Hintze, L.F., 1980, Geologic Map of Utah: Utah Geological and Mineral Survey, Salt Lake City, Utah.

Hobbs, B.E., Means, W.D., and Williams, P.F., 1976, An outline of structural geology: John Wiley and Sons, Inc., New York, 571 p.

Hollet, D., 1979, Petrological and physiochemical aspects of thrust faulting in the Precambrian Farmington Canyon Complex, Utah: University of Utah, Masters thesis, 99 p.

Hopkins, D.L., and Bruhn, R.L., 1982, Geometry and mechanics of basement deformation beneath major Laramide folds in the Rocky Mountains, western U.S.: A.G.U., Eos Transactions, v. 63(45), p. 1115.

Johnson, M.R.W., 1970a, Torridonian and Moinian: in The Geology of Scotland, G. Y., Craig ed., Oliver and Boyd, Edinburgh, 556 p.

Kerrich, R., Beckinsale, R.D., and Durham, J.J., 1977, The transition between deformation regimes dominated by intercrystalline diffusion and intracrystalline creep evaluated by oxygen isotope thermometry: Tectonophysics, v. 38, p. 241-257.

King, P.B., 1977, Precambrian geology of the United States; an explanatory text to accompany the geologic map of the United States: Geological Survey Professional Paper #902, p. 85.

Kohlman, N.A.J., 1980, The polymetamorphism of the Little Willow Formation, Wasatch Mountains, Utah: University of Minnesota-Duluth Masters thesis, 114 p.

Lapworth, C., 1885, The highland controversy in British geology; its causes, course and consequences: Nature, v. 32, p. 558-559.

Lister, G.S. and Snoke, A.W., 1984, S-C mylonites: Journal of Structural Geology, v. 6, #6, p. 617-638.

Little, T.A., 1987, Stratigraphy and structure of the metamorphosed upper Paleozoic rocks near Mountain City, Nevada: Geological Society of America Bulletin, v. 98, p. 1-17.

Love, J.D. and Christiansen, A.C., 1986, Wyoming Geologic Highway Map, scale 1:1,000,000: Wyoming Geological Survey and Western Graphics.

Misch, P., 1960, Regional structural reconnaissance in central-northeast Nevada and some adjacent areas--Observations and interpretation: in Geology of east-central Nevada: Intermountain Association of Petroleum Geologists 11th annual field conference guidebook, p. 17-42.

Mullens, T.E., 1971, Reconnaissance study of the Wasatch, Evanston, and Echo Canyon Formations in part of northern Utah: U.S.G.S. Bulletin 1311-D, 31 p.

Mullens, T.E. and Crittenden, M.D., 1969, Cretaceous age of the Willard thrust, Weber County, Utah: Geological Society of America abs. progs., Rocky Mountain Section 22nd annual meeting, # 5, p. 57.

Myers, J.S., 1978, Formation of banded gneisses by deformation of igneous rocks: Precambrian Research, v. 6, p. 43-64.

Naeser, C.W., Bryant, B., Crittenden, M.D. Jr., and Sorensen, M.L., 1983, Fission-track ages of apatite in the Wasatch Mountains, Utah: An uplift study: Geological Society of America Memoir #157, p. 29-36.

Parry, W.T. and Bruhn, R.L., 1987, Fluid inclusion evidence for minimum 11 km offset on the Wasatch Fault, Utah: Geology, v. 15(1), p. 67-70.

Ramsay, J.G., 1967, Folding and fracturing of rocks: Mcgraw-Hill Inc., 568 p.

Ramsay, J.G. and Graham, R.H., 1970, Strain variation in shear belts: Canadian Journal of Earth Sciences, v. 7, p. 786-813.

Rismeyer, N.W., 1981, Geology of the Precambrian Farmington Complex, Bountiful Peak, Morgan and Davis Counties, Utah: University of Minnesota-Duluth, Masters thesis, 99 p.

Roberts, R.J., Crittenden, M.D., Tooker, E.W., Morris, H.T., Hose, R.K., and Cheney, T.M., 1965, Pennsylvanian and Permian basins in northwestern Utah, northeastern Nevada, and south-central Idaho: A.A.P.G. Bulletin, v. 49, p. 1926-1956.

Robin, P-Y.F., 1979, Theory of metamorphic segregation and related processes: Geochemica Cosmochemica Acta, v. 43, p. 1587-1608.

Royse, F. Jr., Warner, M.A., and Reeves, D.L., 1975, Thrust belt structural geometry and related stratigraphic problems, Wyoming, Idaho and northern Utah: Rocky Mountain Association of Geologists Symposium, Deep Drilling Frontiers of the Rocky Mountains, p. 41-54.

Schmid, S.M., Casey, M. and Starkey, J., 1981, The microfabric of calcite tectonites from the Helvetic Nappes (Swiss Alps): in Thrust and Nappe Tectonics: McClay, K.R. and Price, N.J., eds., Geological Society of London Special Publication 9, p. 151-158.

Sibson, R.H., 1977, Fault rocks and fault mechanisms: Journal of the Geological Society of London, v. 133, p. 191-213.

Simpson, C., 1981, Ductile shear zones: A mechanism of rock deformation in the orthogneisses of the Maggia Nappe, Ticino, Switzerland: ETH Zurich, Switzerland, (Ph.D. thesis), 265 p.

Simpson, C., 1986, Determination of movement sense in mylonites: Journal of Geological Education, v. 34, p. 246-261.

Simpson, C. and Schmid, S.M., 1983, An evaluation of criteria to deduce the sense of movement in sheared rocks: Geological Society of America Bulletin, v. 94(2), p. 1281-1288.

Stewart, J.H., 1980, Regional tilt patterns of late Cenozoic Basin-Range fault blocks, western United States: Geological Society of America Bulletin, v. 91, p. 460-464.

Suppe, J., 1983, Geometry and kinematics of fault bend folding: American Journal of Science, v. 283, p. 684-721.

Tooker, E.W., 1983, Variations in structural style and correlation of thrust plates in the Sevier foreland thrust belt, Great Salt Lake area, Utah: Geological Society of America Memior #157, p. 61-74.

U.S. Geological Survey, 1955, Peterson, Utah 7 1/2 minute topographic quadrangle, one sheet.

U.S. Geological Survey, 1952, Bountiful, Utah 7 1/2 minute topographic quadrangle, one sheet.

Vernon, R.H., 1976, Metamorphic processes: reactions and microstructure development: George Allen and Unwin, Boston, 247 p.

Wernicke, B, 1985, Uniform-sense normal simple shear of continental lithosphere: Canadian Journal of Earth Science, v. 22(1), p. 108-125.

Wojtal, S. and Mitra, G., 1986, Strain hardening and strain softening in fault zones from foreland thrusts: Geological Society of America Bulletin, v. 97(6), p. 674-687.

Zoback, M.L., 1983, Structure and Cenozoic tectonism along the Wasatch fault zone, Utah: Geological Society of America Memior #157, p. 3-27.

APPENDIX

TERTIARY AND YOUNGER FAULTING

The Basin-and-Range province is characterized by horsts and grabens bound by Tertiary normal faults. The grabens contain thick sediments and the horsts are subject to erosion. Zoback (1983) has used gravity and seismic data to determine the nature and extent of the fault systems in north-central Utah. Armstrong (1972) has re-evaluated the subhorizontal faults of northwestern Utah. Three fault systems are evident, Mesozoic compressional faults, Tertiary extensional faults and a presently active fault zone that dips gently to the east.

Gently dipping Tertiary normal faults were unrecognized in northwestern Utah before a classic paper by Armstrong (1972). Prior to 1972, flat-lying faults in that area were mapped as Mesozoic thrusts or decollements. Many of the faults place younger on older sediments, the kind of geometry expected from listric normal faulting. Armstrong has argued convincingly that the faults were formed during Tertiary extension as either normal or listric normal or glide faults (gravity induced), and occasionally as reactivations of eastward verging Mesozoic thrusts. The thrust faults show an opposite sense of movement from the normal faults and some are cut by plutons dated at 109 Ma. Thrusts and decollements are thought by Armstrong (1972) to be less extensive in northwestern Utah at the hinterland edge of the Sevier thrust sheets.

According to Zoback (1983) the normal faults are listric, flattening out at depth to dips as low as 30°. Some of these faults are still mildly active, responding to the present-day E-W least principal stress axis. At

Armstrong (1972) to be less extensive in northwestern Utah at the hinterland edge of the Sevier thrust sheets.

According to Zoback (1983) the normal faults are listric, flattening out at depth to dips as low as 30°. Some of these faults are still mildly active, responding to the present-day E-W least principal stress axis. At least some of these faults penetrate the Precambrian crystalline basement, at greater than 10 km. depth, suggesting that perhaps the basement has been retrograded and involved with cover rocks during eastward thrusting and low-grade metamorphism (see rock descriptions, chapter 3). Individual fault blocks are 10-15 km. wide and up to 60 km. long. Grabens are truncated by E-W trending transverse fault zones that are probably normal faults. There is little evidence to relate these faults to weaknesses associated with older structures (Zoback, 1983; Stewart, 1980). However, the Salt Lake Salient interrupts the Wasatch fault east of Salt Lake City where the high-grade Precambrian rocks of the Uinta axis intersect the fault. Also, the trace of the Charleston-Nebo thrust fault runs perpendicular to the Wasatch fault in the same area. These two structures trend at a high angle to the Wasatch Fault and may account for the E-W trending oblique-slip fault on the northern edge of the salient.

In north-central Utah, east-dipping, low-angle fault zones have been recognized from gravity data and seismic moment tensor solutions of active faults (Zoback, 1983 and Arabasz et

al., 1980 respectively). The faults may have gentle dips depending on the prefered nodal plane and should not be confused with Mesozoic thrust faults, those that crop out at the base of many range blocks (Armstrong, 1972) or show as low-angle reflectors on seismic lines (Zoback, 1983). Neither should they be confused with Tertiary, high-angle normal faults. The activity along the faults occurs below the Wasatch Range and is not confined to the Basin-and-Range. Earthquakes with clear and definable fault plane solutions occurred at 7-16 km. depth (Arabasz et al., 1980). They were located a few kilometers to the east and west of the Wasatch fault in the vicinity of Salt Lake City, beneath Cache Valley (Fig. 2) and along the Utah-Idaho border beneath the Bear River Range. All of these faults presumably dip to the east and define a zone of present extension in northern Utah.

Wernicke (1985) disagrees with the notion of upper crustal extension by ductile stretching of the lower crust. He believes that convection in the asthenosphere has caused extension, that is still active today, by uniform-sense normal simple shear. Extension of the whole crust is accomplished on low-angle normal faults that dip to the east below the Wasatch Mountains. During the past 14 m.y., exposure of deeper crust has occurred in part due to movement on these faults during denudation, and in part to isostatic uplift, erosion and arching of the region between the Wasatch Range and northwestern Utah (Fig. A-1). This arching is corroborated by the tilt of

range blocks either to the east or west about a N-S anticlinal axis that essentially bisects northern Utah (Stewart, 1980). Tertiary faulting can only account for 20-30% of the extension observed in the Great Salt Lake area (Stewart, 1980; Wernicke, 1985).

The model of Wernicke (1985) accounts for the fault geometry and depth of the Moho in northern Utah. His model also agrees with the geometry of active normal faults below the Wasatch Range as explained by Zoback (1983). In general, fault planes dip either gently east or steeply to the west. Armstrong (1972) has hypothesized that gravity gliding was the mechanism by which Tertiary fault blocks in NW Utah were displaced. This hypothesis is not at odds with Wernicke's geometry, but is opposed to his sense of vergence ajacent to breakaway ranges. Note on Figure A-1 how depth to the Moho decreases and gravitational intensity increases westward from a Moho hinge. Wernicke (1985) defines a "discrepant zone" where the Moho should be at 45 km. or more as a result of crustal thickening during Sevier thrusting. Crustal thickness below the Wasatch Mountains today is only 28 km. This discrepancy in thickness cannot be accounted for by normal faulting or backslipped thrusts. The geometrical model of Wernicke explains this anomalously shallow Moho as well as the magnitude of extension and the geometry of active faulting.

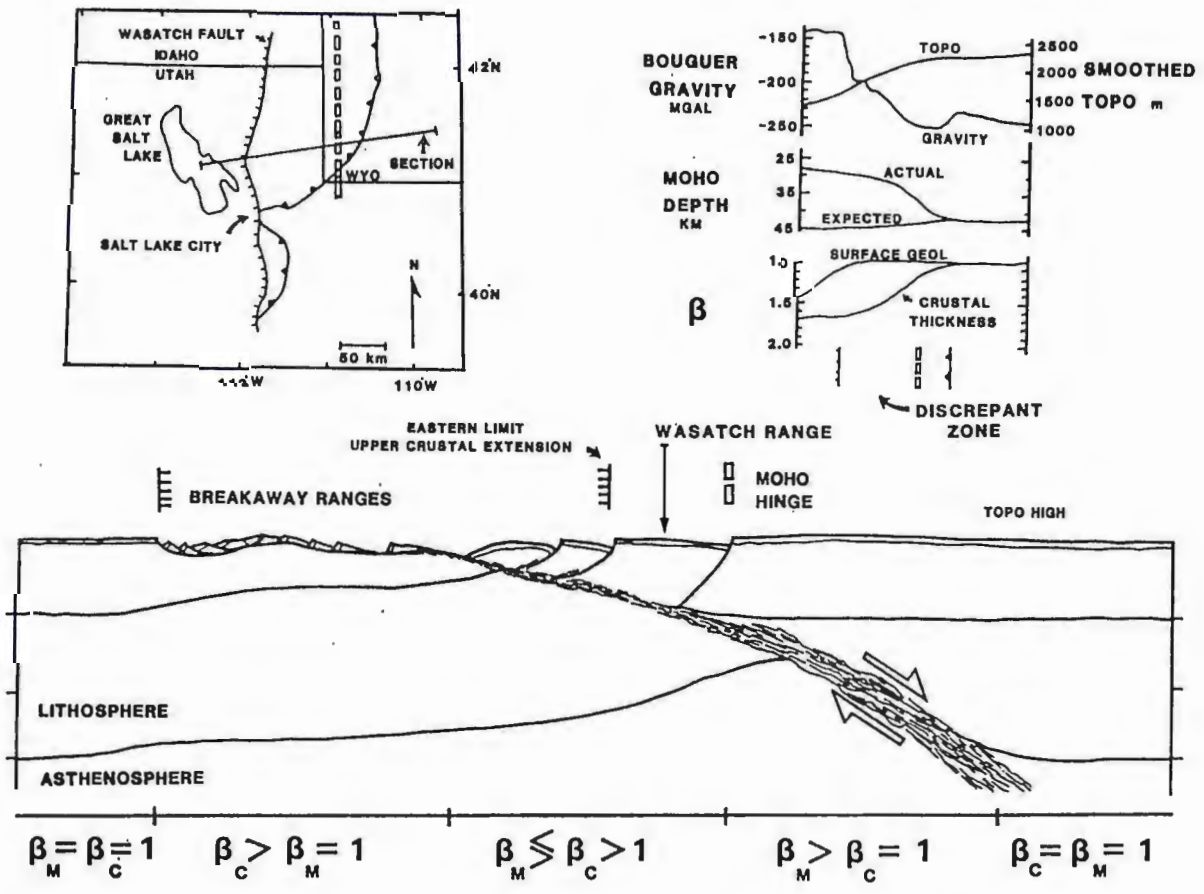

Fig. A-1 Hypothetical cross-section through present study area. Model accounts for variations in gravity, depth to Moho and crustal thickness across discrepant zone of Wernicke (1985). β_m and β_c are mantle and crustal extension respectively. Note: upper and lower cross-sections are not same length.